NTNU

Norwegian University of
Science and Technology

Review of Current control strategies in Modular Multilevel Converter

Jianzhao Wei

Wind Energy
Submission date: June 2016
Supervisor: Lars Einar Norum, ELKRAFT
Co-supervisor: Amin Hajizadeh, ELKRAFT

Norwegian University of Science and Technology
Department of Electric Power Engineering

THESIS REPORT, EUROPEAN WIND ENERGY MASTER PROGRAM, ELECTRIC POWER SYSTEM TRACK

Review of Current Control Strategies in Modular Multilevel Converter

By Jianzhao Wei (763398)

in partial fulfillment of the requirements for the degree of
MSc Electrical Engineering at Delft University of Technology (TU Delft)
& MSc Wind Energy at Norwegian University of Science and Technology (NTNU)

To be defended
on Friday, July 1st, 2016
at NTNU

Supervisors :	Prof. Lars Einar Norum (NTNU) Prof. Pavol Bauer (TU Delft)
Thesis Committee :	Prof. Lars Einar Norum (NTNU) Prof. Pavol Bauer (TU Delft) Dr. Henk Polinder (TU Delft)

TU Delft Delft University of Technology

EWEM

NTNU Norwegian University of Science and Technology

Abstract

With the rapid development of offshore wind farms, the demand for high power, high quality transmission system becomes more urgent. Modular Multilevel converter (MMC) based high voltage direct voltage (HVDC) technology provides a promising solution. In the past decade, intense research has been done on challenges related to the control of MMC, including the outer dynamic control and two inner dynamic controls: capacitor balancing and circulating current suppressing. Many algorithms have been proposed, but an overview of them still lacks. This paper provides a review of most of control strategies for MMC in the literature about all three control purposes with clear classification and detailed explanations. In addition, the traditional proportional-integral (PI) controller based cascade control and model predictive control for AC side current control are compared by simulation in Matlab/Simulink. Different control strategies for capacitor voltage balancing and circulating current eliminating are also tested and compared. Finally, an option of comprehensive control of HVDC system for offshore wind farm is proposed and verified by simulation.

Key words

Modular Multilevel Converter HVDC Current control strategies Capacitor voltage balancing Circulating current suppression

Preface

This is the master thesis 'review of current control strategies for modular multilevel converter'. It is written to fulfill the graduation requirements of European Wind Energy Program, Electric Power System track. I was engaged in researching and writing this thesis from October 2015 to June 2016 in Norwegian University of Science and Technology (NTNU).

There are two main reasons to choose this topic. Firstly, the electrical part of wind energy area is what I am learning and interested. In addition, I focused my direction on power electronics field during the two year master study. Modular multilevel converter (MMC) is one of the latest technologies in this field. Secondly, the offshore wind farm become a hot trend in the future energy system and MMC based HVDC system becomes a very attractive solution for the transmission system of offshore wind farm. I believe that the breakthrough in converters and HVDC technologies would bring more wind energy to grid with high efficiency and stability in future energy system.

Therefore, the thesis focused on the control strategies of MMC with application in offshore wind farm HVDC transmission system. As my background on control theory is not so strong, I spent one chapter to review the current control for two-level voltage source converter and made a good start to extend to multilevel converter. After that, a detailed overview of control strategies for MMC was done. At last, some of the reviewed methods were simulated and compared in Simulink/matlab environment. So, this thesis targeted the readers who wants to study MMC and know the development of MMC in literature, providing them a good reference for more advanced study in MMC or similar topologies. Also, the simulation results can also be used for comparing.

This thesis could not have been done without the help of many people. Firstly, I would like to thank my two supervisors, Pro. Lars Einar Norum in NTNU and Pro. Pavol Bauer for providing me such interesting topic and valuable feedbacks. I also wish to thank my two daily supervisors, associate professor Amin Hajizadeh for guiding me to decide the direction of project at the beginning and PHD Anirudh Budnar Acharya for patient and timely help in simulations, as well as teaching me the efficient methods and deep way of thinking and learning for academic research. I also appreciate their guidance on writing and modifying thesis. I learned a lot from them.

Last but not least, I also want to give my appreciation to my flatmate Milan, who kept forcing me to study every day using all means. Without him, I cannot finish it in time. Also, my lovely girlfriend Lindo deserves a particular note of thanks: your persistent encourage and support kept me always motivated. My parents' care is always the warmest and makes me keep moving.

Jianzhao Wei
09/06/2016

Content

List of Figures

List of Tables

Abbreviation

APOD	Alternate Phase Opposition Disposition
CSC	Current Source Converter
COG	Center of Gravity
CD-PWM	Carrier-Disposition PWM
CPS-PWM	Carrier Phase Shifted PWM
CCSC	Circulating Current Suppressing Control
DFCS-MPC	Direct finite control set MPC
DOF	Degree of Fulfillment
EWEA	European Wind Energy Association
FC	Flying Capacitor
HVAC	High Voltage Alternating Current
HVDC	High Voltage Direct Control
IFCS-MPC	Indirect Finite Control Set MPC
MMC	Modular Multilevel Converter
MPC	Model Predictive Control
NLM	Nearest Level Modulation
NPC	Neutral Point Clamped
OWF	Offshore Wind Farm
PWM	Pulse Width Modulation
PI	Proportional Integral
PR	Proportional Resonant
PLL	Phase Locked Loop
PD	Phase Disposition
POD	Phase Opposition Disposition
RES	Renewable Energy Source
SM	Sub Model
S&H	Sampling & Holding
VSC	Voltage Source Converter

1. Introduction

1.1 Background and Motivation

Due to the economic development, the demand for energy increases dramatically over the past 30 years. On the other hand, the depletion problem of fossil resources and the negative effects of traditional energy combustion are becoming more and more serious, which give an increasing amount of interest and attention on renewable energy source (RES). Among all the RES, wind energy is one of the leading technology. Over the past ten years, globe accumulated installed wind power capacity has increased from about 47.6 GW in 2004 to 369.6 GW in 2014, an average annual growth of 20%, as shown in figure 1.1 [1]. In Europe, wind energy has the highest installation rate among all new installed energy technologies in 2014, accounting for 43.7% [2]. At the end of 2014, the share of wind energy in total installed generation capacity is 14.1% [2] and it will have a deeper penetration in the future. For example, Denmark has a goal of 50% of power consumption from wind energy in 2020[3].

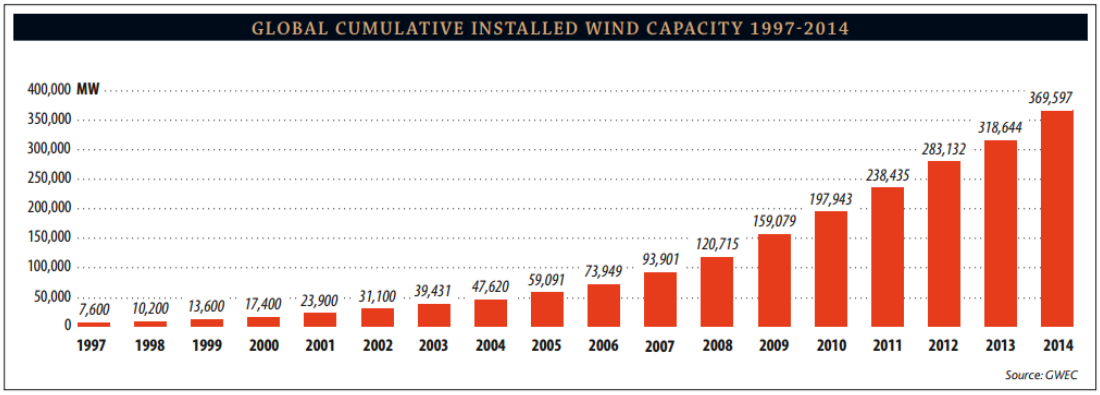

Figure 1.1 Global cumulative installed wind capacity 1997-2014 [1]

Among all the new installed wind energy in Europe in 2014, 12.6% is from offshore wind energy [2] and it shows an increasing trend in the future system [4]. Compared to onshore counterpart, the offshore wind farm (OWF) can capture stronger and more stable wind, thus better and sustained electricity can be generated. And big wind turbine, large wind farm space and high power rating can be achieved by OWF. In addition, low visibility and less noise for public are also the merits. These make OWF a very attractive approach to satisfy RES demand.

However, the large capacity and long distance from coast of OWF increase the requirement of transmission. That makes high voltage DC (HVDC) transmission technology more preferable and it is believed that HVDC will be dominated technology in future energy system, especially for OWF [5]-[10]. One of the idea under discuss about OWF and transmission is referred as 'DC Supergrid', which is proposed by European Wind Energy Association (EWEA) as shown in Figure 1.2. It is called 'EWEA's

20 year offshore network development master plan' and assumes to build a large grid network to connect all the wind farms in the North sea and the countries lie between Scandinavia in northern Europe and France in southern Europe together using HVDC transmission line. This topology is motivated by two reasons:

- The need for interconnection between countries and their power market to provide support and competition
- The demand for connect the offshore wind farm economically and efficiently in order to use offshore wind energy better

HVDC technology could be a useful approach to solve these two challenges [11]. The 'DC Supergrid' plan not only shows the potential of offshore wind energy but also emphasizes the importance of HVDC technology.

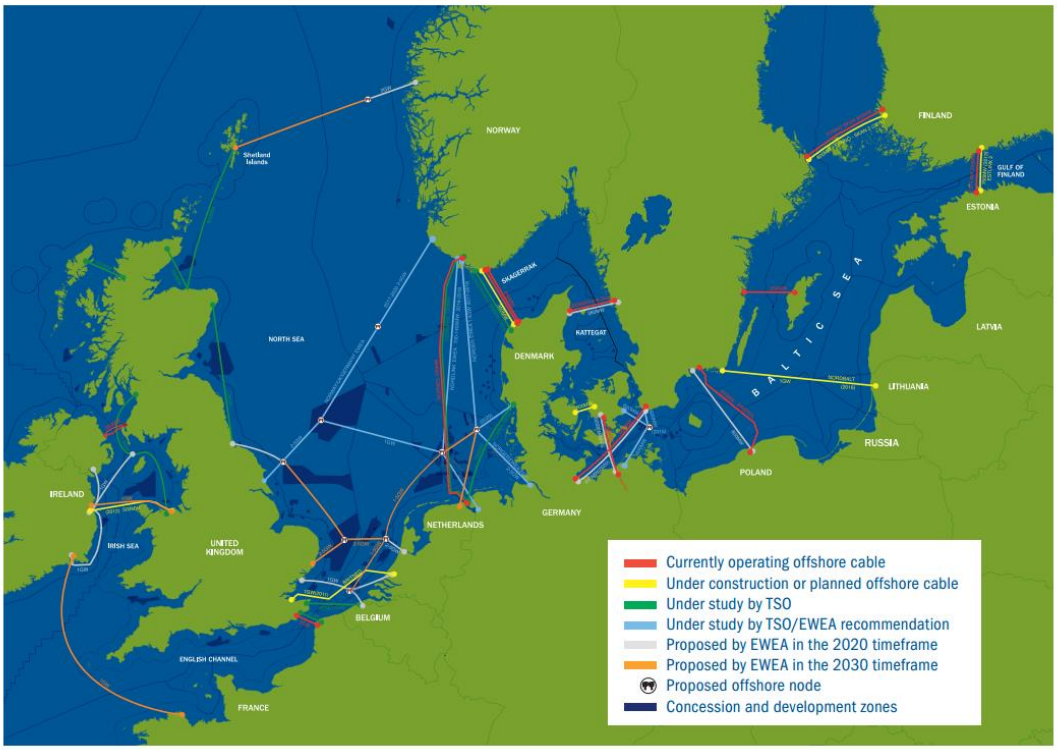

Figure 1.2 EWEA's 20 year offshore network development master plan [11]

The high power, high voltage transmission demands also increase the requirement for power converters. The modular multilevel converter (MMC) proposed in 2002 has offered the solution. It uses modular structure to achieve high voltage levels and less harmonics, thus is widely promoted, especially in HVDC applications [12]-[18]. It is also accepted in the industry. Many companies has implemented MMC into HVDC application: the HVDC-PLUS, HVDC-LIGHT and HVDC-MAXSINE concepts are from Simens, ABB and Alston respectively. With the trend of higher power rating of OWF, MMC is becoming the most promising components in the future system.

Based on the introduction above, it is meaningful to study these technologies as they

are still not mature. This thesis will focus on the current control strategies of MMC. And for better understanding, it is applied in HVDC transmission line for offshore wind energy.

1.2 Problem Statement

Although, intense research has been done on MMC since it is first proposed in 2002, the control technologies of MMC are still not mature because of the multilevel of voltage increases the complexity of control system. Two main extra technical challenges about control of MMC are capacitor voltage balancing and circulating current elimination [19].

As the Sub-model(SM) capacitors are charged and discharged by the arm current, there will be voltage variations in capacitors, which will cause output DC voltage fluctuation and make control system inaccurate and unstable. In addition, unbalanced SM capacitor voltage will cause circulating current problem, which will be discussed below [20]. Also, the switching frequency for each SM will reduce, the capacitors will be charged or discharged at longer time, thus, capacitor voltages become even more unbalanced. Therefore, keeping SM capacitor voltage at constant value is a key issue.

Another problem for MMC is circuiting currents among three phase legs, which is caused by the voltage differences among the three phase as a result of SM capacitor voltage variation. Because circuiting currents only flow in three phase legs, they will not affect the ac-side voltages and currents, however, if they are not properly reduced, they will increase the RMS values of arm currents, thus increase the losses and give more stress on components. Although, the arm inductors can limited the circuiting current, they cannot eliminate the currents completely. Effective algorithms need to be used.

As the MMC is used in high voltage and high power applications, the switching frequency must be limited for safe operation of IGBTs. At such sampling-to-fundamental low frequency ratios, the dynamic performance of the control loops, i.e. AC side current control, becomes a challenge. Reduced switching frequency algorithms of current control should be used.

The MMC applied in HVDC system will be investigated in this thesis, so AC side current control of MMC will also be studied and the control system mainly has two functions:

- Independent active and reactive power control following the desired values.
- Regulation of the dc-bus voltage at its nominal value.

Motivated by the promising future of the MMC and HVDC system for offshore wind power, as well as the technical challenges introduced above, this thesis will focus on the current control of MMC in HVDC systems especially on the wind farm side MMC. The current control methods introduced in existing academic papers are reviewed first and some of the algorithms are simulated and compared.

1.3 Objectives

The objective of the thesis is to study and simulate the control strategies of MMC (both inner and outer dynamic control) applied in HVDC system for offshore wind farm. In order to focus more on control algorithms, only the wind farm side MMC will be studied. The main goals are:

- Understanding the operation characteristics of MMC in both inner and outer dynamics.
- Studying relevant papers and making a review of the most control algorithms in existing papers including AC side control, circulating current elimination control and SM capacitor voltage balancing control.
- Modelling and simulating at least two of the control strategies for each control purpose in Matlab/Simulink environment.
- Analysis and comparison of the simulation results

1.4 Thesis Outline

In Chapter 1, the motivation and objectives of the thesis are introduced. In Chapter 2, some background knowledge about MMC and HVDC system is explained. The advantages of voltage source converter based HVDC system and MMC are presented. In addition, a mathematical model of MMC was derived and the configuration of HVDC system is chosen.

In Chapter 3 and Chapter 4, the current control strategies for two-level voltage source converter and MMC in literature are reviewed respectively. The control strategies for MMC have been classified into three aspects: voltage balancing control, circulating current suppression control and AC side current control.

In Chapter 5, the system used for simulation is proposed. The simulated methods are summarized and the reasons for choosing these methods are explained briefly. The simulation methods and results are introduced in Chapter 6. The results are analyzed and compared for each control purposes. And the comparison between two overall control schemes are made, which are traditional PI based control and model predictive control.

At last, in chapter 7, the conclusions of this thesis are presented. The contribution and future work are summarized.

2. Background Knowledge

In this chapter, some background knowledge about MMC and HVDC system will be introduced. Firstly, the advantages of MMC over other converter topologies are introduced. After that, the basic structure and the mathematical model of MMC are presented. Secondly, the different topologies for HVDC system are reviewed and different power converter technologies in HVDC system are compared. At last, the control algorithms for HVDC system are presented.

2.1 Modular Multilevel Converter

The demands of high voltage applications and better power quality lead to the emergence of multilevel converters, which can achieve lower switching frequency and lower harmonics compared to two-level converters, so that the switching losses are comparably decreased and the filter size is significantly reduced. In addition, because of more voltage levels, the voltage stress (dv/dt) is reduced, which mitigate the electromagnetic interference [21]-[23]. The multilevel converter topologies are summarized in [21]-[23], in which the neutral point clamped (NPC) and flying capacitor (FC) are two widely known topologies. The applications of multilevel converters in HVDC system are reviewed in [24]. However, they need a large number of semiconductor components and the complexity of structure will increase with the increase in number of voltage levels, which will bring large difficulties for control. Also the complex structures complicate the insulation and cooling design, so that for HVDC application, the number of voltage level higher than 3 is seldom considered [21].

MMC is a new form of multilevel converter and it is a big breakthrough in this area especially for high voltage system. Besides the advantages mentioned above, MMC also avoids the drawbacks of other multilevel converter topologies. Due to its modularity and scalability characteristics, the identical small subsystems can be easily added to achieve higher power and voltage levels and the number of voltage steps is considerably expanded [25].

2.1.1 Basic structure

The MMC concepts and basic operation principles were firstly introduced in [25]-[26]. Figure 2.1(a) shows the structure of a three-phase MMC. Three phases are three legs (shown by dotted red circle) and each leg consists of two arms (shown by dotted blue line), the upper arm and lower arm. Both of which comprise *N* series-connected identical sub-modules (SM), which is shown in Figure 2.1(b). In addition, each arm has a series inductor, which is used to limit high frequency components in the arm current [19]. Each SM will be controlled to generator the desired phase voltages.

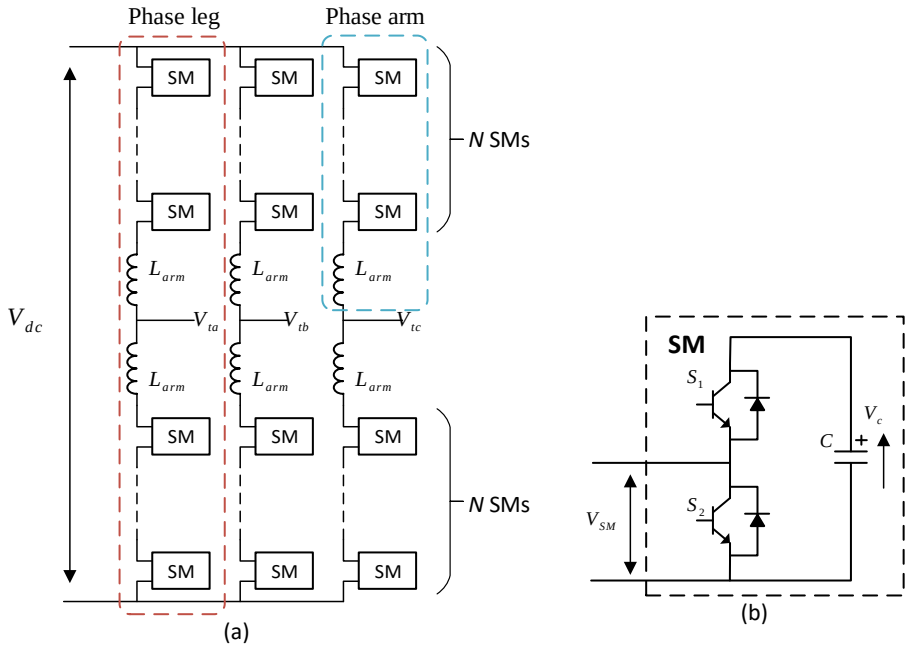

Figure 2.1 a) structure of MMC b) structure of sub-modular

There are different structures for SMs of MMC, the one shown in Figure 2.1(b) is half-bridge circuit. The other types are summarized in [19], which will results in different voltage level at the terminal of SMs. Among all the configurations, the half-bridge SM has been the most popular one, because only two switches are used, thus smaller switching losses and less complexity [19],[27]. Therefore, in this thesis, the half bridge configuration is used.

As shown in Figure 2.1(b), the SMs has two switches and one capacitor. By controlling the switches, the output of SM V_{sm} has three states: when S2 is on, S1 is off, V_{sm} is equal to capacitor voltage, which is called switch-on or inserted state; when S2 is off, S1 is on, V_{sm} is equal to 0, which is called switch-off or bypassed state; when both switches are off, the SM is blocked which is usually used when fault happens. S1 and S2 cannot be both switched on, otherwise, the capacitor will be short-circuited. In addition, the direction of arm current will also affect the output voltage of SMs. At the state that SM is inserted, if current is positive, the capacitor is charged; if current is negative, the capacitor is discharged. Which is very important for balancing the capacitor voltage and will be discussed later. The states of SMs by considering the direction of current is shown in Figure 2.2.

The desired output AC voltages are achieved by controlling the SMs to be inserted or bypassed. As all the SMs are identical and the addition of voltages of all inserted SMs in one leg is equal to DC voltage, in order to balance the DC voltage, the number of inserted SM in one phase should be the same and equal to *N* (*N* is the number of SMs per arm) for maximum number of voltage levels:

$$n_u+n_l=N \tag{2.1}$$

where n_u and n_l are the number of inserted SMs in upper and lower arm respectively.

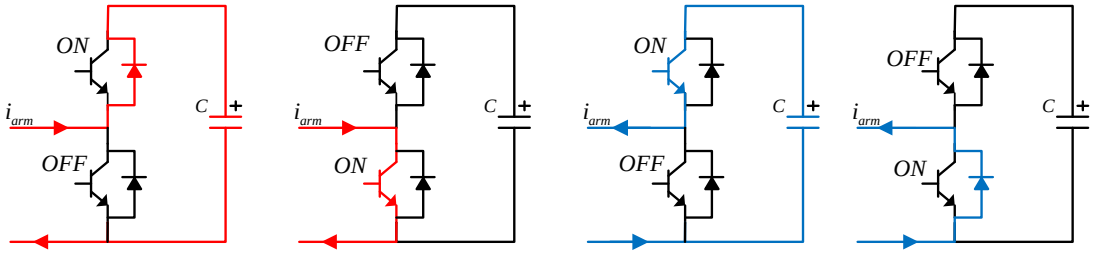

a) Charging b) bypass c) discharging d) bypass

Figure 2.2 Different state of SMs with different current directions

So the level of output voltage is decided by the difference between the number of inserted SMs in upper and lower arm. And the number of phase voltage levels for a MMC with *N* SMs per arm is *N*+1. And 2*N*+1 levels for line voltages

As we can see, the change of output voltage level of MMC is achieved by altering the state of only a few SMs, so the switching frequency is dramatically reduced and the stress to the semiconductor is much smaller compared to two-level converter because of small step of voltage change.

2.1.2 Mathematical Model of MMC

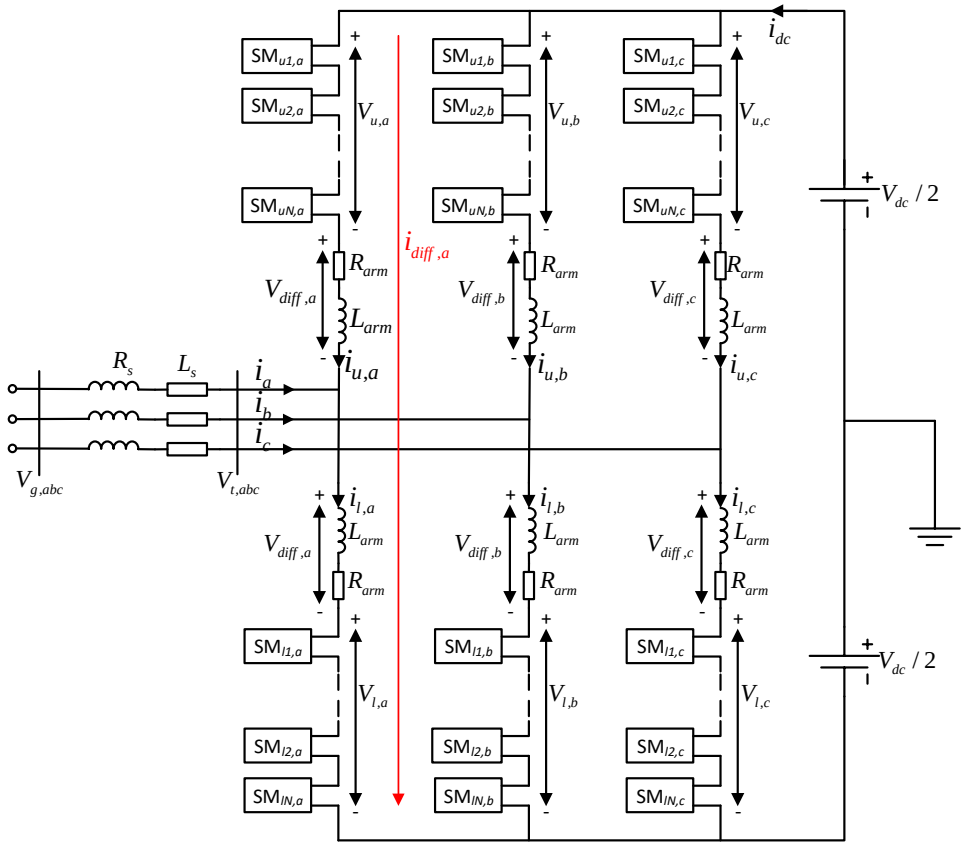

Figure 2.3 The detailed diagram of MMC

A detailed diagram of MMC is shown in Figure 2.3. Each arm consists of *N* SMs, the arm resistor (modeling the losses within each arm) and inductor. The voltage of inserted SMs on each arm is defined by $V_{k,j}$, where subscript *k* represents arms (*k=u, l,* representing upper arm and lower arm respectively); subscript j represents phase (*j= a, b, c*). $V_{diff,j}$ represents the voltage drop on the arm impedance. Circulating current of phase A is shown by dotted red line in Figure 2.3 using symbol $i_{diff,j}$. In AC side, the converter is assumed to be connected to the grid with voltage $V_{g,j}$ and grid impedance R_s and L_s. The DC side of converter is connected to voltage sources with midpoint grounded. The directions of all quantities are shown in the diagram.

Based on Figure 2.3 and Kirchhoff voltage law, the dynamic equations of MMC in phase *j* can be expressed by:

$$\frac{V_{dc}}{2} - V_{u,j} - R_{arm} i_{u,j} - L_{arm} \frac{di_{u,j}}{dt} + R_s i_j + L_s \frac{di_j}{dt} - V_{g,j} = 0 \qquad (2.2)$$

$$-\frac{V_{dc}}{2} + V_{l,j} + R_{arm} i_{l,j} + L_{arm} \frac{di_{l,j}}{dt} + R_s i_j + L_s \frac{di_j}{dt} - V_{g,j} = 0 \qquad (2.3)$$

Because of the symmetry between upper arm and lower arm, the AC side current will be equally divided into two parts flowing to upper and lower arm respectively. Similarly, due to the symmetry between three phases, the DC current will be equally divided into three parts for three phases. Therefore, the arm current can be expressed as:

$$i_{u,j} = \frac{I_{dc}}{3} + i_{diff.j} - \frac{i_j}{2} \qquad (2.4)$$

$$i_{l,j} = \frac{I_{dc}}{3} + i_{diff.j} + \frac{i_j}{2} \qquad (2.5)$$

where the $i_{diff.j}$ only represents the AC components.

Combing (2.4) and (2.5), the circulating current and AC side current can be represented by arm currents as:

$$i_{diff,j} = \frac{i_{u,j} + i_{l,j}}{2} - \frac{I_{dc}}{3} \qquad (2.6)$$

$$i_j = i_{l,j} - i_{u,j} \qquad (2.7)$$

Adding (2.2) and (2.3), and substituting i_j using (2.7), the outer dynamic equation for MMC is yielded:

$$(L_{arm} + 2L_s)\frac{di_j}{dt} = -(R_{arm} + 2R_s)i_j + V_{u,j} - V_{l,j} + 2V_{g,j} \qquad (2.8)$$

Subtracting (2.3) from (2.2) and substituting $i_{diff,j}$ using (2.6), the inner dynamic equation for MMC is yielded:

$$V_{diff,j} = L_{arm} \frac{di_{diff,j}}{dt} + R_{arm} i_{diff,j} + R_{arm} \frac{I_{dc}}{3} = \frac{V_{dc}}{2} - \frac{V_{u,j} + V_{l,j}}{2} \qquad (2.9)$$

According to equation (2.8), the AC side current can be directly controlled by $V_{u,j} - V_{l,j}$ and according to equation (2.9) $V_{u,j} + V_{l,j}$ (or $V_{diff,j}$) can be used to control the circulating current. These will be the basic theories for most of control algorithms for MMC introduced later.

The arm voltages can be calculated by the formula below assuming that all the capacitors are balanced equally:

$$V_{u,j} = n_{u,j} V_{cu,j} \tag{2.10}$$

$$V_{l,j} = n_{l,j} V_{cl,j} \tag{2.11}$$

where $V_{ck,j}$ is the individual SM capacitor voltages, $n_{k,j}$ is the inserted number of SMs in upper and lower arms.

So that the power processed by each arm can be calculated by:

$$P_{u,j} = V_{u,j} i_{u,j} = n_{u,j} V_{cu,j} i_{u,j} \tag{2.12}$$

$$P_{l,j} = V_{l,j} i_{l,j} = n_{l,j} V_{cl,j} i_{l,j} \tag{2.13}$$

The power of each arm can also be calculated by the derivative of energy $W_{k,j}$:

$$P_{u,j} = \frac{dW_{u,j}}{dt} = \frac{d(0.5NCV_{cu,j}^2)}{dt} = NCV_{cu,j}\frac{dV_{cu,j}}{dt} \tag{2.14}$$

$$P_{l,j} = \frac{dW_{l,j}}{dt} = \frac{d(0.5NCV_{cl,j}^2)}{dt} = NCV_{cl,j}\frac{dV_{cl,j}}{dt} \tag{2.15}$$

Compare (2.12),(2.13) with (2.14),(2.15) respectively, the dynamics of each SM capacitor is:

$$\frac{dV_{cu,j}}{dt} = i_{u,j}\frac{n_{u,j}}{N} \tag{2.16}$$

$$\frac{dV_{cl,j}}{dt} = i_{l,j}\frac{n_{l,j}}{N} \tag{2.17}$$

It should be noticed that equation (2.16) and (2.17) represent the average dynamics of SMs, because the switched-on SMs will have higher voltage ripples and switched-off SMs will have no voltage variations during each switching period.

According to paper [19], equation (2.4), (2.5), (2.8), (2.9) and (2.16), (2.17) give a generalized dynamic model of MMC. The control algorithms introduced in Chapter 4 will be explained based on this model and using the same symbols.

2.2 HVDC transmission system

Offshore wind farm can be connected to the main gird through high voltage AC (HVAC) or HVDC transmission. As offshore wind farm are far from the coast, HVDC has shown many advantages over HVAC system, which can be summarized as below [5]-[7]:

- The length of AC transmission is limited by surplus of reactive power due to charging from shunt capacitances. As shown in Figure 2.4, which shows the relationship between transmission distance and power capacity, the active power capacity reduces with the increase of length, at certain length the power transmitted is zero. For longer length, the compensation equipment is needed. But for DC transmission, this problem is avoid.
- Losses and voltage drop in the DC link are very low. And there is no resonant between cables and other AC equipment.
- DC cables are cheaper than AC cables because DC lines only need two conductors while AC lines need three. Thus smaller footprint and simpler tower design for DC.
- HVDC can connected two asynchronous system.
- HVDC system can achieve fast and accurate control of power flow, whereas the ac link provides no or slow control.
- The fault can be quickly isolated as two system are decoupled by DC system.

The disadvantage of HVDC system is that it needs expensive converters, which increase the cost. [5] and [28] made evaluation between HVAC and HVDC transmission line for offshore wind farm and the conclusions are as expected, for short distance, HVAC is more economic and for long transmission distance, HVDC is cheaper and the boundary condition is about 55-70 km in [28]. Because of the trends that wind farms are further from coast, the HVDC system is more and more preferable.

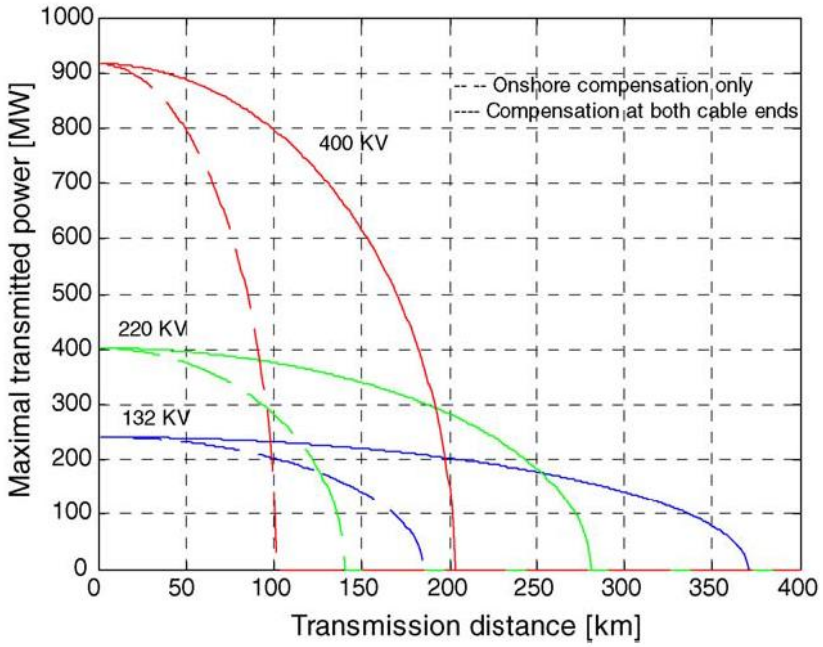

Figure 2.4 Transmission capacity of HVAC system with three different voltage levels [12]

2.2.1 The Topologies of HVDC System

The topologies of HVDC system can be mainly divided into monopole and bipolar systems. In addition, monopole can be further distinguished as asymmetrical and symmetrical configurations [9][10]. They will be introduced below:

- **Asymmetrical monopole systems**. Each station has only one converter and two stations are connected by only one high voltage DC cable. The current return path can be through earth, sea water or low resistance metallic conductor. Both configurations are shown in Figure 2.5 (a) and (b).
- **Symmetrical monopole systems**. Each station has only one converter but two stations are connected by two high voltage DC cables, one for positive polarity and one for negative polarity, so that each of cable is only subjected to half DC voltages, thus transfers half power. Usually the middle point of the converter is ground [10] as shown in Figure 2.5 (c).

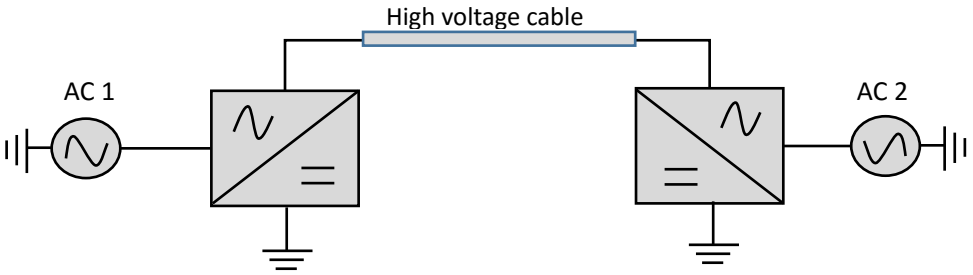

(a) Asymmetrical monopole- Earth return or sea water return

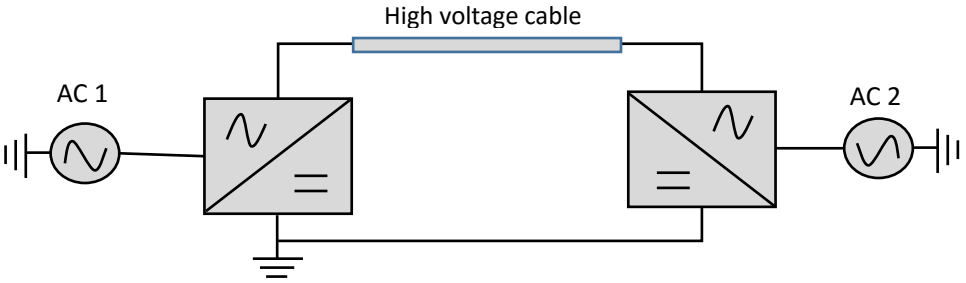

(b) Asymmetrical monopole- Metallic return

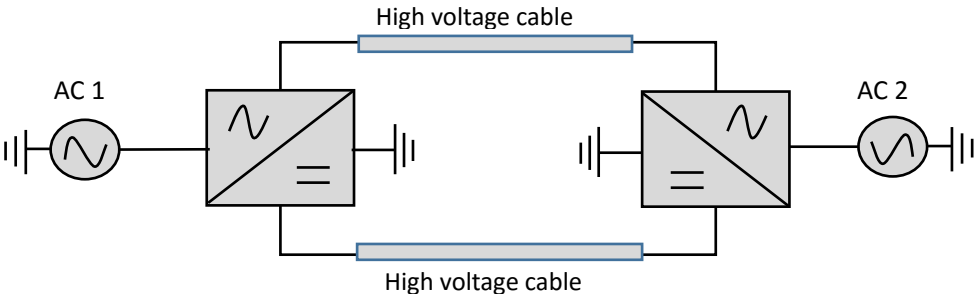

(c) symmetrical monopole

Figure 2.5 Monopole configurations for HVDC system

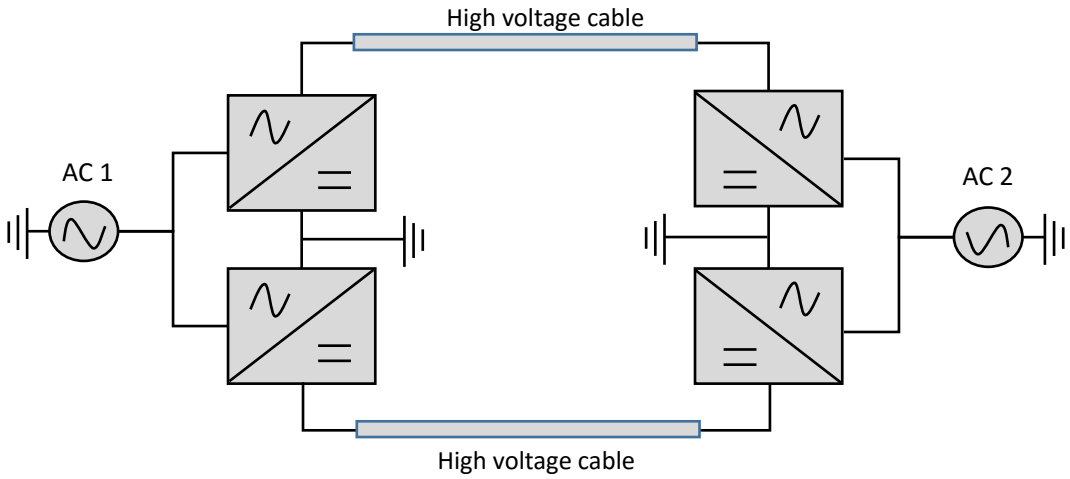

Figure 2.6 Bipolar Configuration for HVDC

- **Bipolar systems**. Each station has two converters in order to achieve high rated power and reduce harmonics for classical current source converter based systems. Bipolar systems basically consist of two asymmetrical monopole systems connected in series, which have same DC amplitude but opposite polarities. The advantage is that if one pole is broken, the other pole can still work as a monopole system. The system is shown in Figure 2.6.

According to [10], for classical current source converter based HVDC system, the bipolar systems are most commonly used, however VSC based HVDC transmission usually uses symmetrical monopole systems. As the thesis is focus on VSC-HVDC system, the symmetrical monopole configuration is used in the rest of the thesis.

2.2.2 Converter Technologies for HVDC Systems

There are basically two converter technologies to achieve HVDC transmission: Line-commutated current-source converters (CSC) and voltage-source converters (VSC) [5]-[7].

The CSC based HVDC system with asymmetrical monopole configuration is shown in Figure 2.7. It is classic HVDC technology using thyristors based line-commutated converters. As we can see, converters are connected to AC systems through transformers and both AC side and DC side need filters to reduce the harmonics. Moreover, the Var capacitors are needed in ac side to compensate the reactive power required by the converters. Inductors L_d are used to reduce the voltage ripple in DC side.

The power is controlled by changing the firing angle of thyristors in both rectifier and inverter. Normally, the inverter controls the DC voltage and rectifier controls current. The power transmission can be reversed in this system, however, no matter the

directions of power flow, the converters will always consume reactive power.

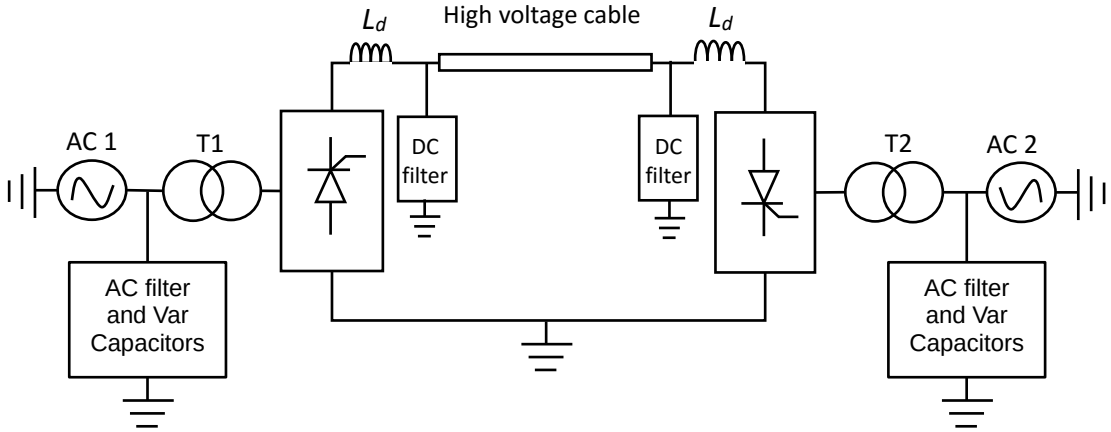

Figure 2.7 CSC-HVDC system

Although, this technology can handle very high power, it has more drawbacks compared with VSC based HVDC system. They are listed below [24][29]:

- VSC can control active and reactive power independently, so four-quadrant operation is possible. While CSC always consume reactive power and VAR compensation are needed
- VSC can be controlled to operate close to unity power factor, thus lower harmonics content and smaller filter size.
- VSC makes it easier to realize multi-terminal HVDC system, which is a hot trend in the future energy system.
- Possible to connect VSC based HVDC system to a 'weak' system, while CSCs need strong synchronous voltage source in order to commutate.
- VSC based system avoid the commutation failures due to disturbance
- VSC-HVDC can provides black-start of offshore grid
- Fast dynamic response due to high PWM frequency.

Because of these numerous advantages, VSC-HVDC system is gaining more and more attention and will be dominated in the future system [24]. The diagram of the system with symmetrical monopole configuration (the midpoint of DC side capacitor is grounded) is shown in Figure 2.8. Compared to Figure 2.7, the AC side VAR capacitors and the DC side filters, smoothing inductors are not needed.

Normally, the IGBTs are used as the switches of converters in above system. Antiparallel diode are needed to achieve 4 quadrant operations. DC bus capacitors not only filter DC harmonics but also provide energy storage for better control of power flow. In the diagram, there are AC filters at the ac source side in order to further reduce the harmonics in the ac source currents. The phase reactor L is used to provide the phase angle between AC source voltage and the input voltage of converter to ensure

the control of power flow. The transformer $T_{1,2}$ is used to adjust the ac system voltages for converter and also joins the voltage amplitude control using tap changers.

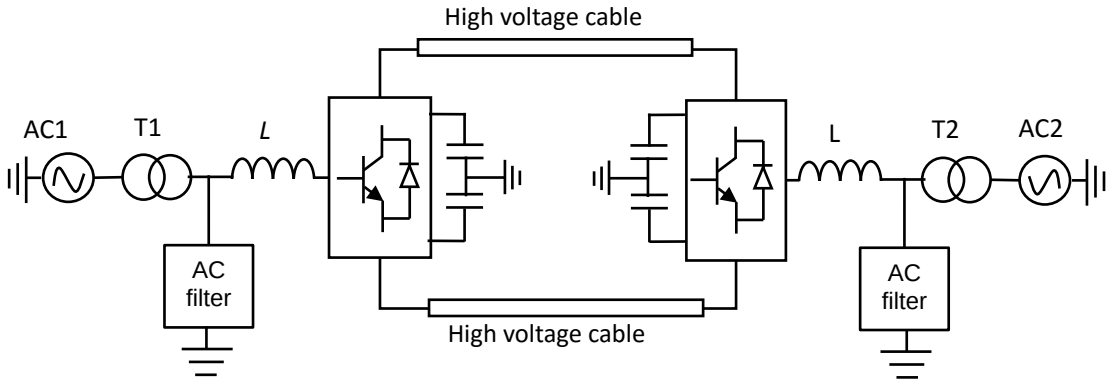

Figure 2.8 Two-level VSC-HVDC system

Although VSC based HVDC system has numerous advantages, it still has drawbacks [12]:

- The transmitted power is not high because of the inherent characteristics of IGBTs. Series connection of IGBTs is needed to achieve high voltage, which was different and easy to fail into an open circuit
- The shape change of arm currents (di/dt) causes undesired electromagnetic interference and increase the stress of components
- The stored energy in the DC-bus results extremely high current during short circuit fault, which will cause damage

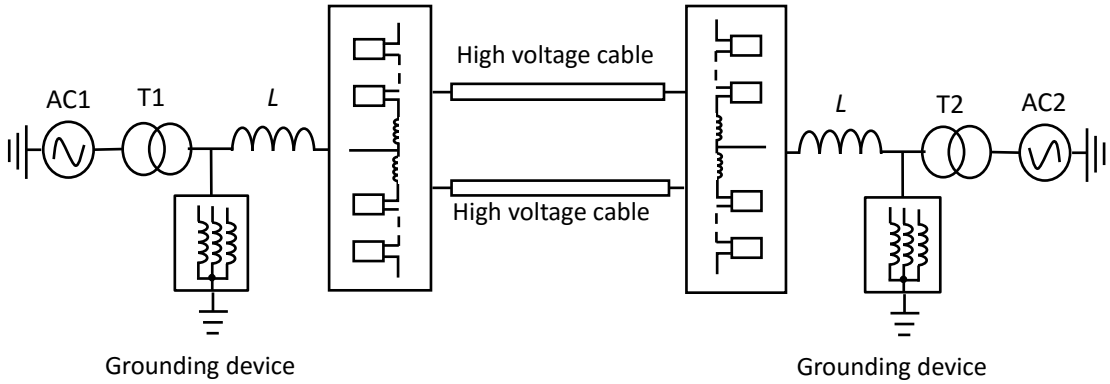

Figure 2.9 MMC based HVDC system

The introduction of the MMC has provide a good solution due to its inherent advantages like: modularity, scalability, high efficiency and good power quality. The diagram of HVDC system using MMC is shown in figure 2.9. Because the DC capacitors of MMC are located in each SMs, the grounding scheme cannot be the same as that for2-level VSC. One scheme used by Simens is shown in diagram by using star

connected reactors (SR) in AC side [30], which is located between converter and transformer providing a low impedance path to ground for DC current.

Compare Figure 2.9 with Figure 2.8, it is found that in MMC based HVDC systems:

- The AC filters are not necessary because multilevel of voltage can create staircase waveform and reduce the harmonics. The arm current are not chopped, so small di/dt.
- The DC-link capacitor are not need because each SM has a capacitor inside. So the dc-bus current and voltage are smooth and can be controlled by converters dynamically
- Most important, the rated voltage and power can be added freely.

Therefore, MMC perfectly solve the problems of two-level VSC-HVDC system and makes it most suitable for offshore wind energy transmission system.

2.2.3 The control of VSC based HVDC system

The control of the VSC in HVDC system usually consists of a fast inner current control loop and outer control loops. The inner current control is responsible for tracking the current reference and generating the switching states for converters. The outer control loops are used to generate reference current for inner control loop

According to [9], both reactive and active power control should take place on both sending end converter and receiving end converter. Active power control can be achieved by DC voltage control, frequency control or set an active power reference; while reactive power control can be realized by AC voltage control or set a reactive power reference. As for HVDC system, DC voltage control is necessary for power balance between two terminals, thus one of the converters must have DC control and the other applies active power reference control.

Neglecting frequency control, the control diagram is shown in Figure 2.10, only one side converter is presented here, the one on the other side has more or less the same control scheme.

For VSC-HVDC application, the control system in dq frame is usually used as the d axis current control corresponds to active power control, while q axis current control corresponds to reactive power control as shown in the diagram. The park transformation is used to transfer currents and voltages from abc to dq0 frame. The transfer matrix is shown in Appendix. Besides, the phase lock loop (PLL) is used to generate angle θ for park transformation. The basic principle of PLL is to use a close loop control to force the q axis component to be zero and output grid angle θ and frequency. It is the most commonly used technique for synchronization with grid.

The detailed explanations for outer and inner control loop will be introduced in Section4.4.

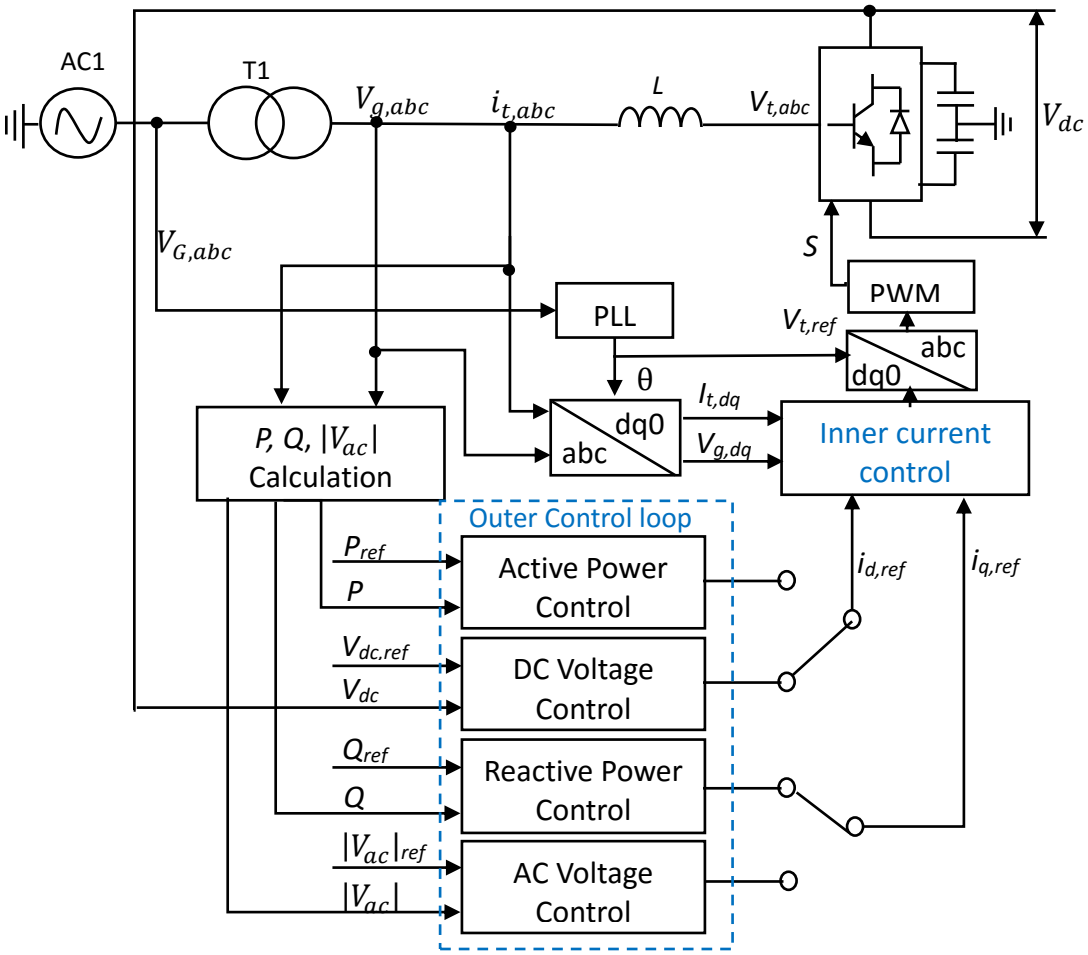

Figure 2.10 Control diagram for VSC-HVDC system

2.3 Summary and Discussions

The basic knowledge about MMC was introduced in the first part of this chapter. It began with the advantages of multilevel converters and the specific merits of MMC. Then, the basic structure of MMC was presented and operating states were explained. Furthermore, a complete mathematical model was derived, resulting both inner and outer dynamic equations.

The second part of this chapter focused on the HVDC system. The superiority of HVDC system over HVAC system was discussed. And the different topologies of HVDC system were introduced. After that, different converter technologies were compared and the advantages of MMC based HVDC system were emphasized. Finally, the general control methods for VSC-HVDC system were introduced and control diagram was shown.

Some decisions has been made for the rest of the thesis:

- The SMs adopts half bridge structure in the rest of paper.
- The mathematical model derived in this chapter will be the basic model for the

explanations of all control strategies and the same symbols for quantities will be used.

- The HVDC system uses symmetrical monopole configuration in the following chapters.
- The control of AC side current for MMC-HVDC system will base on Figure 2.10. However, AC voltage control will not be studied in this thesis as it is more or less the same as DC voltage control.

3. Current Control Algorithms for Two-Level VSC

As MMC is one type of voltage source converter, most of current control strategies for two-level VSC may be extended to control MMC. Thus, the current control algorithms for two-level VSC in the literature are reviewed in this chapter. Compared to traditional open-loop voltage PWM converter, current controlled PWM converters have the advantages as below [31]:

- Control of instantaneous current with high accuracy
- Peak current protection and overload is avoided
- Good dynamics performance
- Goode response to load parameter changes
- Compensation of the DC-link voltage and ac-side voltage change

3.1 The Basic Control diagrams

The closed loop current control system for VSC can be simply represented by Figure3.1. i_A (i_B, i_c) is measured for instantaneous output AC current of VSC; i_{Ac} (i_{Bc}, i_{cc}) is reference phase current. The functions of current controllers is to force the phase currents follow the references and generate the gate states S_A (S_B, S_C), which can decrease the current error ε_A (ε_B ε_C). Thus, current controller actually has two functions: error compensation (reducing ε_A,ε_B ε_C) and modulation (generating gate states) [32].

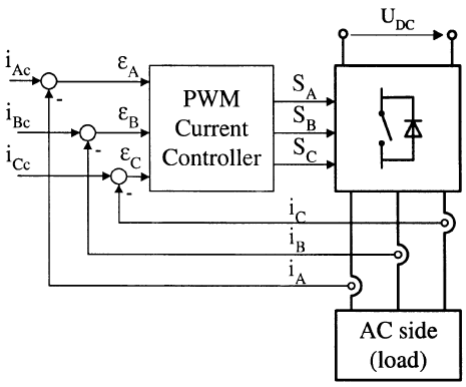

Figure 3.1 Current control system for VSC [32]

According to [31], the existing current control techniques can be classified into two main groups, linear and nonlinear controllers. Generally, linear controllers separate the error compensation and voltage modulation parts, the modulation part uses conventional voltage modulators. While nonlinear controllers do not need modulation part as shown in Figure 3.2. Linear current control algorithms includes: PI stationary and synchronous control, resonant control, state feedback control and deadbeat

control. While model predictive control and hysteresis control belongs to non-linear control. And in [31], neural networks and fuzzy logic controllers are classified into nonlinear current control even though they have modulation part, may because the inherent nonlinearity of the control algorithm. In this thesis, the same classification criteria is adopted.

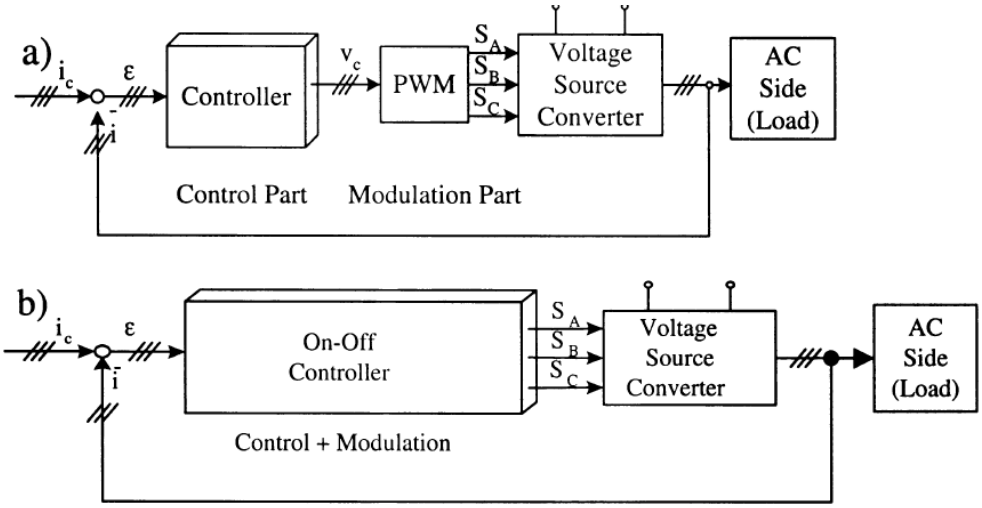

Figure 3.2 a) linear current controller b) non-linear current controller [32]

3.2 Voltage Modulation methods

Linear current control systems separate controller and modulator so that the voltage modulation methods can be used, which mainly including space vector modulation and carrier based PWM methods i.e. sinusoidal PWM modulation. These modulation methods can achieve the advantages like: constant switching frequency and low harmonic in output current.

3.2.1 Sinusoidal PWM Modulation

The sinusoidal PWM modulation is achieved by comparison a triangle carrier signal with three reference sinusoidal signals. If the reference signal is larger than carrier signal, the corresponding output gate signal will be positive, otherwise it is negative. Because of the change of pulse width and high frequency, the output voltages will be nearly sinusoidal, which are shown in Figure 3.3. V_{tri} is carrier signal and $V_{control,}$is reference voltage. The amplitudes of output voltages are decided by the modulation index m_a, which is defined by:

$$m_a = \frac{\hat{V}_{control}}{\hat{V}_{tri}} \tag{3.1}$$

The voltages in above equation are both peak values

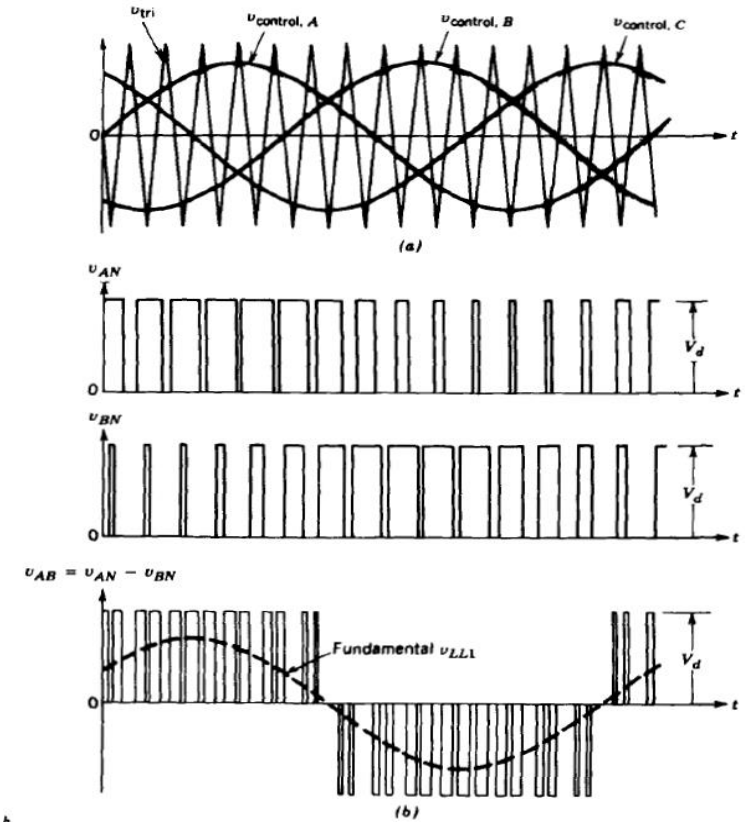

Figure 3.3 Sinusoidal PWM modulation [33]

In order to guarantee the linear relationship between input and output voltages of VSC, m_a should be less than 1. As we can see, the output frequency is defined by the frequency of carrier signal; the amplitude of output voltage is controlled by m_a and the phase of voltage can be controlled by changing the phase of control signal. Thus, by using this method, the output voltage can be fully controlled.

3.2.2 Space Vector Modulation

Space vector modulation is widely used because of its advantages like: possibility of optimal switching sequence and easy digital implementation. Unlike sinusoidal PWM modulation that there are separate modulator for each phase, space vector modulation treat three phase voltages as a space vector, which is described by its amplitude and phase angle. The equation for calculating the space vector V_s is equation (3.2) (balanced three phases): As three phase voltages inherently have 120 degree phase difference with each other, different amplitudes of phase voltages will result in different space vectors.

$$V_s(t) = \frac{2}{3}(V_a(t) + V_b(t)e^{j\frac{2\pi}{3}} + V_c(t)e^{-j\frac{2\pi}{3}}) \tag{3.2}$$

where V_j (j=a,b,c) represent the amplitudes of three phase voltages.

As for VSC, assume there will always be one and only one switch on at each phase leg. Then the phase voltage is either equal to DC voltage or zero. According to equation(3.2), three phases, 6 switches can provide 8 possible switch states including 6 active states and 2 zero states (all the three upper switches are on or all the three lower switches are on) as shown in Figure 3.4 (a). For example, vector(1,0,0) represents the upper switch is on for phase A and lower switches are on for Phase B and C, thus, the vector will have the same phase angle as phase A voltage.

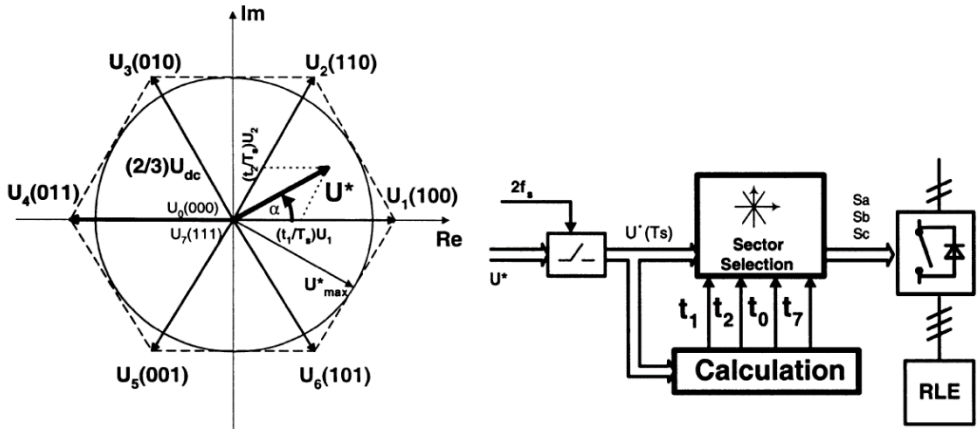

(a) (b)

Figure 3.4 (a) Space vector representation of VSC (b) block diagram of space vector modulation [32]

The reference three phase voltages are represented by U^* in Figure 3.4 (a). It can be seen that the reference vector can be obtained by switching on adjacent two vectors U_1 and U_2 for proper time t_1 and t_2 respectively. Zero states are added to adjust amplitude and also keep the switching period constant.

The block diagram of space vector modulation is shown in Figure 3.4 (b). The reference voltage is sampled at constant frequency Ts and t_1, t_2 can be calculated by angle α in Figure 3.4 (a) and the amplitude ratio between reference vector and DC voltage *M* by formula (3.3):

$$t_1 = \frac{2\sqrt{3}}{\pi} M T_s \sin(\pi/3 - \alpha)$$
$$t_2 = \frac{2\sqrt{3}}{\pi} T_s sin a \tag{3.3}$$

The residual time during one period is for zero vector assuming $t_1+t_2 \leqslant T_s$, Therefore, the two equations below should be satisfied:

$$\vec{U}^* T_s = \vec{U}_1 t_1 + \vec{U}_2 t_2 + \vec{U}_0 T_0 + \vec{U}_7 T_7$$
$$T_s = t_1 + t_2 + t_0 + t_7 \tag{3.4}$$

t_0 and t_7 can be calculated using different equations for different methods.

3.3 Linear current controller

3.3.1 Proportional-integral and Proportional-resonant controller

The proportional-integral (PI) control is the most commonly used control method for VSC because of its advantages of simplicity and robustness [34]-[39]. The integral part of PI controllers will reduce the steady state error and proportional gain are associated with ripple [31]. A proper tuned PI controller can dramatically reduce the oscillations when disturbances are presented. The simplest configuration of PI control system is stationary PI controller [34], which uses three PI controllers as error compensation on three phases respectively and produces reference voltage for sinusoidal PWM modulation part. The diagram is shown below:

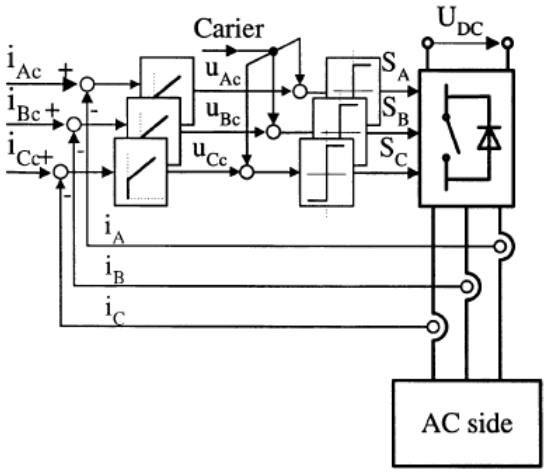

Figure 3.5 stationary PI control system for PWM [32]

The transfer function of PI controller is:

$$G(s) = K_p + \frac{K_i}{s} \tag{3.5}$$

where K_p is the proportional parameter and K_i is integral parameter

By tuning these two parameter, a good dynamic performance can be achieved. The tuning methods is presented in [35]. The sinusoidal PWM method can be replaced by space vector modulation [39].

The drawbacks of stationary PI controller is an inherent racking error on phase or amplitude. However, some applications of VSC need high accuracy. In addition, with the increasing popularity of VSC-based HVDC system, the decoupled controls of active power and reactive power for VSC are needed. In this cases, the control system based on d-q coordination are applied [35]-[37] as shown in Figure 3.6.

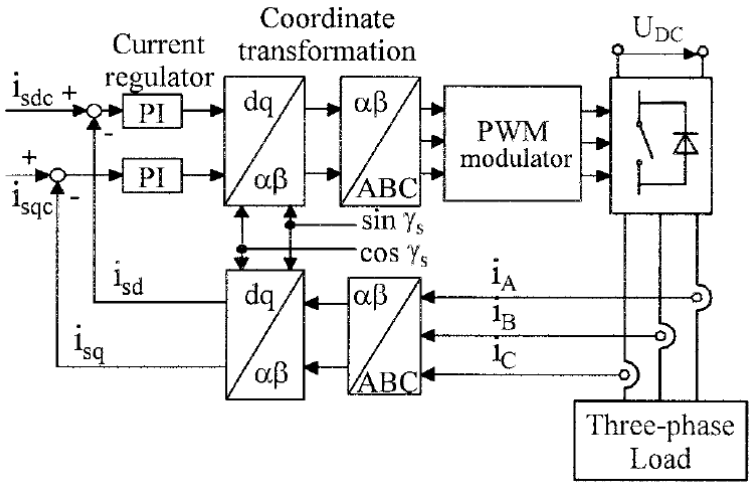

Figure 3.6 Synchronous PI control system for VSC

Transferred from a-b-c coordination to d-q coordination, the currents become DC components for balanced system. By using PI controller, high accuracy can be achieved. In addition, active power and reactive power can be controlled independently, by setting desired d-axis current and q-axis current respectively. For this method, the phase angle of current is required for abc to dq transformation and phase-locked loop (PLL) block is needed.

Proportional resonant (PR) controller is very similar to PI controller. The transfer function is shown below:

$$G(s) = K_p + K_i \frac{s}{s^2 + \omega^2} \tag{3.6}$$

where K_p is proportional gain, K_i is integral gain and ω is resonance frequency.

As we can see, compared to PI controller, PR controller has resonance part. Thus there will be a high gain at frequency ω, which gives PR some advantages over PI controller: no need for coupling or voltage feedforward and easier tuning stand, better compensation for low order harmonics [40]. But the resonance frequency of the system should be known if PR is used. One problem of PR controller is that, the frequency band where good dynamic response can be achieve is narrow around resonance frequency, if the grid frequency varies a little bit, the performance of controller will be dramatically reduced. To solve these problem, [40] uses an adaptive PR control method to adjust parameter of PR controller according to the grid frequency variation provided by PLL.

3.3.2 State Feedback Controller

The error compensator part in Figure 3.2 (a) can also use state feedback controller [41]-[44]. Which can be based on both stationary and synchronous coordinates as well. In addition, both continuous and discrete system model can be used. The simplified

control system is shown in Figure 3.7.

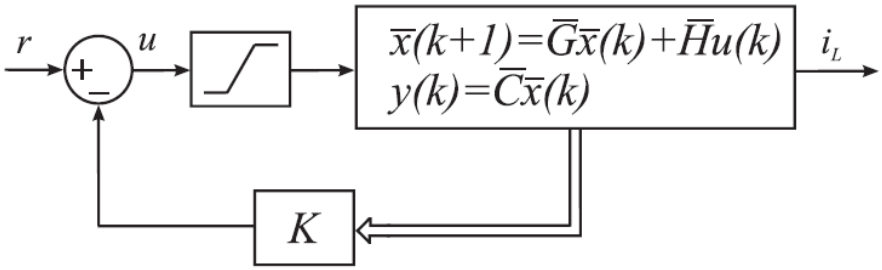

Figure 3.7 state-feedback control diagram [43]

Firstly, the linear state space model of system at operating point is derived. The standard form is shown in Figure 3.7 (discrete-time mode), where *u(k)* is the input and *x(k)* represents the state variables, *y(k)* is output, *K* is the state feedback gain vector. By adding the feedback loop, the input of system *u* becomes:

$$u(k) = r(k) - K\bar{x}(k) \tag{3.7}$$

And the state space equation become:

$$\bar{x}(k+1) = \overline{(G} - \mathrm{K}\bar{H})\bar{x} + \bar{H}r(k) \tag{3.8}$$

The performance of the system is mainly described by the characteristic equation, $\overline{(G} - \mathrm{K}\bar{H})$ and the purpose of state feedback control is to solve matrix *K* to get the desired performance. With different requirement, there will be different methods to calculate matrix *K*. The [41][43]and [44] design state vector controller based on pole placement to ensure stability and guarantee sufficient damping. [41] uses linear quadratic regulator algorithm to design the controller.

The disturbance of the system can be minimized by adding it to feedback loop. As the state space equations of the VSC based system are usually complex, the design process involves large computation of linear algebraic equations, which is one drawbacks of state feedback control. However, when state feedback control is used to control motor drives, it ensures the dynamically correct compensation for the EMF voltage. In this aspect, state feedback is better than conventional PI controllers [31]

3.3.3 Predictive Control-Deadbeat controllers

The main idea of the predictive current control is to use the model of the system and the present operating state to predict the future behavior of the controlled variables. The predicted behavior can be used to get desired performance by predefined optimization criterion. Based on different criterions, reference [45] classifies predictive control methods into four categories: Hysteresis based, trajectory based, deadbeat control and model predictive control (MPC). Hysteresis based and trajectory based predictive control aim to keep the controlled variable within a boundaries and following a predefined trajectory respectively, which has more knowledge of hysteresis

control (which will be introduced in section 3.4.2) and will not discuss here. In addition, as MPC does not need a modulation part, it is classified into non-linear controller according to section 3.1. Thus only deadbeat control is introduced in this section.

The deadbeat controller uses the model of system to calculate the required voltages once every sample period, which can make the controlled variable follow the reference value in next sample period. Then, the voltages are fed into the modulation part to generate desired switch states [45]-[48]. Thus, compared the control scheme in Figure3.6, deadbeat control scheme only replace PI controller by deadbeat controller.

To explain deadbeat control better, a normal RLE load system is used and the model of it can be described by the equation below [45]:

$$v = Ri + L\frac{di}{dt} + e \tag{3.9}$$

where *v* is the output voltage i.e. of three phase VSC, *i* is the current and *e* is grid voltage. In discrete-time model, current change rate can be written as:

$$\frac{di}{dt} \approx \frac{i(k+1) - i(k)}{T_s} \tag{3.10}$$

Assuming T_s is the sampling time. jn

Combing (3.9) and (3.10), the reference voltage for modulation part can be get:

$$V^*(k) = \left(\mathrm{R} + \frac{\mathrm{L}}{T_s}\right) i^*(k+1) - \frac{L}{T_s} i(k) + e(k) \tag{3.11}$$

where $i^*(k+1)$ is the reference current and $i(k)$ is the measured current.

As we can see, the algorithm can force the controlled variables to desired value in one sample period, it can achieve fast dynamic response and the complexity is small. As modulation part is used, the switching pattern is good and harmonics are small.

3.4 Nonlinear current controllers

3.4.1 Model Predictive Control

Unlike deadbeat control, MPC uses a cost function to represent the desired behavior and the optimal actuation is achieved by minimizing the cost function [49-52]. According to [45], MPC can be further classified into continuous control set and finite control set. Considering the discrete nature, the optimization process only takes into account the finite switching states in this thesis, thus only finite control set model predictive control (FCS-MPC) method is studied in the rest of the thesis. The diagram of FCS-MPC system is shown in Figure 3.8.

In the diagram, the predictive model is used to calculate predicted quantities one step forward based on the measured quantities and dynamic model of system. For example,

the same RLE model in section 3.3.3, the predictive current can be calculated by equation 3.11 but voltage is known quantity and current is the calculated one.

The cost function is defined by the desired behavior. For example, if the output current is desired to follow the reference value, then the cost function can be defined as [49]:

$$g = |i^*(k+1) - i(k+1)| \tag{3.12}$$

where $i^*(k+1)$ is the reference current and $i(k+1)$ is the predicted current.

The purpose of the controller is to minimize the cost function, which can be achieved by evaluating all the possible switching states and choosing the one, resulting in minimum value of cost function. As for 2-level VSC, there are total 8 switch states as discussed in space vector modulation part (section 3.2.2), so 8 possible situations are compared.

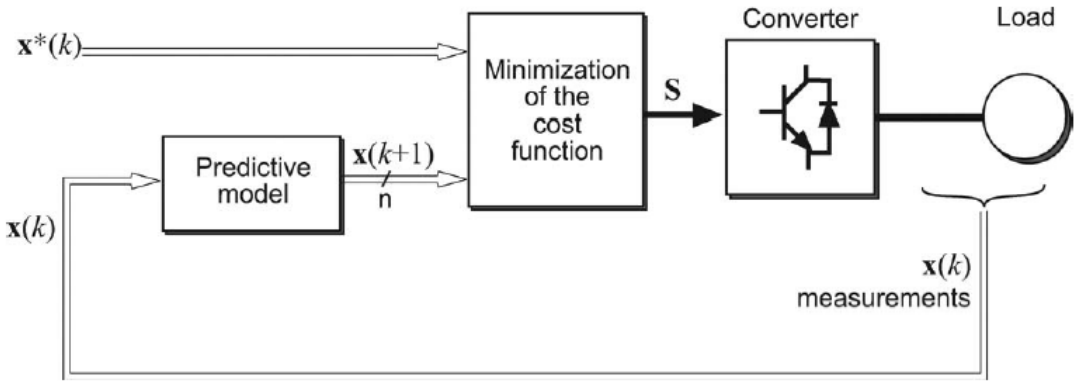

Figure 3.8 The diagram of MPC system [45]

One of the advantage of MPC is that the cost function can include more than one desired behavior, thus more variables can be controlled at the same time. Which is attractive as most applications have more than one requirement. In [52], the voltage balancing and switching reduction requirements are added to the cost function besides the current error as shown below:

$$g = |i^*(k+1) - i(k+1)| + \lambda_1 |V_{dc1} - V_{dc2}| + \lambda_2 N_s \tag{3.13}$$

where V_{dc1} and V_{dc2} are dc link capacitor and N_s is number of the commutations need. λ_1 and λ_2 are weight factor in order to deal with the different unit and magnitude of the controlled variables. They can be used to adjust the importance of each variables.

As we can see, the modulation part is eliminated in MPC system, and optimal switching state is applied during each sample period, which makes the switching frequency variable. In addition, for every period, the cost function needs to be calculated at each switch state, which increase the computation effort and time. Reference [50] proposed a switching reducing method that allows only one switching transition at maximum at each period, so only four neighbor switch states are considered for 2-level VSC each period, which reduce the switching frequency and the computation effort.

3.4.2 Hysteresis current control

The Hysteresis current control uses two-level hysteresis comparators on each phase as the combination of error compensator and modulation part, the diagram is shown in Figure 3.9. The waveform of one phase current is shown in Figure 3.10. As we can see, the hysteresis controller will force the current in a tolerance band around reference current. As for one phase of VSC, when the upper switch of leg is on, the output voltage is positive, current in inductor will increase, while the lower switch is on, output current will decrease. Therefore, the switching state is decided by the manner that when current reach lower band, upper leg switch is on to increase the current; when upper band is reached, lower switch is on to reduce the current.

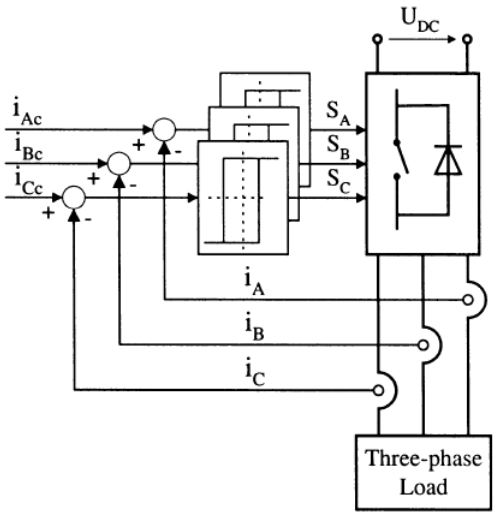

Figure 3.9 Hysteresis current control diagram [31]

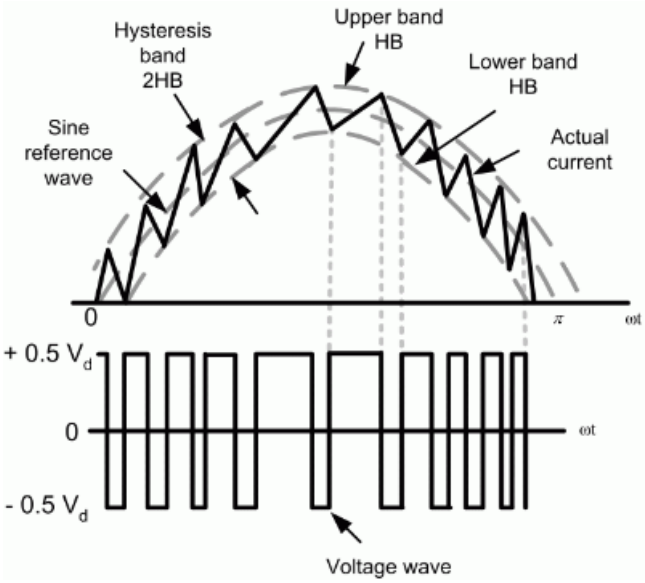

Figure 3.10 The output current waveform of hysteresis current [31]

The hysteresis current control has many advantage, such as Simplicity, outstanding

robustness, lack of tracking error, independent of system characteristics and load parameter change. However, the main disadvantage of this method is that the switching frequency is variable, which may be undesired for some application.

One method to reduce the switch frequency is using a sampling and hold (S&H) block [31], which can keep the switch state for a sample period, so that the switching frequency is limited by the sampling frequency. Some papers have proposed method to get constant switching frequency by varying tolerance band amplitude [53][54], which shows that the tolerance band *h* and switching period *T* has the relationship as blew:

$$T = \frac{4hL}{E(1-(2V^*/E)^2)} \tag{3.14}$$

where *E* is the DC voltage, V^* is the reference voltage. In order to keep *T* constant, *h* should be varied with reference voltage.

Another problem of the control system shown in Figure 3.9 is that the instantaneous error can reach double value of the hysteresis band because of the interaction between three phases [55]. One way to avoid the influence between three phases is to treat the three phase as a whole using space vector based control method [56][57]. Reference [56] introduce the method based on both $\alpha\beta$ plane and dq plane. Two hysteresis comparators are used in two directions, each combination of the outputs of two directions corresponds to one switch state, which can minimize the error between reference value and measured values. Normally, the output values of hysteresis comparators are fed into a switching table to generator the switch states. The method based on dq coordinator in [57] has divided rotating plane into 24 sections, each one corresponds to one switch state, which make control system has a fast dynamic responds.

A good switching table can reduce the switching frequency. Reference [57] uses a three level hysteresis comparator and designing the switching table in the manner that only on step changes in voltage to get desired value very time, thus, only adjacent voltage states are chosen. Simulation verified that these algorithms can considerably decrease the switching frequency.

The hysteresis control method can be combined with predictive control method. The main idea can be shown by Figure 3. 11.

The error boundary is decided by the reference current i_s^* as shown in Figure 3.11. When current reaches the boundary, the next step is determined by the prediction and optimization. The change direction of current for each switch state is predicted based on the mathematical model of system, which has been introduced in section 3.3.3. The time interval that the current reaching error boundary again for each switch state is predicted as well. The one results maximum time is chosen, which corresponds to the minimum switching frequency.

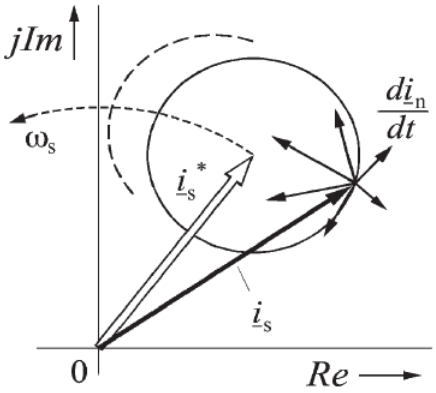

Figure 3.2 hysteresis based predictive current control [45]

3.4.3 Fuzzy Logic Current Controller

Fuzzy logic current control is another replacement for traditional PI control. The advantages of Fuzzy logic can be summarized as [58]-[61]:

- Do not need precise mathematical model, so well suited for nonlinear, time-variant system.
- Can cope with the nonlinear properties of system
- Fuzzy logic is flexible and tolerant of imprecise data
- Can control multi-input, multi-output system

The control diagram is shown below:

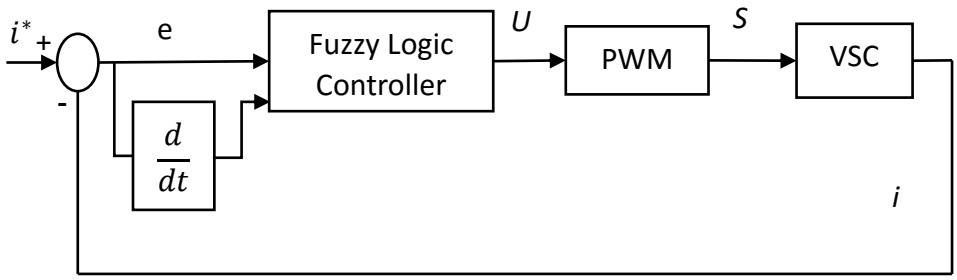

Figure 3.3 Control diagram of fuzzy logic control

The inputs of the fuzzy logic controller are typically the error e and the derivative of the error. The output is the reference voltage for PWM modulation block. The basic configuration of the fuzzy logic controller is shown in figure 3.13 [58].

It mainly consists of three parts: fuzzyfication, fuzzy inference and defuzzyfication. The fuzzyficaiton parts converts input data to suitable linguistic values, which are defined by fuzzy set, such as negative small (NS), positive big (PB). The membership function as the example in Figure 3.14 is a curve that defined how the value of fuzzy set in a certain region are mapped to a membership value. The membership function sharp is

usually triangular, other sharps can also be used. The second part consists of the control rules, which simulate human thinking to generator linguistic values of output variables. The third part defuzzyfication is the reverse of fuzzyficaiton, to transfer linguistic values to the concrete data based on membership function.

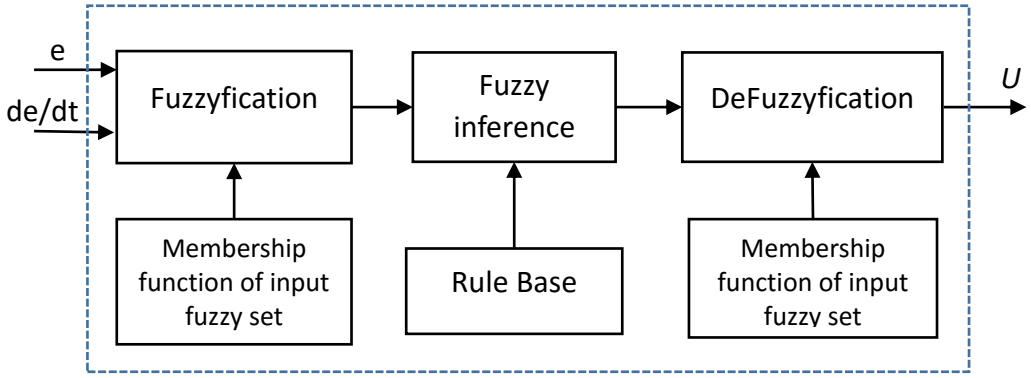

Figure 3.4 The configuration of fuzzy logic controller

The membership function and the control role are derived based on the knowledge of system and experience. The number of fuzzy set is not fixed and depends on the sensitivity needed.

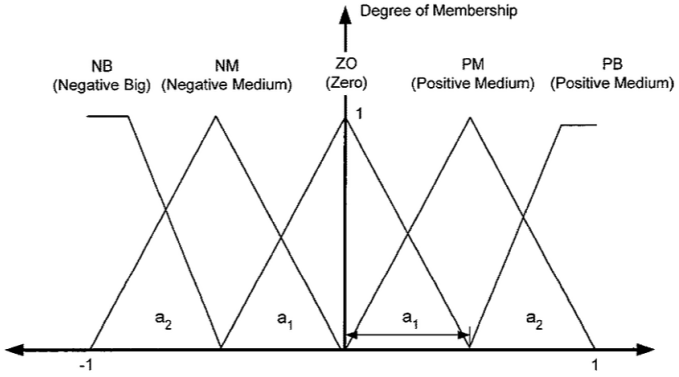

Figure 3.5 An example of membership function.

Taking Reference [59] as an example, this paper presents a fuzzy logic control algorithm for three phase voltage source inverter. The input variables of fuzzy logic controller are current error and the variation of current error. Output variable is reference voltage *V*. For all input and output variables, 7 fuzzy sets are used: negative big (NB), negative medium (NM), negative small (NS), zero (ZR), positive small (PS) positive medium (PM) and positive big (PB). The control rules are generated:

- If both the error and change of error are NB or NM, the control is set to NB to reduce both error and change of error fast.
- If both the error and change of error are PB or PM, the control is set to PB

- If both error and change of error are ZR the control is set to ZR.

In this way, the control table can be generated, there are total 49 control rules for two input variables. Using these rules, the output can be connected with inputs. For example, if the error value is in the common region of NB and NM according to membership function and change of error is in common region of PB and PM, then four situations need to be concerned: 1) error is NB, change of error is PB; 2) error is NB, change of error is PM; 3) error is NM, change of error is PB; 4) error is NB, change of error is PM and each situation corresponds a output fuzzy set. Then implication step should be taken, which is used to evaluate the consequence of a rule, which is defined by degree of fulfillment (DOF). Thus, DOF of four situations need to be calculated by using 'min' operator as shown below:

$$\mu_B(y_q) = min\{\mu_q(e), \mu_q(\Delta e)\} \tag{3.15}$$

where $\mu_q(e), \mu_q(\Delta e)$ are fuzzy set values of two input variable in qth situation.

The defuzzyfication can be achieved by using center of gravity (COG) method, which is defined by the equation below:

$$\mathrm{cog(B)} = (\sum_{q=1}^{Nq} \mu_B(y_q) y_q)/(\sum_{q=1}^{Nq} \mu_B(y_q)) \tag{3.16}$$

Where Nq is the number of situations, B represents the output B. The point y_q is the qth situation of the product space y of the output universe. cog(B) is the output concrete value.

The input and output of fuzzy controller can be changed depending on the control system. In [58] and [60], the outputs of fuzzy controller are integral and proportional parameters for PI controller. [61] uses fuzzy controller to optimize the trade-off between current overshoot and phase delay.

3.4.4 Advanced Nonlinear Current control in Recent Decade

The nonlinear control methods introduced above is not based on system mathematical model. The linear control methods are designed based on the eliminating of the nonlinearities of the system. If there are some uncertainties in the system i.e. some parameter is not constant, the linear control methods will cause a constant error when operation point is shifted [62]. Therefore, for better tracking and regulating state set point, reducing the sensitivity to the system parameters and good stability and transients, many nonlinear control methods based on nonlinear mathematical model of VSC has been proposed in recent decade, especially for HVDC system. An adaptive backstepping method has been proposed in [62] to compensation for the uncertainties given by change of parameters like line impedances in HVDC system. Sliding mode control (SMC) methods are another nonlinear control methods to compensate the

uncertainties. The design of SMC involves finding a sliding surface that the system states are forced towards the surface and stay on it. The tracking error will converge to 0 on the surface. In [63], a SMC algorithm for VSC-HVDC system is proposed based one Lyapunove direct method. The nonlinear mathematical model is derived and independent control of active and reactive power, stabilization of DC voltage are achieved. In addition, second order SMC is designed to avoid the chattering problem. Input–output linearization with sliding mode control is shown in [64]. [65] proposes an optimal control method based on bilinear state-space model for HVDC system.

3.5 Summary and Discussions

In this chapter, most of current control strategies for two-level VSC in the literature were reviewed. The principle of each method was explained and necessary control diagrams were illustrated. In addition, the advantages and disadvantages of some methods were pointed out and corresponding solutions to avoid disadvantages were proposed. All the reviewed control methods were classified into two groups, linear current control and nonlinear current control. They are summarized below:

- Linear current controller
  - Based on PI controller or PR controller
  - State feedback controller
  - Deadbeat controller
- Non-linear current controller
  - Model Predictive control
  - Hysteresis current control
  - Fuzzy logic control

Some of the strategies are extended to control AC side current of MMC in HVDC system, which will be reviewed in the next chapter.

4. Current Control Algorithms for MMC

In this Chapter, The current control algorithms for MMC in literature are reviewed. Some control methods for 2-level VSC introduced above can be extended to control MMC, but the complexity increase with the increase of number of voltage levels. In addition, MMC has some new control challenges, of which two main problems are SM capacitor voltage balancing and circulating current eliminating. In sections below, different modulation methods, capacitor voltage balancing methods, circulating current eliminating methods and AC side current control methods for MMC will be introduced in detail separately.

4. 1 Modulation Methods

There are three main modulation methods for MMC: PWM modulation, space vector modulation and nearest level modulation.

4.1.1 PWM modulation

The basic principles of PWM modulation for MMC is the same as that for 2-level VSC by comparing the reference waveform with high frequency triangular carrier waveform to generator the switch states. However, the number of carrier waveforms increases as the number of voltage levels increases. In 2-level VSC, there are two switches in one phase leg corresponding to two-level phase voltage and one carrier waveform is needed as upper and lower switch can be controlled together with opposite switch states. For MMC, there are 2*N* SMs in one phase leg corresponding to *N*+1 phase voltage levels, thus, *N* carrier waveforms is need. As the number of total inserted SMs on one leg is *N*, each carrier waveforms will control two SMs (one in upper arm and one in lower arm) with opposite switching states. There are two main PWM techniques by using one single reference waveform: Carrier-disposition PWM (CD-PWM) and Carrier phase shifted PWM (CPS-PWM) (also called subharmonic techniques) [19][66].

A) CD-PWM. The *N* carrier waveforms have same amplitude and frequency. They are displaced symmetrically with respect to zero axis. Each carrier will be compared with the single sinusoidal reference waveform and produce the desired phase voltage level. The resulted switching state is used to control a particular upper SM (and its corresponding lower SM). Thus, independent SM modulation is achieved. According to the phase shift among carrier waveforms, CD-PWM can be further classified into phase disposition (PD), phase opposition disposition (POD) and alternate phase opposition disposition (APOD) [19], the waveforms are shown in Figure 4.1.

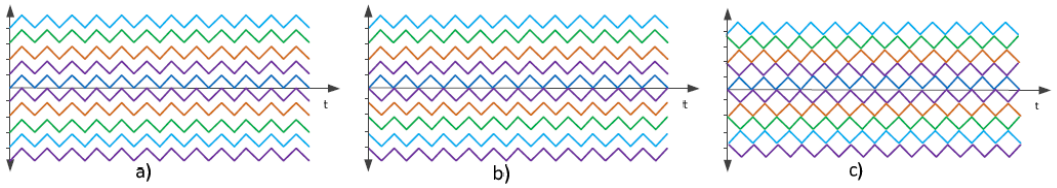

Figure 4.1 carrier displacement PWM methods a) PD, b) POD, c) APOD [19]

One disadvantage of this method is that there is voltage variation for SM capacitors. So these methods should be used together with voltage balancing methods. For better using of balancing method, some modification has been made for CD-PWM method in [67] [68]. These two papers using different voltage balancing methods (which will be discussed later on) but use the same modulation methods base on PD-PWM. Instead of getting voltage transitions to control particular SM, the technique in [67] compares reference waveform and carriers to get the voltage levels, then determine the number of SMs to be inserted/bypassed in the upper and lower arms. The waveform in shown in Figure 4.2 and the output AC voltage and its corresponded number of inserted SM is shown in table 4.1. In [67] N=6 and DC side voltage is V_{dc} and it is middle grounded.

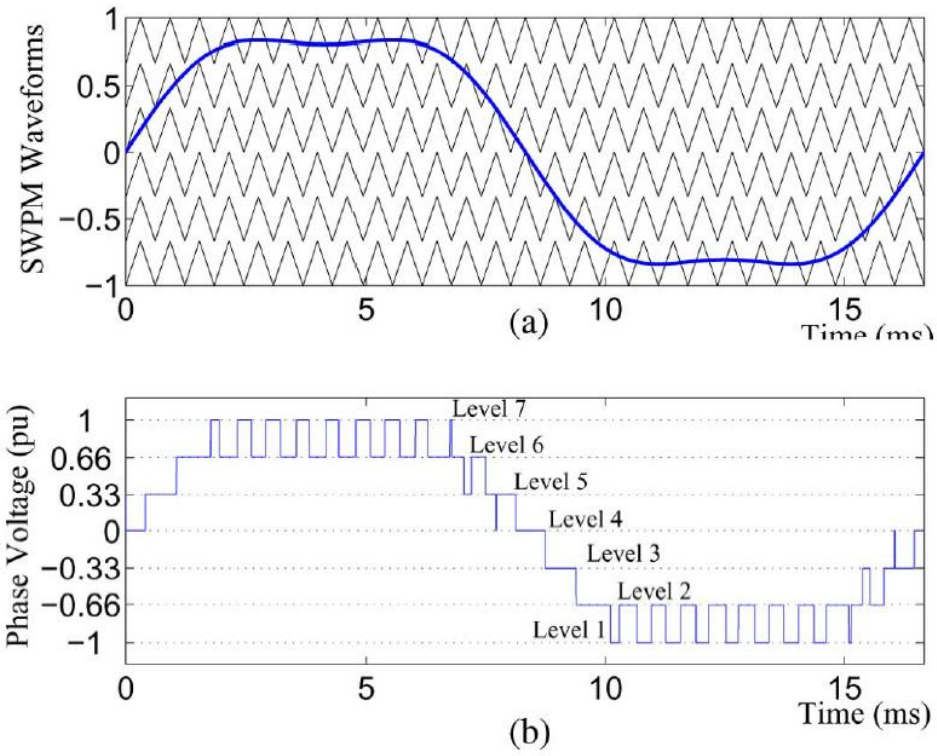

Figure 4.2 PD-PWM method of MMC (a) carrier and reference waveforms (b) voltage levels [67]

Table 4.1 The number of inserted SMs and corresponding Voltage level

Voltage Level	AC side phase voltage	$n_{u,j}$	$n_{l,j}$
1	$-V_{dc}/2$	6	0
2	$-V_{dc}/3$	5	1
3	$-V_{dc}/6$	4	2
4	0	3	3
5	$V_{dc}/6$	2	3
6	$V_{dc}/3$	1	5
7	$V_{dc}/2$	0	6

n_u and n_l are the number of SMs inserted in the upper and lower arm respectively.

In this strategy, only the number of inserted SMs is concerned, so the traditional sorting voltage balancing method can be used to decide which SMs should be inserted.

As the sum of voltage on upper and lower arm is equal to DC voltage and assuming the SM capacitors are balanced, the number of inserted SMs can be calculated by reference voltage at different levels by the formula below:

$$n_{u,j} = N\left(\frac{1}{2} - \frac{V_{ref}}{V_{dc}}\right)$$
$$n_{l,j} = N\left(\frac{1}{2} + \frac{V_{ref}}{V_{dc}}\right) \quad (4.1)$$

which extended the method to N+1 voltage levels. In the simulation part of this thesis, this method is used to combine the PWM with sorting method for voltage balancing.

B) CPS-PWM. The number of carriers are also *N* corresponding to *N*+1 voltage levels and all the carriers should have the same amplitude and frequency. The difference with CD-PWM is that the carriers have phase shift with each other, which is 360˚/*N*. The shape of carrier waveforms could be triangular or sawtooth. They are shown in Figure 4.3.

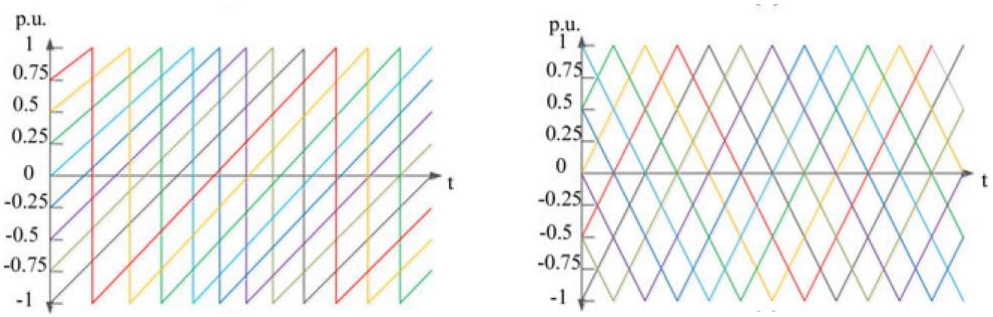

Figure 4.3 The sawtooth and triangular carriers of CPS-PWM method [19]

The further difference between CD-PWM and CPS-PWM are not studied in this thesis and in simulation part, the CPS-PWM method are chosen.

The methods above are based on single reference waveform, in [69], the reference voltage for each SM has been derived and each SM has its own controller, which

compares the reference waveforms with carrier, thus multi-reference waveforms are used. The choosing of carriers for SMs is based on CPS-PWM method: carriers have a phase difference with each other.

4.1.2 Nearest Level Modulation (NLM)

This method is not based on the carrier waveforms. Its main idea is to choose the voltage levels, which is nearest to reference values, for MMC. As a result, the numbers of inserted SMs in upper and lower arms are calculated by using formula (4.1). However, as the reference voltages are usually between two voltage levels, so the results by using (4.1) need to be rounded to get the nearest level. Thus, it is similar to the method used in paper [67] introduced above, but without PWM between two voltage levels. This will bring some error especially the number of voltage level is not big. To compensate this error, one SM can be controlled by using PWM method, the reference voltage amplitude for PWM is equal to the difference of chosen voltage level and reference value. In this way, this method is almost the same as that used in [67].

This method can be used for MMC with a high number of voltage level because the switching frequency can be reduced (fundamental switching frequency can be achieved), thus low losses. In addition, as the resolution is increased, the errors between voltage level value and reference are reduced.

4.1.3 Space Vector Modulation

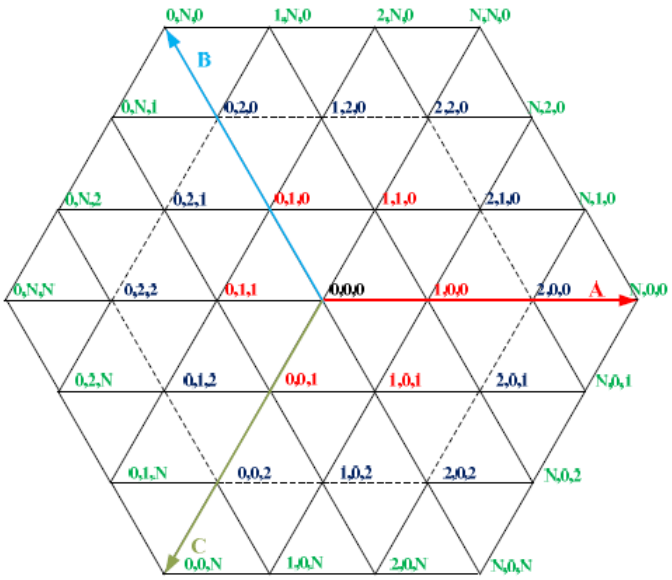

Figure 4.4 The switch states of space vector modulation with *N* levels

The space vector modulation for VSC can be extended for MMC. For a MMC with *N* SMs per arm, the number of space vectors is equal to $(N+1)^3$ [25]. So that the switching state diagram is expanded as shown in Figure 4.4. The number of space vector on each

phase represents the voltage level. For example, (4, 2, 0) represents at phase A, voltage is at 5th level, phase B voltage is at 3rd level, phase C is at 1st level. To realize this vector, the formula (4.1) can be used to calculate the number of inserted SMs on each phase.

Each reference voltage needs to be normalized on each phase and transferred to space vector diagram in Figure 4.4. Similar to two level modulation method, the reference vector can be achieved by operating the nearest three space vectors, $\vec{V}_1\ \vec{V}_2\ \vec{V}_3$ (The vectors pointing to the three vertices of the triangle where reference vector is) for proper time respectively during one sample period to satisfy the equations below:

$$\begin{aligned} \vec{V}^* T_s &= \vec{V}_1 t_1 + \vec{V}_2 t_2 + \vec{V}_3 t_3 \\ T_s &= t_1 + t_2 + t_3 \end{aligned} \tag{4.2}$$

4.2 Voltage Balancing Algorithms

4.2.1 Sorting Method

The sorting method is the most widely used for SM capacitor voltage balancing control[19]. Normally, the number of SMs to be inserted or bypassed is known after modulation. Sorting method is used to decide which SMs should be inserted or bypassed to balance the capacitor voltages. The capacitor voltages of all SMs are measured and sorted and the algorithm can be concluded as [70]:

- If the arm current is positive, SMs with the lowest voltages are inserted so that the capacitors are charged and their voltages increase
- If the arm current is negative, SMs with the highest voltages are inserted so that the capacitors are discharged and their voltages decrease

If the SMs are bypassed, the voltages will not change. In this way, the capacitor voltages are kept balanced relatively. This algorithm is simple and can be used for MMCs operating at all conditions. However, there is a main disadvantage that the switching frequency will increase. Even if the operating condition is not changed, the switching of SMs may occur, which increase the losses. There are many methods proposed to reduce the switching frequency, they are based on:

A) sorting limited SMs [20]. In this technique, If additional SMs need to be inserted compared to last control period, only the SMs, which is bypassed during last control period, are sorted and the SMs with lowest voltage are inserted if current is positive, otherwise, the SMs with highest voltage are inserted; If additional SMs need to be bypassed compared to last control period, then only the SMs, which is inserted during last control period, are sorted. The principle of selection of SMs are the same as above. Therefore, there will be no unnecessary switching transitions and the switching frequency is effectively reduced, however, it sacrifices the effect of balancing voltages.

B) a hybrid strategy combining predictive method and sorting method [71]. Considering a tolerant range for voltage ripple in SM capacitors, the sorting method may be not necessary to be applied in every period. Therefore, a simple method could be applied that reduce the sorting frequency but keep the modulation frequency unchanged, this will avoid unnecessary voltage transitions and reduce the frequency. However, this method need to make tradeoff between switching frequency and ripple amplitude. For more accurate control, a hybrid strategy is applied by setting a limit ripple value, ΔV. The main idea is:

- Calculating the voltage differences between SM capacitor voltages and the reference voltage, if the maximum voltage difference is larger than predefined value ΔV, which define the maximum allowable ripple, the conventional voltage sorting method is used.
- If all the voltage difference is less than ΔV, a predictive method is used.

The predictive method is used to predict the voltage error between SM capacitor voltages and reference voltage one step forward and choose the SMs, which result in minimum voltage error, to insert. The predicted capacitor voltages can be calculated by the formula below:

$$V_{c,j}(t + T_s) = V_{c,j}(t) + \frac{i_{k,j}}{C} T_s \tag{4.3}$$

where $i_{k,j}$ is arm current, C is SM capacitor and T_s is the control period. The voltage errors are calculated by:

$$e_j = \left| V_{c,j}(t + T_s) - V_{ref} \right| \tag{4.4}$$

where V_{ref} is the reference SM capacitor voltage.

Using these method, some of SMs may not be switched for a few cycle [72], so that the switching frequency is reduced.

C) Fundamental frequency strategy [72]. If NLM is used and the reference voltage is sinusoidal, there is only 2N switching transitions, so fundamental frequency for each SM. However, if voltage balancing method based on sorting is used, the switching frequency will be increased by the 'unnecessary switching'. For example, if N/2 SMs are inserted on upper arm of MMC and the number of inserted SMs on upper arm is still N/2 in next control period, there should be no switching occur for NLM, however, the sorting algorithm may turn some inserted SMs off and turn some bypassed SMs on, which will cause additional switching transitions. This situation will not happen if all the SMs on the upper arms are on or all of them are off. Therefore, this fundamental frequency strategy only sorts the SM voltages when all the SMs on the upper arms are on or off, at other time, the sorting index list are kept unchanged.

D) strategy that the SM voltages are adjusted before sorting [72]. In this method, a maintaining factor is used and the limit of voltage ripple is set. The algorithm is:

- If the arm current is positive, the SMs with lowest voltage should be inserted. So the capacitor voltages of the SMs at OFF state, whose voltages are above the lower voltage limit are multiplied by a maintaining factor, which is higher than 1, to increase their possibility to stay at OFF state in next period. In addition, the voltages of the SMs at ON state are also multiplied by a maintaining factor (larger than 1) to increase their possibility to stay at ON state.
- If the arm current is negative, the SMs with highest voltage should be inserted. So the capacitor voltages of the SMs at OFF state, whose voltages exceed the upper limit, as well as the SMs at ON state are multiplied by a maintaining factor, so that their possibilities to be inserted are increased.

This method is actually based on the idea that try to control the SMs to stay at their original states and only change the states of SMs that the most need to.

D) predictive algorithm [73]. In this algorithm, the inserted or bypassed SMs are decided by comparing the predicted capacitor voltages and reference voltage. Both of predicted capacitor voltages and reference voltage are based on the predicted total transferred charge. The main steps are:

1. The total amount of charge transferred to SMs during two zero crossing points of arm current is predicted
2. The reference voltage is calculated assuming that the total charge predicted in step 1 is evenly distributed among all the SMs
3. Assume a pulse pattern and predict the capacitor voltages of each SMs if the assumed pulse pattern is used.
4. Compare the reference voltage and predicted voltage to insert or bypass SMs. Basically, if the current is positive, only insert the SMs whose predicted voltage is lower than reference value and if current is negative, only inert the SMs whose predicted voltage is higher than reference value.

As classified by the reference voltage, only a part of SMs is sorted and switched, therefore, the switching frequency is reduced.

4.2.2 Method Based on Carrier Rotation

In [74], a voltage balancing method based on CPS-PWM method is proposed. As for CPS-PWM method, *N* carriers can produce *N* pulse sequence with different phase angle. In this method, the pulses are not assigned to control random SMs. The selection of pulse sequences for particular SMs can be varied to achieve voltage balancing. The current and capacitor voltages after CPS modulation are analyzed first in [74] and the conclusion is made that the SM with the pulse whose middle point is close to $\pi/2$ could absorb more power, thus its voltage tends to be higher. The further from $\pi/2$ the SM with pulse whose middle point is, the less power it can get. Based on this conclusion, the pulse sequences can be assigned by the algorithm below:

- If current is positive, the pulse sequences whose middle point is the closest to $\pi/2$ are assigned to the SMs with lowest capacitor voltages.
- If current is negative, the pulse sequences whose middle point is the closest to $\pi/2$ are assigned to the SMs with highest capacitor voltages.

So the SM capacitor voltages need to be measured and sorted. This method is more complex than traditional sorting method, but it provides another way to combine PWM with sorting method.

4.2.3 Methods Based on Averaging and Balancing control

In [69], the voltage balancing is achieved by using close-loop controller on each SM. In addition, the control algorithm is divided into averaging control and balancing control.

The MMC used in [69] has 8 SMs per phase. The averaging control is used to force the average capacitor voltage of all SMs per leg to follow the reference value $\bar{V}_{c,j}^{*}$. The average voltage is calculated by:

$$\bar{V}_{c,j} = \frac{1}{8}\sum_{x=1}^{8} V_{c,j}(x) \tag{4.5}$$

where $V_{c,j}(x)$ is the xth SM on the phase j

Two PI controllers are used to get the average control command $V_{A,j}^{*}$ as shown in Figure 4.5(a). The circulating current is defined by equation (4.6), so in this paper, the circulating current contains DC components compared to equation (2.6):

$$i_{diff,j} = \frac{1}{2}(i_{u,j} + i_{l,j}) \tag{4.6}$$

where $i_{u,j}$ and $i_{l,j}$ are upper arm current and lower arm current of phase j respectively. The first PI controller can be explained that if reference average voltage is higher than measured values, circulating current will increase to charge the inserted SMs and average voltage increases. As circulating current is affected by SM capacitor voltages, the second PI controller is used to force the circulating current to follow the reference value so that to minimize the error of average voltage.

The balancing control aims to force the individual SM capacitor voltage to follow the reference value V_{c}^{*}, as shown in Figure 4.5 (b). The command voltages are $V_{B,j}^{*}(i)$, which have linear relationship with error between reference value and measured value. In addition, the command balancing voltage is affected by current direction. When current is positive, a positive voltage should be added to the SM capacitor, when current is negative, a negative voltage is added to produce positive power for the SM.

After both average command voltage and balance command voltage are obtained, the reference voltage for each SM can be derived:

$$V_{c,j}^*(x) = V_{A,j}^* + V_{B,j}^*(i) - \frac{V_{t,j}^*}{4} + \frac{V_{dc}}{8} \ (x: 1-4)$$
$$V_{c,j}^*(x) = V_{A,j}^* + V_{B,j}^*(i) + \frac{V_{t,j}^*}{4} + \frac{V_{dc}}{8} \ (x: 5-8) \quad (4.7)$$

where $V_{t,j}^*$ is the ac side voltage reference for phase *j*. Now the modulation part can be used to generator the switch state for each SMs.

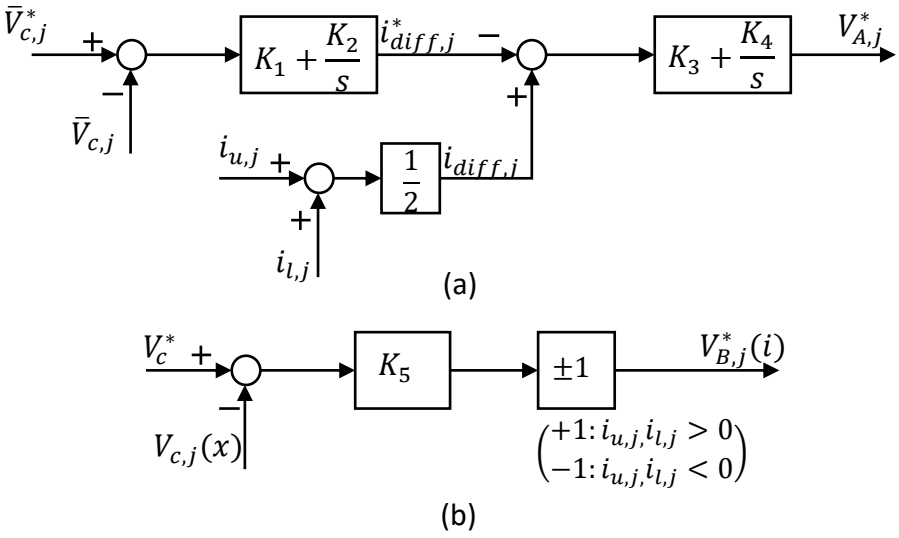

Figure 4.5 Voltage balancing control diagram (a) averaging (b) balancing control [69]

4.2.4 Method Based on Model Predictive Control Method

In Paper [75], a model predictive control method is proposed to control AC side current, voltage balancing and circulating current at the same time by using a single cost function. The SM capacitor voltage is predicted by the formula below:

$$V_{c,j}(t + T_s) = V_{c,j}(t) + S\frac{i_{k,j}}{C}T_s \quad (4.8)$$

S=1: switched-on SM
S=0: switched-off SM

where $i_{k,j}$ is the arm current, T_s is the sampling period, C is the capacitor value. The voltage balancing part of cost function is shown below:

$$\mathrm{J} = \lambda\left(\sum_x \left|V_{c,j}(t + T_s) - \frac{V_{dc}}{N}\right|\right) \quad (4.9)$$

where λ is the weighting factor and the expression in the brackets is the sum of capacitor voltage errors of all SMs. Minimizing cost function will reduce the voltage error and voltage balance can be achieved.

4.3 Circulating Current Suppressing Algorithms

4.3.1 Methods Based on Energy Control

In paper [76], a method based on total energy control and energy balancing control between upper and lower arms is proposed. According to [76], by analyzing the model of MMC, the equations below can be derived:

$$i_{u,j} = -\frac{i_j}{2} + i_{diff,j} \tag{4.10}$$

$$i_{l,j} = \frac{i_j}{2} + i_{diff.j} \tag{4.11}$$

which is the same as equation (2.4),(2.5), i_{diff} here represents circulating current with both DC component and AC component.

The voltages has the relationships below:

$$V_{u,j} = \frac{V_{dc}}{2} - V_{t.j} - V_{diff,j} \tag{4.12}$$

$$V_{l,j} = \frac{V_{dc}}{2} + V_{t,j} - V_{diff,j} \tag{4.13}$$

In this paper, the SMs on the upper and lower arms are treated as voltage sources and their voltages are $V_{u,j}$ and $V_{l,j}$ in the above equations. $V_{t.j}$ is the AC side phase voltage and V_{diff} is the difference voltage, which has the relationship with circulating current as below:

$$L_{arm}\frac{di_{diff,j}}{dt} + R_{arm}i_{diff,j} = V_{diff,j} \tag{4.14}$$

Based on these equations, the derivative of energy in upper and lower arms can be derived:

$$\frac{dW_{u,j}^{\Sigma}}{dt} = i_{u,j}V_{u,j} = (-\frac{i_j}{2} + i_{diff,j})(\frac{V_{dc}}{2} - V_{t.j} - V_{diff,j}) \tag{4.15}$$

$$\frac{dW_{l,j}^{\Sigma}}{dt} = i_{l,j}V_{l,j} = (\frac{i_j}{2} + i_{diff,j})(\frac{V_{dc}}{2} + V_{t,j} - V_{diff,j}) \tag{4.16}$$

where $W_{u,j}^{\Sigma}$ and $W_{l,j}^{\Sigma}$ are the total energy of upper and lower arm respectively. So the derivative of total energy per phase W_j^{Σ} and the energy difference of upper and lower arms W_j^{Δ} are:

$$\frac{dW_j^{\Sigma}}{dt} = (V_{dc} - 2V_{diff,j})i_{diff,j} + V_{t,j}i_j \tag{4.17}$$

$$\frac{dW_j^{\Delta}}{dt} = -2V_{t,j}i_{diff,j} - (\frac{V_{dc}}{2} - V_{diff,j})i_j \tag{4.18}$$

As we can see from (4.17), the derivative of total energy is highly dependent on the circulating current. The production of DC part of circulating current and DC voltage balances the power between DC side and AC side, also compensates for the losses on the inductor and resistor on each arm. However, the DC part of $i_{diff,j}$ has no relation with derivative of energy difference between two arms according to equation (4.18). As there are no DC component in $V_{t,j}$ and i_j. However, the fundamental part of the circulating current will affect the voltage balance, the $V_{t,j} \times i_{diff,j}$ will result in a DC component and break the balance. Therefore, the purposes of control circulating current is to control the DC component to get the desired energy transfer and try to eliminate the AC component of circulating current. Therefore, two control loops are needed: total energy control loop and energy balancing loop. The control diagram in paper [76] is shown below:

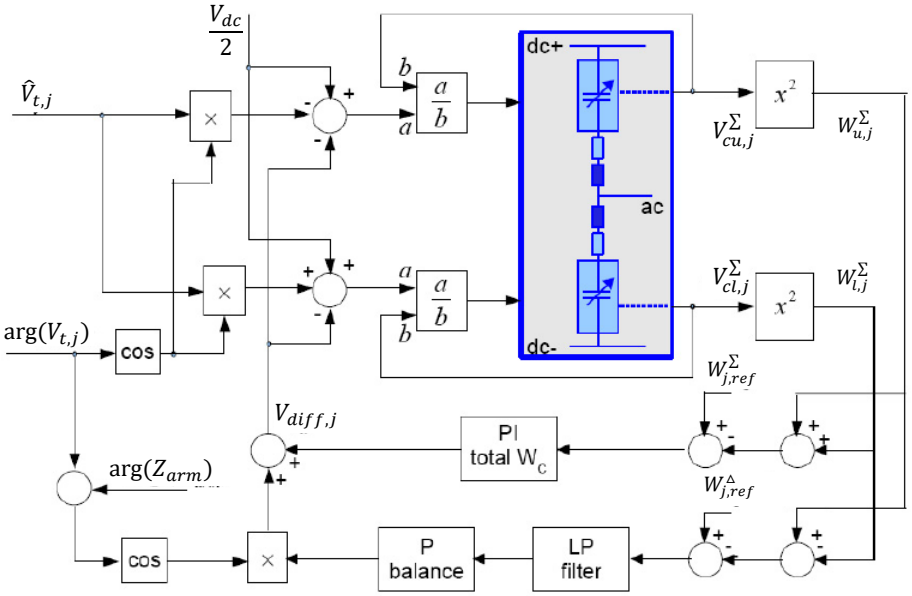

Figure 4.6 The control diagram of total energy control and energy balancing control [76]

As shown in the diagram, the voltages of SMs are measured. The sum and difference of energy are the inputs of total energy control and energy balancing control respectively. Total energy control uses a PI controller to eliminate the static error in the average energy and the reference can be chosen freely according to the desired performance. The energy balancing control uses P controller to suppressing AC component of circulating current. A filter is need to get the desired average value of energy difference. Two 'cos' blocks are used to control the command $i_{diff,j}$ in phase with $V_{t,j}$. The outputs of two controllers are added to difference voltage $V_{diff,j}$ as $i_{diff,j}$ can be directly controlled by it according to (4.14). Thus according to equation (4.12) and (4.13) the reference value of SM voltage can be calculated.

In this method, the voltages of SMs are needed to be measured consistently, which will be a problem if the number of SMs are big. In [77], a similar method is proposed but the energy is based on estimations. So that an open-loop control is achieved. The estimations are achieved by solving the equations (4.15),(4.16). The output current is measured and circulating current is set to be purely DC current. The control diagram is shown in Figure 4.7[77].

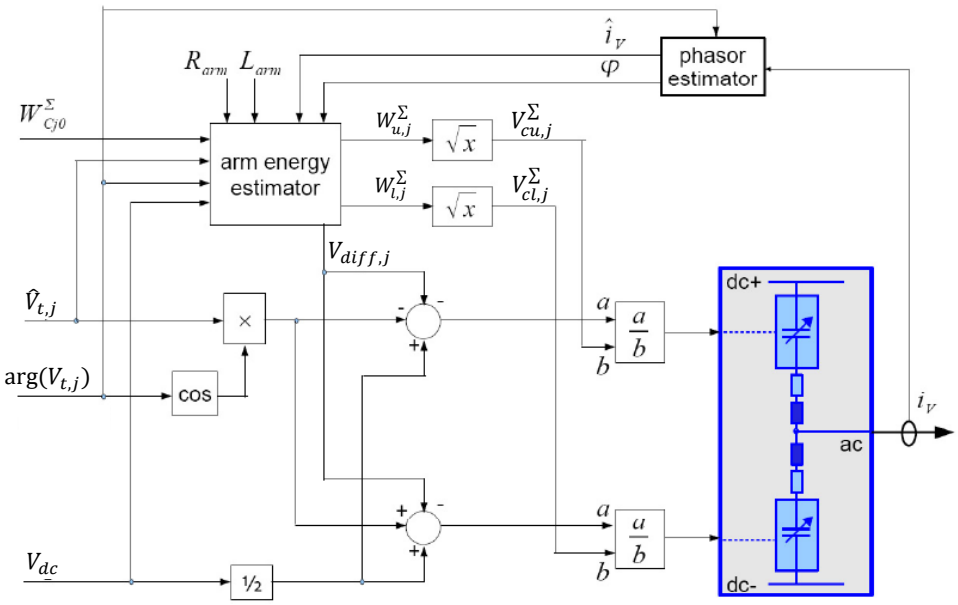

Figure 4.7 Diagram of control method based on energy estimation [77]

Based on the idea of controlling total energy and difference energy between upper and lower arm, a similar approach based on mathematical optimization is proposed in [78], in which the reference circulating current is obtained by lagrange-based multiobjective optimization. This method is compared with the closed-loop method mentioned above and shows better performance than the closed-loop method.

Based on the idea that DC component of circulating current is related to the power transfer and AC component will cause unbalance of voltage distribution, more methods are proposed [79][80]. Paper [79] actually uses the same methods as above

one, only replaces the energy by the square of SM voltages. Two methods are proposed in [79], first one is to separate the AC component from DC component and force it to be zero by using a high-pass filter based on moving average filter. The second one is to get the DC component and AC component reference of circulating current separately. DC reference is achieved by calculating the DC side current and AC reference is achieved by controlling the average SM capacitor voltage. Arm current is measured and circulating current is calculated. The control diagram is shown in 4.8.

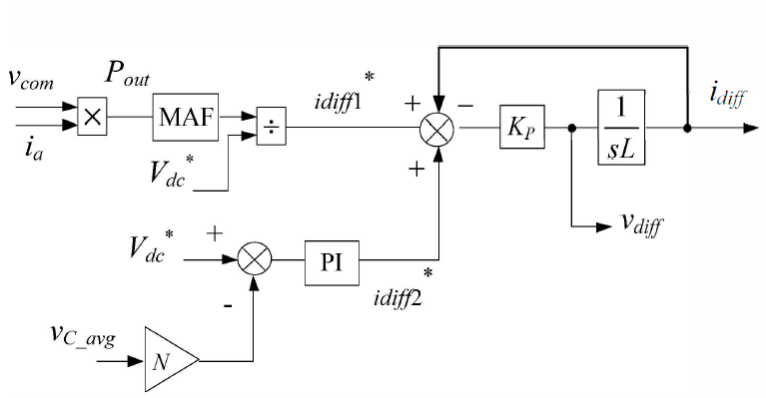

Figure 4.8 Control diagram of AC and DC component control [79]

4.3.2 Method Based on Double Line-frequency d-q Coordinate

In [20], a circulating current suppressing control (CCSC) method is proposed based on the theory that the circulating current is in the form of negative sequence with double line frequency, besides the DC component. Thus, the three phase circulating current can be represented as:

$$i_{diffa} = \frac{I_{dc}}{3} + I_{2f}\sin(2\omega_0 t + \varphi) \tag{4.19}$$

$$i_{diffb} = \frac{I_{dc}}{3} + I_{2f}\sin[2(\omega_0 t - \frac{2}{3}\pi) + \varphi] \tag{4.20}$$

$$i_{diffc} = \frac{I_{dc}}{3} + I_{2f}\sin[2(\omega_0 t + \frac{2}{3}\pi) + \varphi] \tag{4.21}$$

where I_{2f} is the peak value of AC component, I_{dc} is the DC current and ω_0 is the fundamental frequency and φ is the phase angle

Based on equation (4.14) and transfer to dq frame, the following relationship can be achieved:

$$\begin{bmatrix} V_{diffd} \\ V_{diffq} \end{bmatrix} = L\frac{d}{dt}\begin{bmatrix} i_{2fd} \\ i_{2fq} \end{bmatrix} + \begin{bmatrix} R_{arm} & -2\omega_0 L_{arm} + R_{arm} \\ 2\omega_0 L_{arm} + R_{arm} & R_{arm} \end{bmatrix}\begin{bmatrix} i_{2fd} \\ i_{2fq} \end{bmatrix} \tag{4.22}$$

where V_{diffd} and V_{diffq} are the difference voltage in d, q direction respectively and i_{2fd}, i_{2fq} are the d, q component of circulating current respectively. Equation (4.22) can also be represented by diagram as shown in Figure 4.9[20].

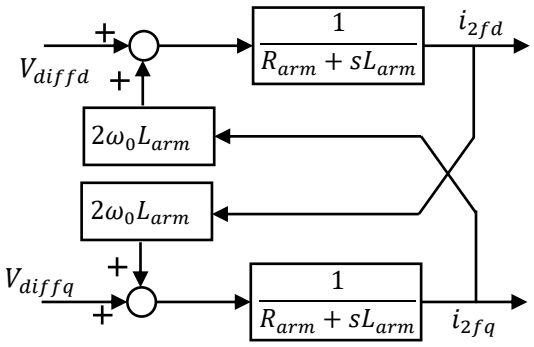

Figure 4.9 Relationship between circulating current and corresponding voltage

According to equation (4.22), circulating current can be controlled directly by difference voltage. Thus two PI controllers can be used on d and q directions and the control diagram is shown below. The output of the controller V_{diff_ref} will be subtracted from both upper and lower arm voltage reference as shown in diagram.

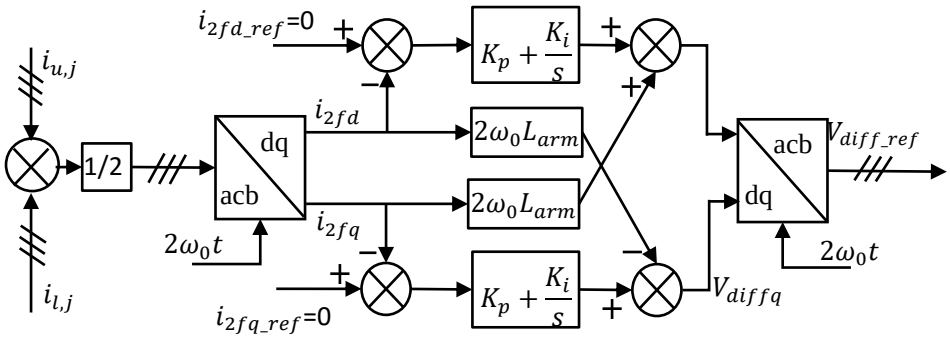

Figure 4.10 Control diagram of the Method Based on Double Line-frequency d-q Coordinate

As we can see, the d, q component reference of circulating current are both set to be zero to suppress the circulating current and the characteristics of double frequency and negative sequence can also been observed from diagram.

Following the original paper, the abbreviation name CCSC will only represent this method in the rest of the thesis.

4.3.3 Method Based on Model Predictive Current Control

In [75], a method based on model predictive current controller is proposed. The mathematical model derived in Section 2.1.2 can be used in this method. Based on equation (2.8), and assume R_{arm}=0, the circulating current can be predicted as:

$$i_{diff,j}(t+T_s) = i_{diff,j}(t) + \frac{T_s}{2L_{arm}}[V_{dc} - V_{u,j}(t+T_s) - V_{lj}(t+T_s)] \quad (4.23)$$

As introduced, cost function is minimized to achieve the desired performance. The circulating suppressing part is:

$$J = \lambda \left| i_{diff,j}(t + T_s) \right| \tag{4.24}$$

4.3.4 Methods Based on PR controller and Repetitive Controller

[81],[82] use the PR controller in the circulating current suppressing control system. The PR controller is used because there are not only double line frequency components in the circulating current, but also even harmonics i.e. components with forth, sixth fundamental frequency.

As introduced in Chapter 3, PR controller can achieve high gain at the resonant frequency, so that the components with known frequency can be regulated well. In this case, based on the pre-introduced control algorithms, several parallel connected PR controllers are used to eliminate the higher order harmonics in the circulating current. [81] is based on voltage balancing method introduced in section 4.2.3 and [82] just uses PR controllers to generator command control voltage V_{diff_ref}, similar to CCSC method but in abc frame.

For the same purpose, the repetitive controller is used to eliminate the multiple harmonics in the circulating current. In [83], repetitive-plus-PI control scheme is proposed and the control diagram is shown below (i_{zx} is circulating current).

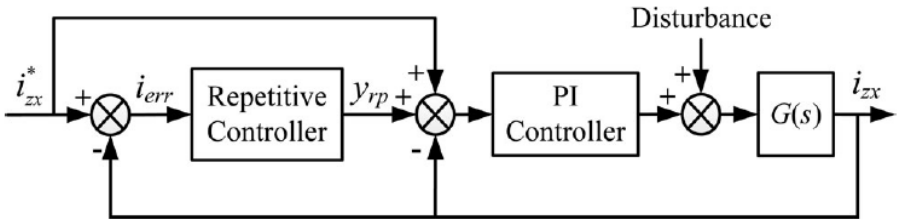

Figure 4.11 diagram of repetitive-plus-PI control [83]

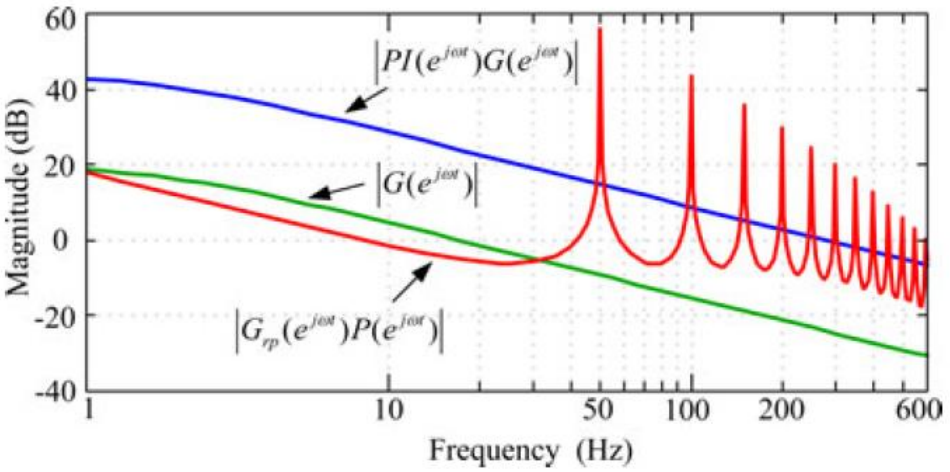

Figure 4. 12 Open-loop gains of three control systems [83]

Figure 4.12 compares the open-loop gains of original system $\left|G(e^{j\omega t})\right|$, the system only using PI controller $\left|PI(e^{j\omega t})G(e^{j\omega t})\right|$ and the system using repetitive controller $\left|P(e^{j\omega t})G(e^{j\omega t})\right|$. As we can see, the repetitive controller not only has high gain at fundamental frequency but also at multiple harmonic frequency. Therefore, it has good suppression ability of circulating current. Compared with the systems using PR controllers, those using repetitive controllers are much simpler with respect to the number of controllers.

4.4 AC Current Control Methods

4.4.1 PI controller

According to [84], the control scheme for AC side current of MMC applied in HVDC system is almost the same as that for 2-level converters, which is introduced in Section2.3.3. As explained, the control system is usually divided into two control loops: inner control loops and outer control loops. Both of them can be achieved by using PI controllers. In this section, the detailed control diagrams of power control, DC voltage control are introduced. As AC voltage control is more or less the same, it will be neglected here.

1. Active and reactive power control. Under balanced steady-state condition, the d-axis coincides with the load voltage vector, thus the voltage on q axis is zero and the active and reactive power are given by [84]:

$$\mathrm{P} = \frac{3}{2} V_d i_d \tag{4.25}$$

$$\mathrm{Q} = -\frac{3}{2} V_d i_q \tag{4.26}$$

From the equations above, the active and reactive power can be directly controlled by d axis current and q axis current respectively and the control structure should be the same in both directions, which is shown by Figure 4.13

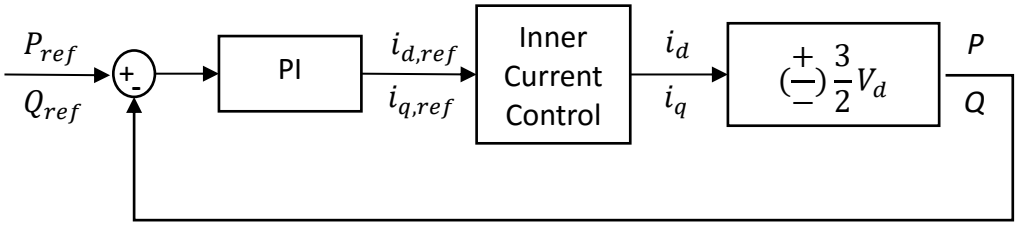

Figure 4.13 Active and reactive power control loop

2. DC power control. DC voltage control is used to generate reference current for d axis. The relationship between d axis current i_d and DC voltage V_{dc} can be achieved by the power balance between AC side and DC side of MMC as shown by the equations below:

$$\mathrm{P} = \frac{3}{2} V_d i_d = V_{dc} i_{dc} \tag{4.27}$$

$$i_{dc} = \mathrm{C} \frac{dV_{dc}}{dt} \tag{4.28}$$

Combining (4.27), (4.28) and transferring to s domain, the transfer function of system can be achieve as:

$$\frac{V_{dc}(s)}{i_d(s)} = \frac{3V_d}{2V_{dc,ref}} \cdot \frac{1}{sC} \tag{4.29}$$

So that the block diagram of DC voltage control is:

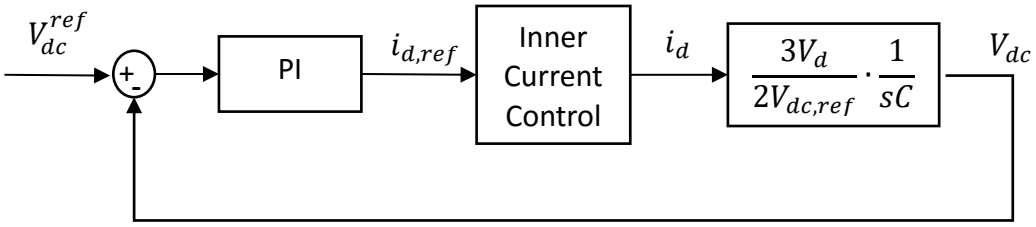

Figure 4.14 DC voltage control loop

3. Inner current control. Based on Figure 2.3, the dynamic equation of AC side of MMC in abc coordinator can be expressed as:

$$L_s \frac{di_j}{dt} = -R_s i_j + V_{g,j} - V_{t,j} \tag{4.30}$$

In order to control reactive and active power independently, the dynamic equations are transferred to dq frame using park transformation as:

$$L_s \frac{di_d}{dt} = -R_s i_d + V_{gd} - V_{td} + \omega L i_q \tag{4.31}$$

$$L_s \frac{di_q}{dt} = -R_s i_d + V_{gq} - V_{tq} - \omega L i_d \tag{4.32}$$

where V_{td} and V_{tq} are MMC output voltage in d, q direction respectively; i_d and i_q are output current in d, q direction respectively; V_{gd} and V_{gq} are the voltage components of supply gird. $\omega L i_d$ and $\omega L i_q$ are coupling terms. Based on the above equations, the inner current control scheme can be achieved as shown below:

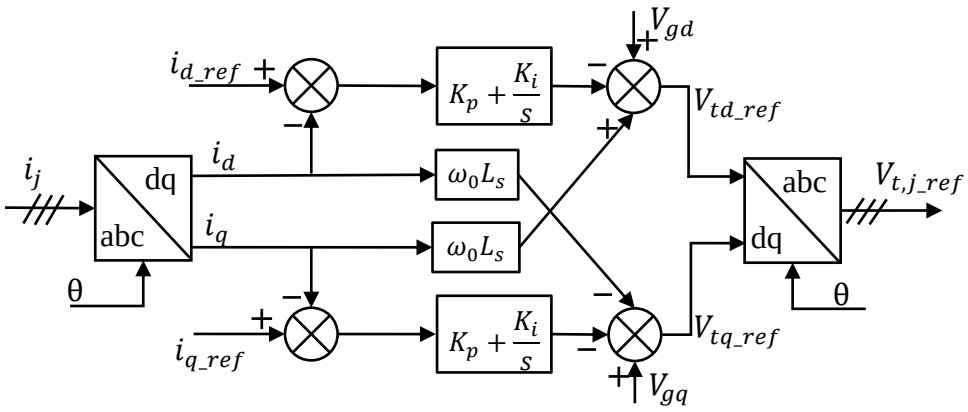

Figure 4.15 inner current control using PI controllers

4.4.2 Model Predictive Control

Model predictive control strategy has been proposed for controlling MMC in many papers [75][85]. In this thesis, as explained in Section 3.4.1, only FCS-MPC is studied, that is to say, the cost function is evaluated based on finite switching states. For simplicity, MPC represent FCS-MPC in the rest of thesis.

The basic principle is the same as that used for 2-level VSC, and the steps are the same:

- Develop discrete time model for the system and predict the variables one step forwards
- Define a cost function to describe desired performance.
- Minimize the cost function by comparing the results of all possible switching states

In [75], Model predictive control is proposed to achieve AC-side current control, capacitor voltage balancing and circulating current suppression control at the same time. The latter two functions have been introduced in this report and the AC-side current control is based on the MMC ac-side dynamic equation (2.8), which is repeated here, if the arm resistance is neglected:

$$V_{l,j} - V_{u,j} = (L_{arm} + 2L_s)\frac{di_j}{dt} + 2R_s\frac{di_j}{dt} + 2V_{g,j} \tag{4.33}$$

Using Eular approximation and assuming a sampling period T_s, the current can be predicted one step forward by the formula below:

$$i_j(t+T_s) = \frac{1}{K}\left(\frac{V_{l,j}(t+T_s) - V_{u,j}(t+T_s)}{2} - V_{g,j}(t+T_s) + \frac{L'}{T_s}i_j(t)\right) \tag{4.34}$$

where $L'=L_{arm}/2+L_s$ and $K=R_s+L'/T_s$. The switched-on SM voltages and AC side current need to be measured to make the prediction.

To force the predicted current follow the reference current the cost function below is defined:

$$J = \left| i_{jref}(t + T_s) - i_j(t + T_s) \right| \tag{4.35}$$

In [75], as the SM capacitor voltage balancing control is added to the cost function, all possible switching state should be evaluated, which needs high computation effort. In [85], an indirect finite control set (IFCS) model predictive control is proposed. In which, only the situations for all possible insertion indices are evaluated, which dramatically reduces the computation time for main controller and the voltage balance is achieved by using sorting method executed by another local controller. In addition, further burden reduction is proposed by only selecting neighbor insertion indices.

4.4.3 Hysteresis Current Control

The hysteresis current control algorithms can also be used for controlling MMC [86][87]. In [86], the MMC model is simplified into a one phase diagram shown below:

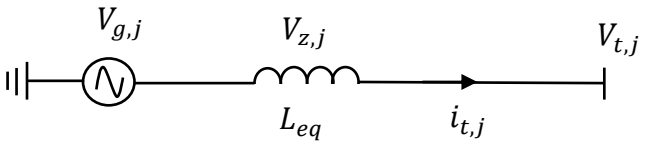

Figure 4.16 one phase simplified MMC circuit

where $V_{t,j}(t)$ is equivalent output voltage of MMC, L_{eq} is the equivalent inductance, which is same as L' in equation (4.34). $V_{g,j}(t)$ is the grid voltage. $i_{t,j}$ is the output current.

A hysteresis band is set around reference current with width *h*. If I_a is higher than the upper limit of the band, $V_{t,j}(t)$ will be set to higher than $V_{g,j}(t)$ so that $V_{z,j}$ is negative and current will decrease; If I_a is lower than the lower limit of the band, $V_{t,j}(t)$ will be set to lower than $V_{g,j}(t)$ so that $V_{z,j}$ is positive and current will increase; otherwise the switch state is unchanged. Each time the regions that $V_{g,j}(t)$ belongs are decided and the adjacent voltage levels are chosen for $V_{t,j}(t)$ depending on the amplitude and sign of errors between real current value and reference value. In this way, the inserting indices of SMs can be decided.

One problem of this method is the variable switching frequency. [86] achieves quasi-fixed frequency control by continuously adjusting hysteresis band width *h* as the frequency is decided by voltage $V_{z,j}$ and the torrent band width *h*.

Paper [87] takes more effort on choosing the voltage level for $V_{t,j}(t)$. If the number of voltage levels is small, the voltage levels adjacent to grid voltage are chosen (which is called constant excitation in [87]). However, if the number of SMs per arm is large, the voltage per SM is much smaller. Therefore, adjacent voltage levels may not be

sufficient to lead the current following the reference and more distant values should be choose to increase the absolute value of $V_{z,j}$ and the speed of response. As a result, the variable excitation is chosen, which is proportional to the error between real current and reference value.

4.4.4 Methods Based on Bilinear Model

Because of the inherent nonlinear dynamics of the MMC, nonlinear modelling and control may achieve more precise performance [88]. In [88], the sum of squares decomposition method is proposed based on a discrete-time bilinear model. The state variables includes the AC side current, the circulating current, the total energy and energy difference of upper and lower arm. Based on the reference real and reactive power, the corresponding steady state point can be calculated and the sum of square decomposition controller converges MMC to this steady state point by generate desired voltage references and PWM modulation can be used.

In [89], an integrated control of the AC side current, circulating current and voltage balancing is proposed by representing all the controlled variables in a bilinear model, which is very similar to that in [88]. A periodic linear quadratic regulator is used to achieve optimal control. By using lifting procedure, the problem become a time-invariant state feedback control.

One of the advantages of the algorithms mentioned above is that they can provide uniform control for all states and the interaction between the states, so that the three control purposes, AC current control, circulating current control and voltage balancing control can be achieved at the same time. Thus, only on controller is needed. However, these methods are complex and require deep mathematical knowledge.

4.5 Summary and Discussions

In this chapter, the control strategies of MMC for SM voltage balancing, circulating current suppressing and AC side current control in HVDC system were reviewed separately, which includes most of control methods proposed in existing papers. They are summarized here:

- Voltage balancing Algorithms
  - Sorting method
  - Method based on carrier shifting
  - Method based on averaging and balancing control
  - Method based on model predictive control
- Circulating current suppressing control
  - Method based on total energy and energy balancing control
  - Method based on double line-frequency dq coordinate
  - Method based on Predictive current control

- Method based on PR controller and repetitive controller

- AC side current control
  - Method based on PI controller
  - Model predictive control
  - Hysteresis current control
  - Methods based on bilinear model

5. Proposed System and Simulated Strategies

In order to verify and compare different control strategies reviewed in Chapter 4, at least two methods for each control purpose were simulated in Matlab/Simulink environment. In this chapter, the system used for simulations will be introduced and the tested control strategies will be summarized. The simulation methods and the results will be shown in Chapter 6.

5.1 Model and Parameters

In this thesis, the study of MMC was based on the application of HVDC transmission system for offshore wind farm. In addition, In order to focus on the control of MMC, only the wind turbine side converter (sending end converter) was studied through simulation. The DC side was represented by DC voltage sources assuming that the other MMC in HVDC system keeps the DC bus voltage constant. Or when DC voltage control was applied to wind farm side MMC, two resistors were connected to DC side to represent the rest of system. The diagram of the system is shown in Figure 5.1.

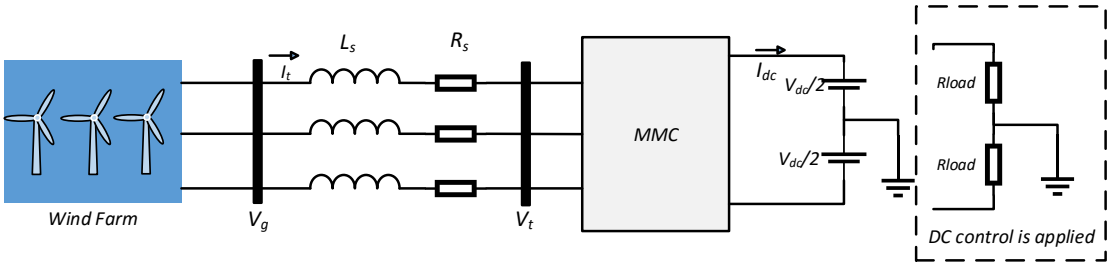

Figure 5.1 The overall diagram of studied the system

The resistors and inductors R_s, L_s between MMC and wind farm represent the impedance of AC system.

The model parameters are summarized in table 5.1, which are mostly based on those used in paper [20]. However, some modifications or comments about several important parameters have been made below:

1. **The number of SMs per arm.** because of limited computation effort, the number of SMs on each arm is chosen as 6 (which is 20 in paper[20]), which results in 7 levels in output AC phase voltages

2. **The SM capacitance.** According to [90], the selection of arm capacitance is decided by energy-power ratio once the rated power and DC side voltage are decided. The ratio is defined below:

$$\mathrm{EP} = \frac{E_{cmax}}{S_n} \tag{5.1}$$

where E_{cmax} is the maximum energy stored in arm capacitors. The ratio actually represents the trade-off between the cost of capacitors and voltage ripples in DC

voltage. Higher EP means higher cost and lower voltage ripple, resulting higher arm capacitors C_{arm} , which is defined below:

$$C_{arm} = \frac{C}{N} \tag{5.2}$$

where *C* is the SM capacitance. As the parameters of system for simulation are chosen based on that in paper [20], the SM capacitance is reduced from 0.026 F to 0.01 F to result a similar arm capacitance and the EP ratio is about 74 J/kVA.

3. Arm inductance. The arm inductance is used to suppression circulating currents and fault currents, thus most of selection criteria depends on the desired circulating current or fault currents [90]. In this thesis, the fault currents were not considered and extra controllers for suppressing circulating current are used, therefore a small inductance can be used, which follows that in paper [20] and is set as 0.05 p.u.

4. Switching frequency. As the number of SMs is decreased compared to that in [20], the switching frequency of SMs is increased to 600 Hz and total switching frequency of MMC is 3.6 kHz.

Table 5.1 Circuit parameters for MMC

Items	Abbreviation	Values
Active power	P	20 MW
Reactive power	Q	6.6 Mvar
Grid voltage (phase, peak)	V_s	14.14 kV
Grid side inductance	L_s	3.17 mH
Grid side resistance	R_s	0.062 Ω
DC bus voltage	$V_{dc}/2$	17.68 kV
Number of SMs per arm	N	6
SM capacitance	C	0.01 F
Arm inductance	L_{arm}	1.59 mH
Arm resistance	R_{arm}	0.1 Ω
SM capacitor voltage	V_c	5892 V
Carrier frequency	f_c	600 Hz
Sampling period (for MPC)	T_s	100 μs

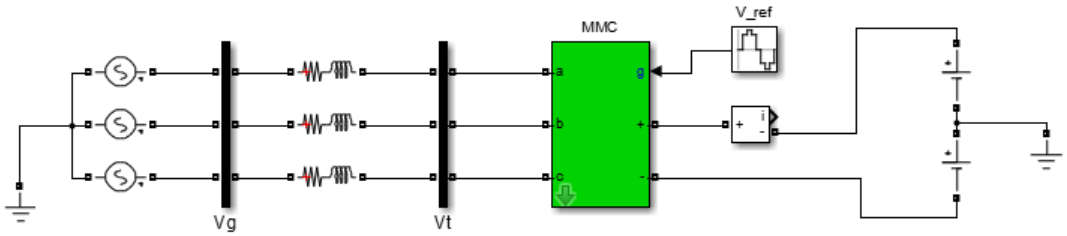

Figure 5.2 The Simulink model used for testing control Algorithms

For the purpose of testing and comparing different control algorithms, the basic model in Simulink as shown in Figure 5.2 was built, in which an ideal grid model was used to represent wind farm. Thus, the oscillations from wind farm were neglected. At the end, an option of overall control scheme for targeted system in Figure 5.1 is proposed and a 21 MW wind farm model was added to simulate and verify the functions of different controllers, which will be shown in Section 6.8.

5.2 Simulated Control Strategies

In Chapter 4, most of control strategies for different purposes were classified and reviewed. Because of limited time, not all strategies could be simulated and verified. In this thesis, only the typical methods were simulated, but at least two methods for each control purpose are guaranteed. They are summarized below:

- Modulation Methods
  - Carrier phase shift modulation
  - Nearest level modulation
- Voltage balancing Algorithms
  - Sorting method
  - Method based on model predictive control
- Circulating current suppressing control
  - Method based on total energy and energy balancing control
  - Method based on double line-frequency dq coordinate
  - Method based on Predictive current control
- AC side current control
  - Method based on PI controller
  - Model predictive control

The reasons for chosen these methods are briefly discussed in following sections

5.2.1 Selection of Modulation methods

There are total three modulation methods introduced in Section 4.1, but only PWM modulation and NLM were simulated. The problem of space vector modulation is that the number of space vectors increase exponentially with *N* and the switching diagram will be huge if more than 3 voltage levels are used, which may not be a good option for MMC. As for PWM modulation, the extension from two-level application to multilevel is easy and it can achieve low harmonics, constant switching frequency and high precise. Thus it was simulated in this thesis. The further comparison between CPS-PWM and CD-PWM is not made and CPS-PWM was chosen in this thesis. The NLM is a new modulation method only for multilevel converters. It is simple and can achieve

fundamental switch frequency, thus it is also simulated and compared with PWM method. The detailed results is shown in Section 6.1.

5.2.2 Selection of Voltage Balancing Methods

There are total four voltage balancing methods introduced in section 4.2. The sorting method is most widely used because it is simple and can be easily used with most of modulation methods. Actually it can be part of modulation that the PWM or NLM generates the inserted number of SMs in upper and lower arm and sorting algorithms decide which SMs should be switched on or off. Therefore, sorting algorithm is simulated. The method based on MPC is also simulated because it can be achieved with circulating current control and AC side current control at the same time. In addition, the control algorithm is totally different with sorting method, thus a good comparison can be made.

As for the method based on carrier rotation, it can be only used with PWM modulation and if precise voltage balancing is need, the sorting of capacitor voltage is also needed, which makes it more complex than sorting method. So it is not simulated. Similarly, the method based on average and balancing control does not have good compatibility as it needs separate PWM modulation for each SM. In addition, the idea of controlling average voltage and difference voltages between SMs is similar to energy control for circulating current control. As the latter will be simulated, the former is not studied in this thesis.

5.2.3 Selection of Circulating Current Control methods

Three out of four strategies introduced in section 4.3 are simulated. The energy control introduced in 4.3.1 and CCSC method introduced in section 4.3.2 are two typical methods widely used in literature. The ideas behind these two methods are different. CCSC is more straightforward that it uses two PI controllers to suppress circulating current in dq frame directly by setting the reference value to be zero, while energy control tries to reduce the circulating current from source by controlling the total energy and balancing the energy difference between upper and lower arm since the circulating current is caused by the energy difference. Thus, it is very meaningful to compare these two methods and they are simulated in section 6.2 and 6.3. For the same reason as in last section, the predictive control for circulating current is also simulated.

The method based on PR controller or repetitive controller can eliminate high order harmonics in circulating current, which can be used as compensation for other control methods. For example CCSC only focuses on second order harmonics, if higher requirement are asked, PR controller can be used for suppressing targeted harmonics. The methods are not simulated as most of components of circulating current are second order as shown by simulation.

5.2.4 Selection of AC side current control methods

The main idea for AC side current control in this thesis is to compare traditional PI controller based method with new non-linear control algorithm. Thus, PI controller based cascade control was simulated. Compared to PI controller, MPC includes the nonlinearity of systems and has a fast dynamics responses. So it gains an increasing attention in literatures recently. As for MMC, MPC can control circulating current, voltage balancing and AC side current at the same time, thus makes system simpler. Because of these, MPC is very promising and it is necessary to simulate and verify these advantages. In section 6.5 and 6.6, PI based method and MPC were simulated respectively and they were compared in section 6.7.

Hysteresis control was not simulated because it cannot be treated as new control method. Also, the methods based on bilinear model were not simulated because they involves many mathematical calculation, which can be studied in the future.

5.3 Summary and discussions

In this chapter, the system used for simulation was introduced, including the system diagram and the parameters. The selections of most important parameters are discussed. In addition, the simulated strategies are summarized and the reasons for choosing these strategies are briefly explained.

The simulation methods and results will be introduced in next chapter.

6. Simulation Methods and Results

In this chapter, a switched model of MMC is built to verify and compare the control strategies summarized in chapter 5. The MMC model is exactly follow the configuration shown in Figure 2.3. The simulation methods were explained and all the results are presented and discussed. In addition, all the results are shown in p.u. value, the way to calculate the base values are shown in Appendix based on the parameters shown in Table 5.1.

6.1 Modulation Methods

1. **CPS-PWM**: six sawtooth carriers with same frequency and amplitude are generated, which have 60 degree phase shift with each other. Then, the carriers are compared with sinusoidal reference voltage, resulting in 6 sequences of switching pulses. Each sequence corresponds to one SM in the upper arm. The configuration of PWM modulation used in Simulink is shown in Figure 6.1. It is seen that the switching pulses for upper arm SMs are reversed to control the SMs in the lower arms by changing the setting of comparator. This method is the same as PWM with bipolar voltage switching for 2-level VSC. The AC side voltage references are the references for both upper and lower arm. The reason to use two separate comparator rather than one comparator and one reversing block is for better connection with circulating current control introduced later, which generate different reference values for upper and lower arm.

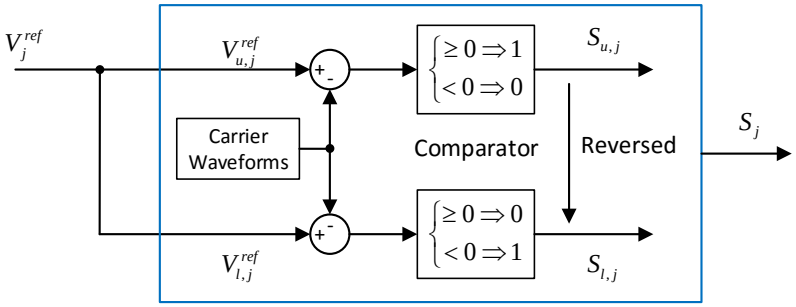

Figure 6. 1 The configuration of PWM modulator

In order to test the MMC model as well as CPS-PWM method, the Simulink model shown in Figure 5.2 was simulated. The desired AC side voltage references were chosen and modulation index was set to 0.8. The results of output voltages and currents, SM capacitor voltages are shown in Figure 6.2.

As we can see from Figure 6.2 (a), the three phase voltages were shaped well as expected with 7 levels. In addition, the amplitudes of voltages reached DC voltage, which was reasonable as when all the SMs in upper arm were on, the output voltage was almost equal to DC voltage if the losses were low. Also, the output currents were almost sinusoidal and the amplitudes were reasonable. The reason that they were not

1p.u. was that the reference voltages was chosen randomly, so the system did not operate at rated power. According to Figure 6.2 (b), the SM voltages were well balanced and the ripples were low.

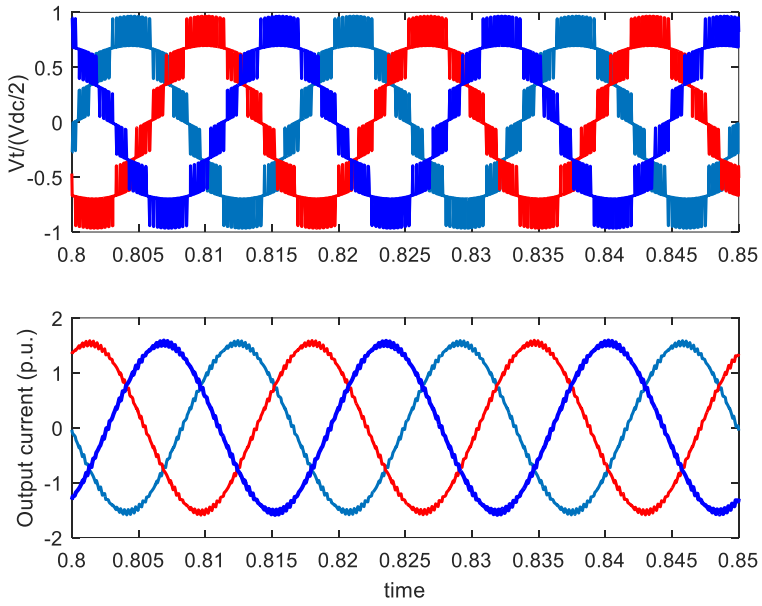

(a)

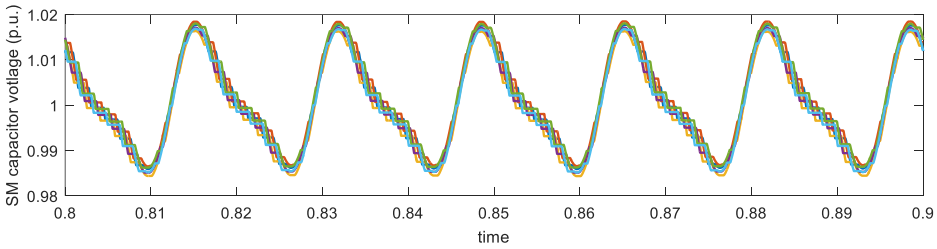

(b)

Figure 6.2 Results of CPS-PWM (a) output voltages and currents of MMC (b) The SM capacitor voltages of upper arm in Phase A

Although, for testing purpose, the reference voltages were chosen randomly, some cautions should be paid that the reference voltages should be have similar amplitude and phase angle to grid voltages. As the operating power was decided by the difference between grid voltages and output voltages, high difference may results high current and makes dynamic go bad. The AC side currents in Figure 6.2 (b) were about 1.5 p.u., which is acceptable for testing purpose. Once the close loop control is added, the current would be go back to 1p.u.

2. **NLM and Sorting method:** By using NLM, the numbers of SMs inserted are calculated by the formula (4.1), which is repeated here

$$n_{u,j} = N\left(\frac{1}{2} - \frac{V_{ref}}{V_{dc}}\right)$$

$$n_{l,j} = N\left(\frac{1}{2} + \frac{V_{ref}}{V_{dc}}\right)$$

Once the inserted index is known the sorting method can be used to decide which SMs should be turned on (or off) in order to keep the SM capacitor voltages balanced. The sorting method simulated here is the basic algorithm introduced in section 4.2.1 that the SMs with lowest voltages are turned on when current is positive and SMs with highest voltages are turned on when current is negative. The comparing between the voltages using and without using sorting method is shown in Figure 6.3.

According to Figure 6.3, the arm with sorting control had very balanced capacitor voltages, while the one without sorting control had a tendency of unbalanced capacitor voltages. This verified the function of sorting method.

The output voltages and currents of MMC by using NLM are shown in Figure 6.4. All three phases used sorting algorithm. Compared Figure 6.4 to Figure 6.2, the output voltages of the system using NLM lost a lot of information as there are only 5 voltage levels shown in Figure 6.2 rather than 7 when the modulation index was 0.8 (0.33p.u. per voltage level).This is because NLM method cannot precisely distinguish the reference value between adjacent two voltage levels. In addition, it introduced much more harmonic to the system, which can be seen from the distorted output current waveforms. The high frequency harmonics around the peak value of currents were caused by the sorting algorithm, which caused more switching transitions even when the inserted index did not change.

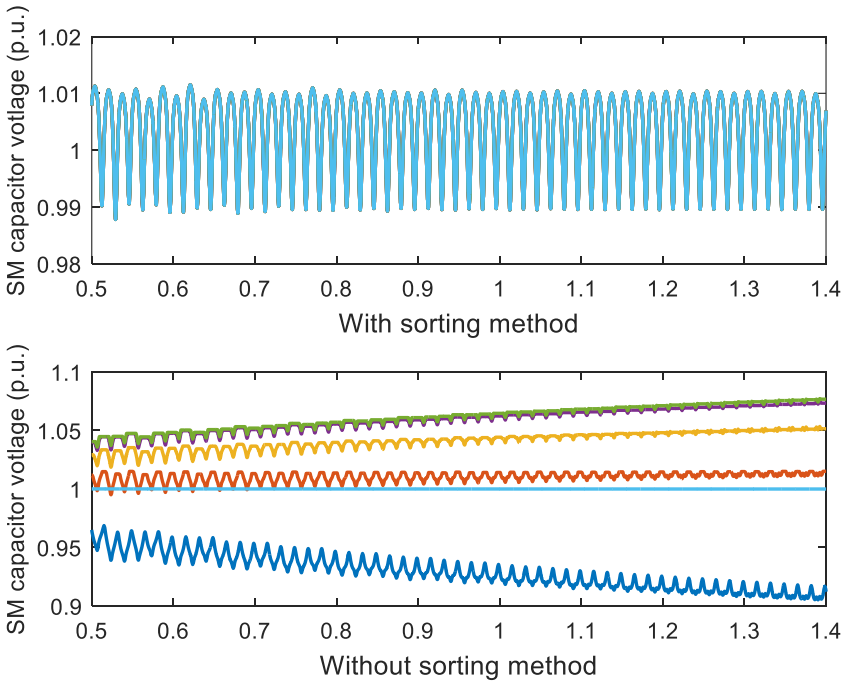

Figure 6. 3 SM capacitor voltages of one arm with and without sorting methods

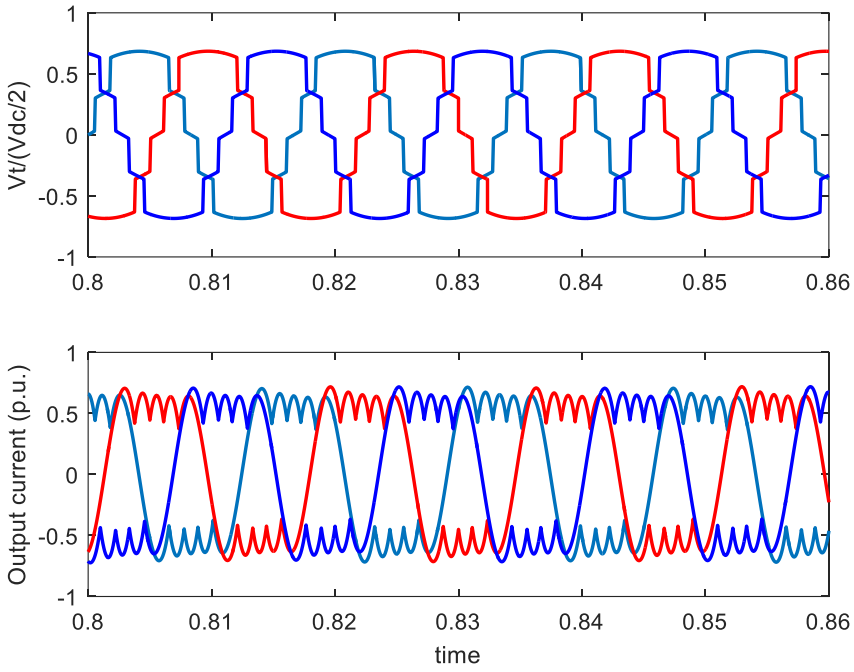

Figure 6.4 The output voltages and currents using NLM when modulation index is 0.8

Comparing these two modulation methods, NLM can achieve fundamental switching frequency, which, however, caused the voltage unbalancing because particular SMs will be charged or discharged at a relative longer time, so that the SM capacitor voltage balancing control is more necessary for NLM, which can be seen by comparing Figure6.2 (b) and Figure 6.3. In addition, CPS-PWM will produce more precise results and less harmonics. As for NLM, it is simple and suitable for MMCs with large number of SMs so that the amount of lost information will be reduced.

As the performance of CPS-PWM is much better than NLM for targeted MMC model, CPS-PWM method will be used in the rest of thesis to test different control methods. The way that CPS-PWM works together with sorting method is that after PWM generator switching pulses for each SMs, the pulses are added to calculate the number of inserted (bypassed) SMs (assuming “1” represents switching on and “0” represents switching off), so that the sorting algorithm can be used to decide which SMs should be turned on or off.

According to simulation, the sorting method slows down the simulation obviously, which means that it needs high computation effort.

6.2 Circulating Current Suppression Control (CCSC)

In this section, the CCSC method proposed in paper [20] is implemented and tested. As introduced in last chapter, this method is based on double line-frequency, negative-sequence rotational dq coordinate because it is proved that the circulating current is in the form of negative sequence with the frequency twice the fundamental one. The

circulating currents are transferred to dq frame and vector current control is used by setting both d and q reference to be zero. The control diagram is repeated in Figure6.5 and the connections with modulation part is also shown. The model in Simulink was built following this diagram.

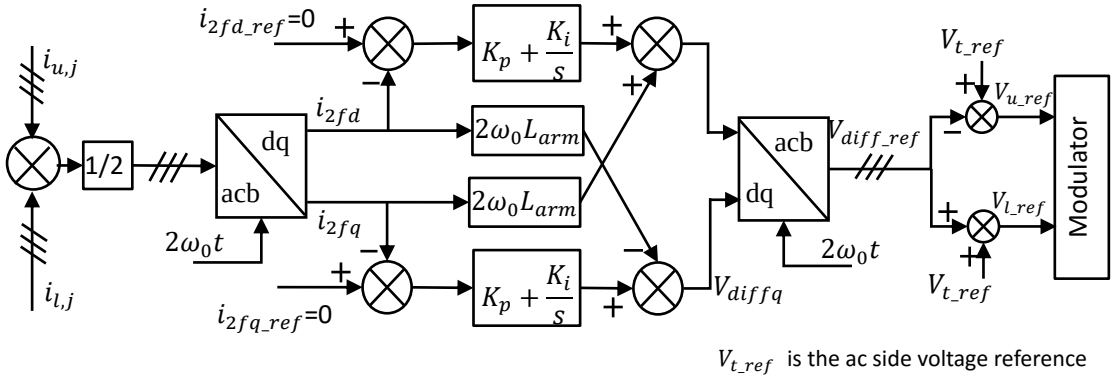

Figure 6.5 Control diagram of the CCSC Method

Two main problems should be noticed are that the frequency used for calculating phase angle 'wt' should be twice the fundamental one, which is got by using phase lock loop (PLL) and the circulating currents should be in negative sequence to get acb-dq transformation.

6.2.1 Modulation for CCSC

The configuration of modulator used for CCSC is the same as that shown in Figure 6.1. The output of the controller V_{diff} should be subtracted from voltage references of both upper and lower arm. Because, the voltage drops on arm impedances have the same direction as voltages of inserted SMs on both upper and lower arm as shown in Figure 2.3. Subtracting V_{diff} from upper and lower arm reference voltage will compensate the voltage drops on arm impedance, so that the voltage difference between DC voltage and phase inserted SM voltages will be reduced and circulating current will be suppressed. However, as shown in Figure 6.5, V_{diff} is added to lower arm reference. That is because the switching pulses for lower arm SMs is achieved by reversing those for upper arm, thus the "+" actually acts as a "-" on the lower arm references. Which can be seen from the configuration of modulator in Figure 6.1.

6.2.2 Tuning the PI Controller- Modulus Optimum

The tuning method for PI controllers are modulus optimum method proposed in paper [35]. According to relationship between circulating current and command voltage V_{diff} described by equation (4.14), the transfer function of the system is derived:

$$\frac{i_{diff}(s)}{V_{diff}(s)} = \frac{1}{R_{arm} + sL_{arm}} \tag{6.1}$$

So that the whole control system can be represented by the block diagram below:

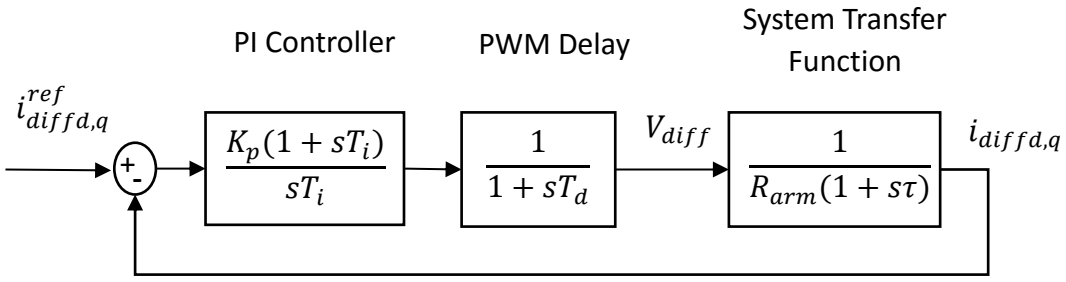

Figure 6.6 Block Diagram of CCSC

the τ in the diagram is the ratio between arm inductance and resistance. Since d and q loops have the same dynamics, so tuning of the two loops are the same.

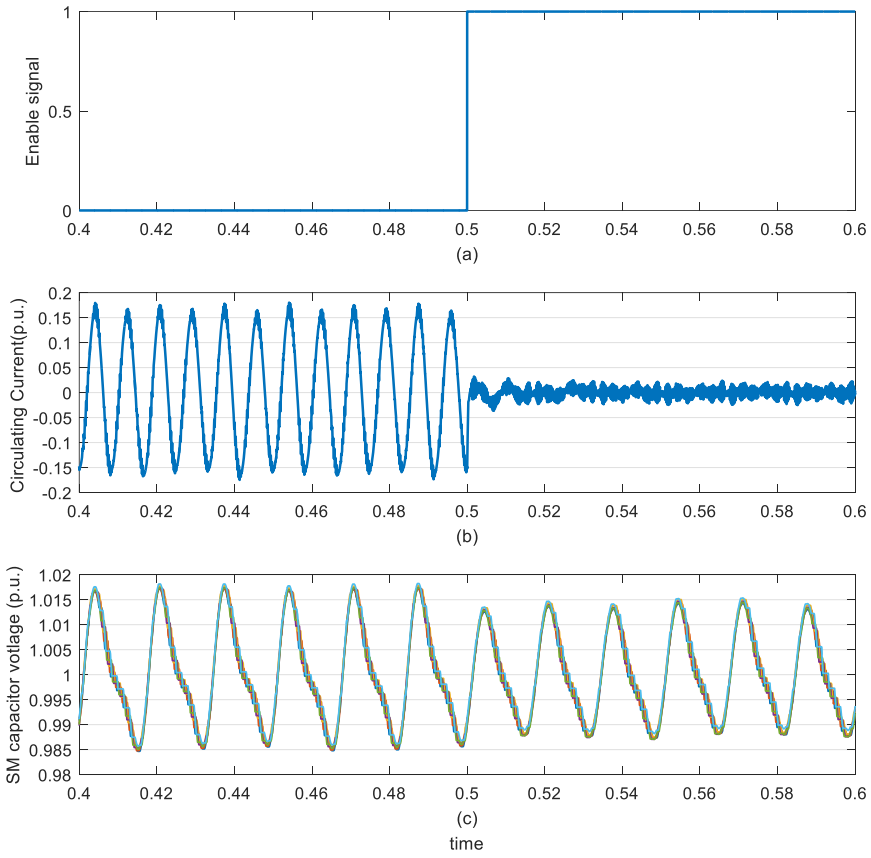

Figure 6.7 (a) the enable signal for CCSC; (b) circulating current (c) the capacitor voltage of phase A

According to modulus optimum method, choose T_i to be equal to τ to cancel the slow system pole. Then the open loop transfer function of the system is:

$$G_{OL} = \frac{K_p}{R_{arm} sT_i} \frac{1}{1+sT_d} \tag{6.2}$$

The proportional parameter of PI is calculated by setting the close loop gain to be 1:

$$\left|\frac{G_{OL}}{1+G_{OL}}\right| = 1 \tag{6.3}$$

And

$$K_p = \frac{\tau R_{arm}}{2T_d} \tag{6.4}$$

where T_d is chosen to be half of switching period.

$$T_d = \frac{1}{2f_{switch}} \tag{6.5}$$

By using the equations above, the parameters are obtained as K_p=5.72, T_i=0.0159. According to simulation, the system showed good robustness that the parameters of PI can vary at a relatively big range to keep the system stable. The results of simulation are shown in Figure 6.7.

The CCSC block was enabled at 0.5s as shown in Figure 6.7 (a). The circulating current is shown in Figure (b) (the DC component was got rid of). As we can see, before CCSC was enabled, the circulating current was about 0.3 p.u. for peak-peak value at double line frequency as expected. After enabling CCSC, it is reduced to less than 0.05 p.u. From Figure 6.7 (c), it is found that the CCSC also reduce the SM capacitor voltage ripple from about 3.25% to 2.75%. These clearly shows well performance of CCSC.

The output voltages and currents are shown in Figure 6.8. There are no noticeable changes to the AC side after using CCSC, which is expected as circulating current only related to inner dynamics of MMC.

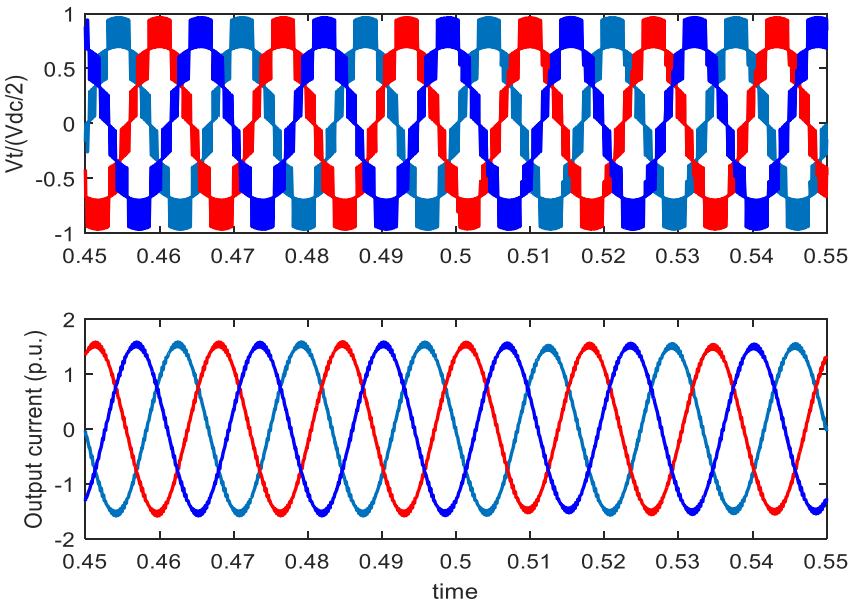

Figure 6.8 Output voltages and currents when CCSC was enabled at 0.5s

6.3 Energy Control

In this section, the closed loop energy control method proposed in [76] was simulated. The principle has already introduced in Section 4.3.1. Basically, the voltages of SM capacitors on each phase are measured and the energy stored in upper and lower arm is calculated. Then, two control loops are used to control the total energy and difference energy respectively. The control diagram are repeated in Figure 6.9. Total energy control will result a DC component to regulate the DC power and balance control will result an AC component to keep the energy balanced. Combination of these two loops aims at eliminating circulating current (AC component) and voltage ripple of SM capacitor.

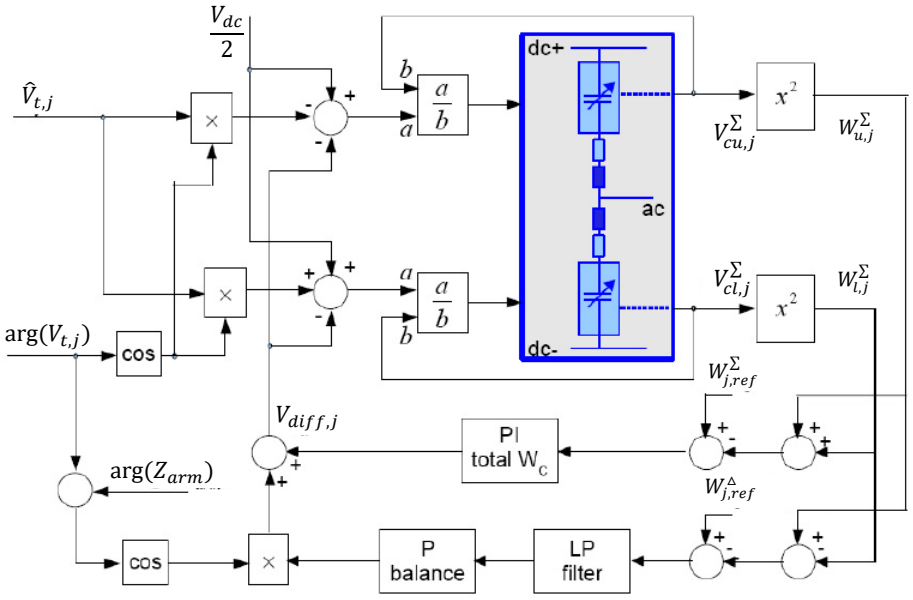

Figure 6.9 Control diagram of closed loop energy control [76]

6.3.1 Modulation for Energy Control

The modulation method for this method is a little different with that introduced by Figure 6.1. According to Figure 6.9, the index of inserted SMs for upper and lower arm are calculated by formula below:

$$D_u = \frac{\frac{V_{dc}}{2} - V_{t.j} - V_{diff,j}}{V_{cu,j}^{\Sigma}} \tag{6.6}$$

$$D_l = \frac{\frac{V_{dc}}{2} + V_{t.j} - V_{diff,j}}{V_{cl,j}^{\Sigma}} \tag{6.7}$$

where D_u and D_l are inserted index for upper and lower arm respectively. They are controlled within 0 and 1 representing 0 and 6 SMs respectively.

Thus, the modulator used in this method had two separate but exactly the same comparators for upper and lower arms respectively. In addition, the amplitudes of carrier waveforms are between 0 and 1 rather than -1 and 1 for that introduced in section 6.1. The SPC-PWM method is used to transfer D_u and D_l to the number of SMs, after that sorting method was used.

6.3.2 Tuning the PI Controllers and Results

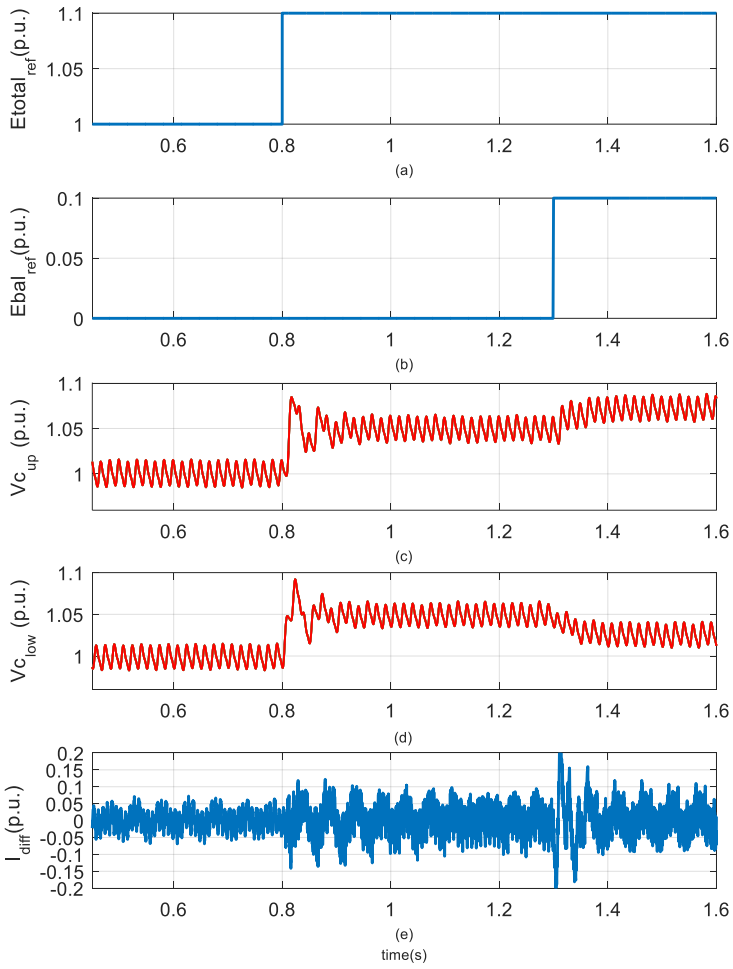

Figure 6.10 (a) reference for total energy control (b) reference for balance control (c) upper arm capacitor voltages (d) lower arm capacitor voltages (e) circulating current

As the transfer function of the system are not straight forward, the try and error method was used for tuning the PI controller and P controller. The basic steps are that firstly set parameter of integral part to be zero and only tune P parameter to make the system stable, then add integral part to eliminate the error between reference value

and real value. In addition, the two control loops are not the same, therefore, the parameters for them were chosen separately. The parameters for total energy control were chosen first to achieve the basic function, transferring desired power from AC side to DC side. Then, the parameter for balance control was decided. Balance control only used a P controller as it tracks reference very well. The values of parameters after tuning were K_p=8e-4, T_i=0.533 for the total energy control; K_p=-1e-3 for balance control. The simulation results are shown in figure 6.10

At t=0.8s and t=1.3, step changes were added to total energy reference and balance energy reference respectively as shown in Figure 6.10 (a) and (b). From Figure (c) and (d), the capacitor voltages followed the reference very well, which show good dynamic response of both control loops.

As shown in Figure 6.10 (e), the circulating current is suppressed well to between 0.1 p.u. to 0.2 p.u. while the original circulating without using controller is more than 0.3 p.u. as shown in Figure 6.7 (b) before t=0.5s. If zoom Figure 6. 10 (c) or (d) as shown in Figure 6.11. The ripple of SM voltages are about 3%. Compared with that shown in Figure 6.7 (c), it reduces by 0.25% of rated AC side voltage. The SM capacitor voltages are well balanced due to the usage of sorting method.

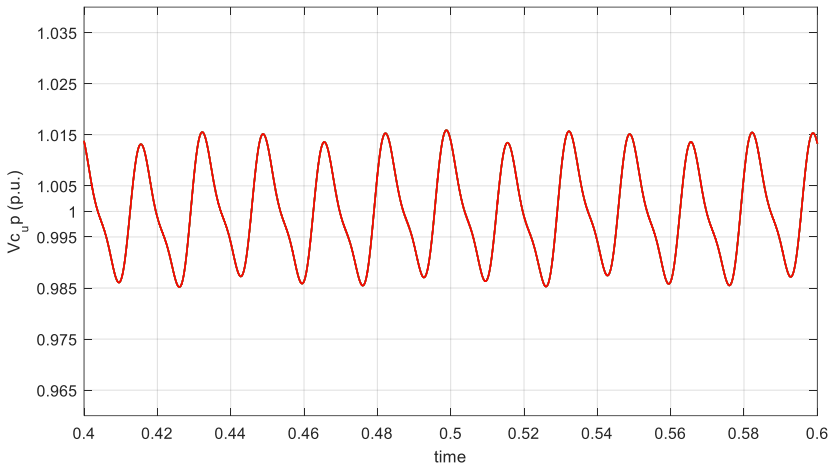

Figure 6.11 SM capacitor voltages

For this closed loop energy control, all the capacitor voltages need to be measured, which need a lot of sensors. To solve this, an open loop energy control based on estimated stored energy is proposed in [77], it will be studied in the future.

6.3.3 Comparing between Energy Control and CCSC

The comparisons the energy control and CCSC method in Section 6.2 are summarized in table 6.1. According to it, The CCSC is better than energy control method both in circulating suppressing and balancing capacitor voltages. In addition, based on the experience of simulation, CCSC is easy to tune and synchronize with other controllers. One good advantage of energy control is that the DC energy can be controlled flexibly.

Table 6. 1 Comparison between Energy Control and CCSC (in p.u. value)

	Without controller	With CCSC	With Energy Control
Circulating Current	0.3	<0.05	0.1
Voltage Ripple	3.25%	2.75%	3%
Tuning		Easy	Hard
Synchronizing with other Controllers		Easy	Hard
Other Functions		No	Energy Control

Based on this, the CCSC method will be used in the overall control schemes in the rest of thesis.

6.4 AC side Current Control for HVDC System

The control methods have been introduced in section 4.4. The simulation process and the results are shown here.

6.4.1 Inner Current Control

The dynamic equations in dq frame and the control diagram for inner current control are repeated here:

$$L_s \frac{di_d}{dt} = -R_s i_d + V_{gd} - V_{td} + \omega L i_q \tag{6.8}$$

$$L_s \frac{di_q}{dt} = -R_s i_d + V_{gq} - V_{tq} - \omega L i_d \tag{6.9}$$

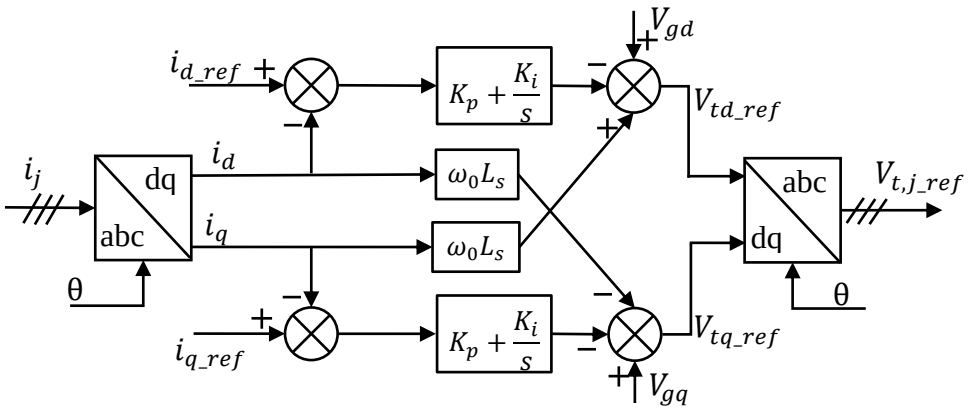

Figure 6.12 control diagram of inner current control

Based on the diagram in Figure 6.12, the control model was built in Simulink using PI controllers. The method for tuning of PI control is modulus optimum as shown in

Section 6.2.2. Neglecting the current cross-coupling terms and feed-forward terms, the block diagram for inner current control is the same as Figure 6.6 and the derivation steps for calculating parameters are almost the same except that the transfer function of system changes a little bit by replacing arm impedance to AC side impedance. So the parameters of PI controllers can be calculated by the equations blew:

$$T_i = \tau$$

$$K_p = \frac{\tau R_s}{2T_d}$$

Using the system values, the parameters of PI controllers are calculated as K_p=11.38, T_i=0.051. by adjusting in the Simulink, the final values are K_p=100.38, T_i=0.025. The dynamic responses are shown in Figure 6.13. It can be observed that the current in dq frame follows reference well and the step change in one axis does not affect the other one.

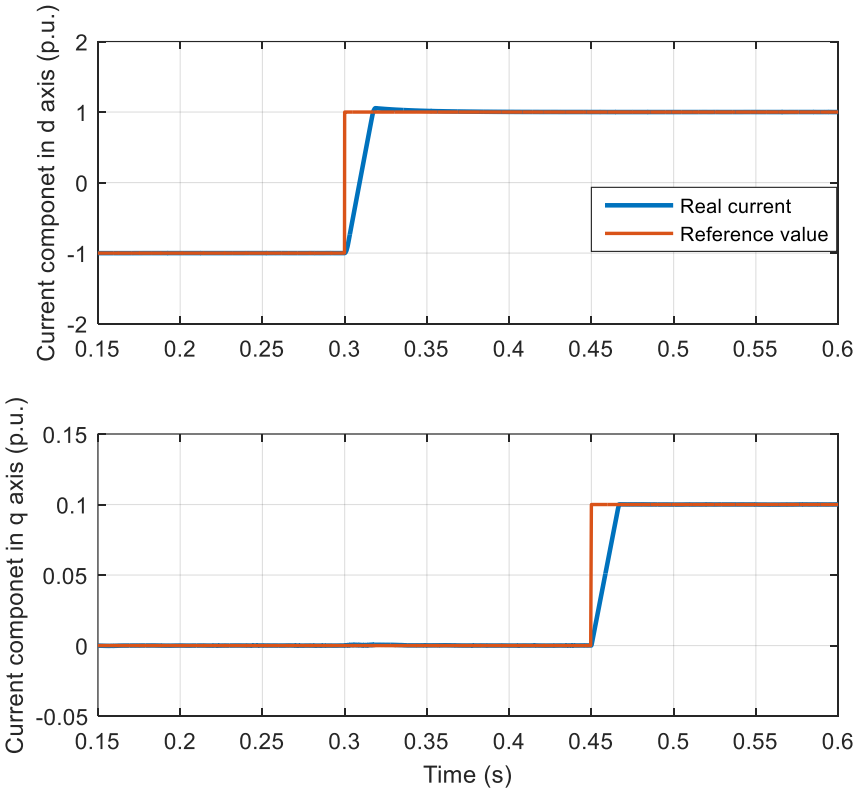

Figure 6.13 Current control response in d, q frame

6.4.2 DC Voltage Control

The control diagram has been shown in section 4.4.1. Here it is repeated with the transfer function of each part shown on the diagram:

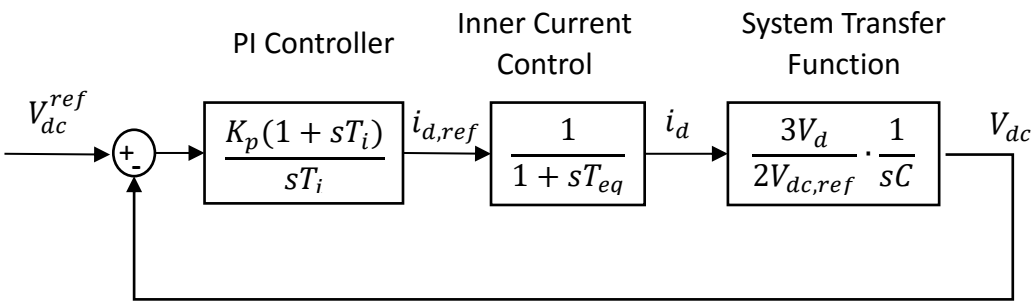

Figure 6.14 DC voltage control loop with transfer function

The transfer function of inner current control is got by approximation. After using modulus optimum method, the closed loop transfer function of inner current control is:

$$G_{cl} = \frac{1}{2T_d^2 s^2 + 2T_d s + 1} \tag{6.12}$$

By neglecting the second order part, the first order transfer function in Figure 6.14 is resulted and $T_{eq} = 2T_d$.

6.4.2.1 Tuning PI controller- Symmetrical Optimum

The open loop transfer function of DC voltage control is:

$$\mathrm{G}_{dc,ol} = \frac{K_p(1+sT_i)}{sT_i} \cdot \frac{1}{1+sT_{eq}} \cdot \frac{3V_d}{2V_{dc,ref}} \cdot \frac{1}{sC} \tag{6.13}$$

In this case, modulus optimum method cannot be used otherwise, two poles at origin will lead the system to be unstable. Therefore, symmetrical optimum method can be used [35]. The tuning criteria of symmetrical optimum is obtained using Nyquist criteria of stability:

$$\left|G_{dc,ol(j\omega)}\right| = 1 \tag{6.14}$$

$$\angle G_{dc,ol(j\omega)} = -180^\circ + \Phi_M \tag{6.15}$$

where Φ_M is the phase margin. The higher is the phase margin, the more stable of the system. By differentiating the angle with respect to ω, the maximum phase margin happens when:

$$\omega_d = \frac{1}{\sqrt{T_i T_{eq}}} \tag{6.16}$$

This means that the crossover frequency ω_d is symmetric about $1/T_i$ and $1/T_{eq}$, so we can get the formula to calculate parameter T_i:

$$T_i = a^2 T_{eq} \tag{6.17}$$

where a is the symmetrical distance between $1/T_i$(or $1/T_{eq}$) and ω_d and usually taken between 2-4. Here, it is chosen as 2.

Using equation (6.14), the proportional gain for PI controller is found by:

$$K_p = \frac{2V_{dc,ref}C}{3V_d a T_{eq}} \tag{6.18}$$

The C used in the formula is the equivalent capacitance in DC side for MMC, equal to:

$$C_{eq} = 3\frac{C_{SM}}{N} \tag{6.19}$$

N is the inserted number of SMs per phase.

Using the system values, the parameters of PI controller for DC voltage control is calculated as K_p=15, T_i=1.11e-3. After adjusting in the Simulink, K_p=3, T_i=0.005. The dynamic response of DC control is shown in Figure 6.15. The DC side voltage source is replaced by two resistors. As we can see, the DC voltage can still track the reference when a 5% step change was set in DC voltage reference. After about 0.1s, DC voltage goes back to steady state and the dynamic response of a typical second order system was observed.

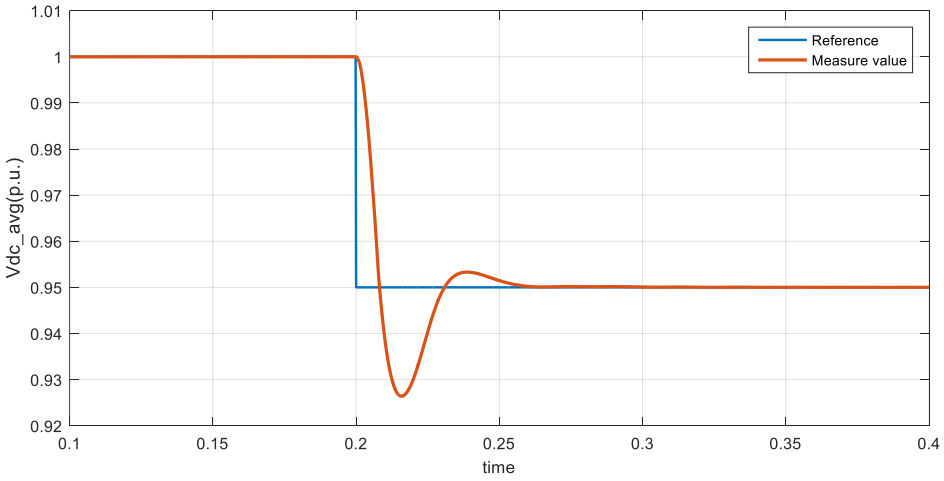

Figure 6.15 Dynamic response for DC voltage control

It should be noticed that only the average DC voltage is plotted in the Figure 6.15, which can be calculated by the formula below：

$$V_{dc\_avg} = \left(\sum_{x=1}^{2N} V_{ca,x} + \sum_{x=1}^{2N} V_{cb,x} + \sum_{x=1}^{2N} V_{ca,x} \right) / 6 \tag{6.20}$$

By using the average value, the high frequency components caused by switching transients of different capacitors were eliminated in step response waveform.

6.4.3 Power Control

The control diagram with transfer function of each part is repeated in Figure 6.16.

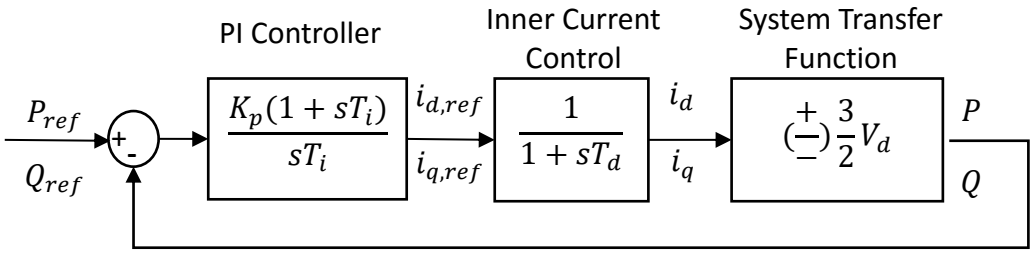

Figure 6.16 Power control Loop with transfer function

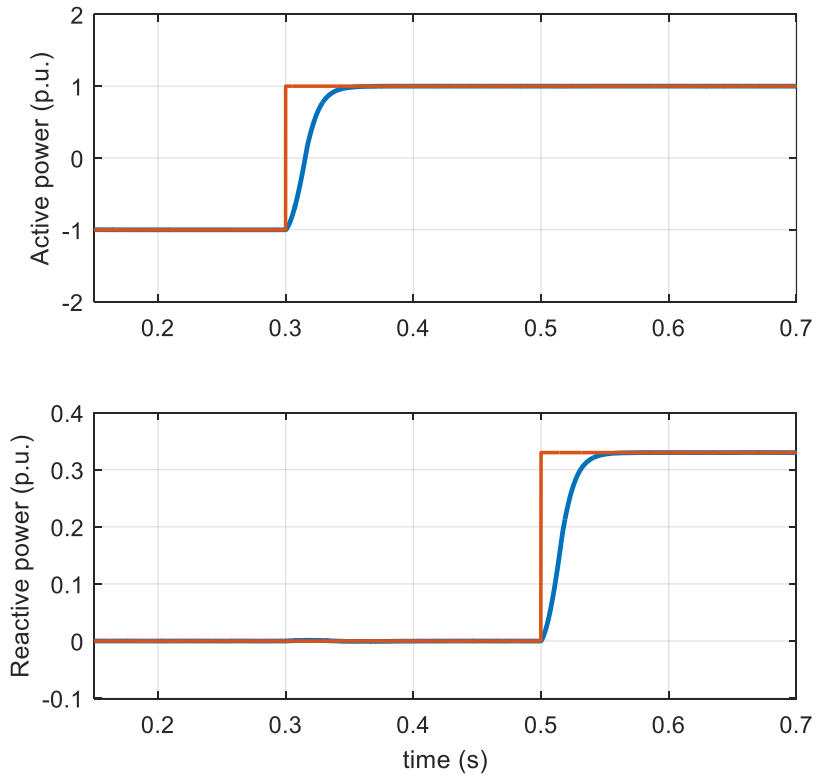

Figure 6.17 Active and reactive control response

The PI controller tuning method is the same as that for DC voltage control: symmetrical optimum. The equations for parameter calculation are:

$$T_i = a^2 T_{eq} \tag{6.21}$$

$$K_p = \frac{2}{3V_d} \tag{6.22}$$

After calculating K_p=4.7e-5, T_i=1.11e-3. After adjusting in Simulink, K_p=8.61e-4, T_i=3.75e-3. The controller is tested by reversing the active power from -1p.u. to 1 p.u. and giving a 0.33 p.u. step change to reactive power. The results are shown in Figure6.17. Both active and reactive power track reference very well and good dynamics are observed.

6.5 Synchronizing Three Controllers to the System

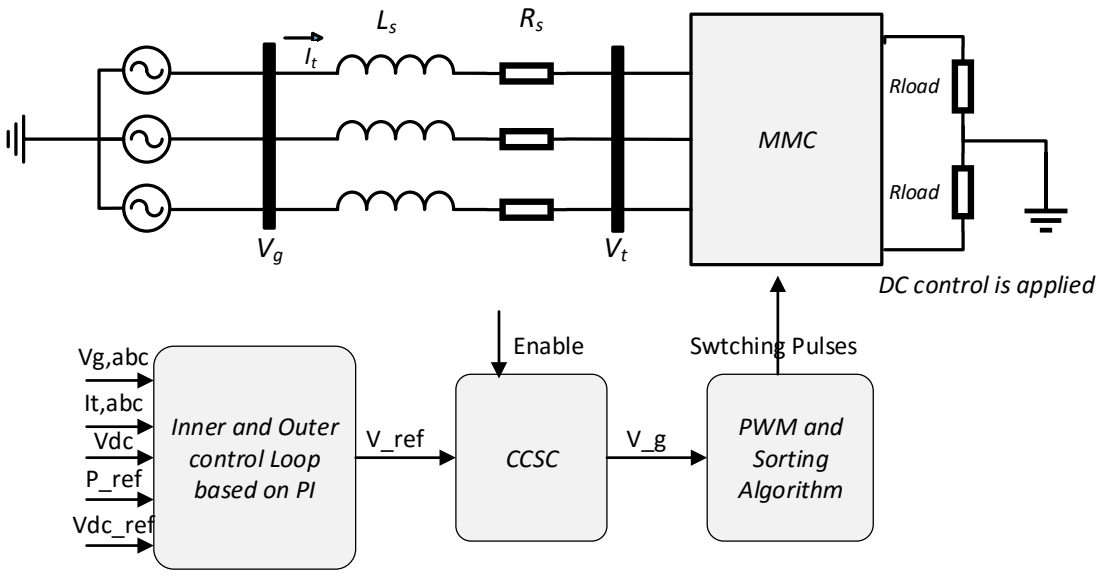

Figure 6.18 The control diagram of System without Wind Farm

In this section, AC side current control (the DC voltage control and reactive power reference control), CCSC introduced in Section 5.3 and sorting algorithm for voltage balancing were combined together and simulated. The system diagram is shown in Figure 6.18. The detailed configuration of each controller has already been shown in above sections separately. The combination of them and the connections between controllers are shown in Appendix.

The ability of reactive control was tested by step response. The CCSC and voltage balancing control behavior during reactive power change was evaluated. At t=0.2s the CCSC is enabled and at t=0.4 the reactive power has a step change from 0 p.u. to 0.33 p.u. The results are shown in Figure 6.19.

It can be seen that the reactive power followed reference in Figure 6.19 (b) and the DC voltages were not affected by the step change of reactive power and kept at 1p.u. by DC control in Figure 6.19 (c). From 6.19 (d) and (e), the CCSC effectively reduced the circulating current and also the capacitor voltage ripples both before and after the

transient. However, it brought DC voltage noise as shown in Figure 6.19 (c), which is inevitable as it is the reason that the circulating current is suppressed. In addition, it is noticed in Figure 6.19 (e), that the CCSC also brought some small frequency harmonics to the SM voltages. The reasons will be studied in the future.

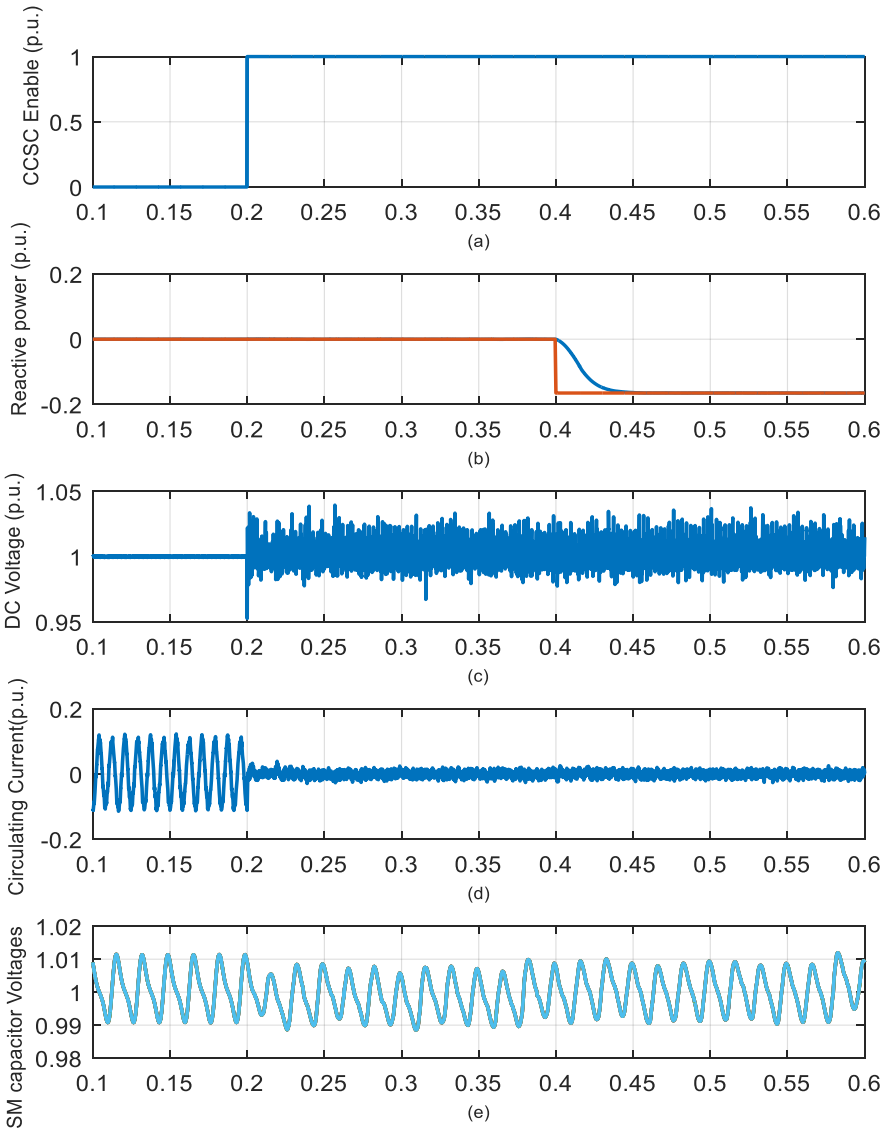

Figure 6.19 (a) enable signal for CCSC (b) reactive power and reference value (c) DC voltage (d) circulating current (e) SM capacitor voltages in upper arm of phase A (the voltages are balanced by using sorting method)

6.6 Model Predictive Control

The traditional PI controller based AC side current control plus extra SM capacitor voltage balancing and circulating current suppressing control were simulated and

introduced in above sections. In this section, the simulation of relatively new control method for MMC, model predictive control will be introduced. Again, the MPC simulated here is simplified name of FCS-MPC. The overall control block diagram of the system using MPC is shown in Figure 6.20. Only the wind farm side MMC is simulated and the DC side is represented by DC sources. Wind farm is represented by an ideal grid in order to focus on the control algorithm of MMC.

The AC side current references were decided by the reference active and reactive power reference according to the energy equations (4.25), (4.26) on dq frame.

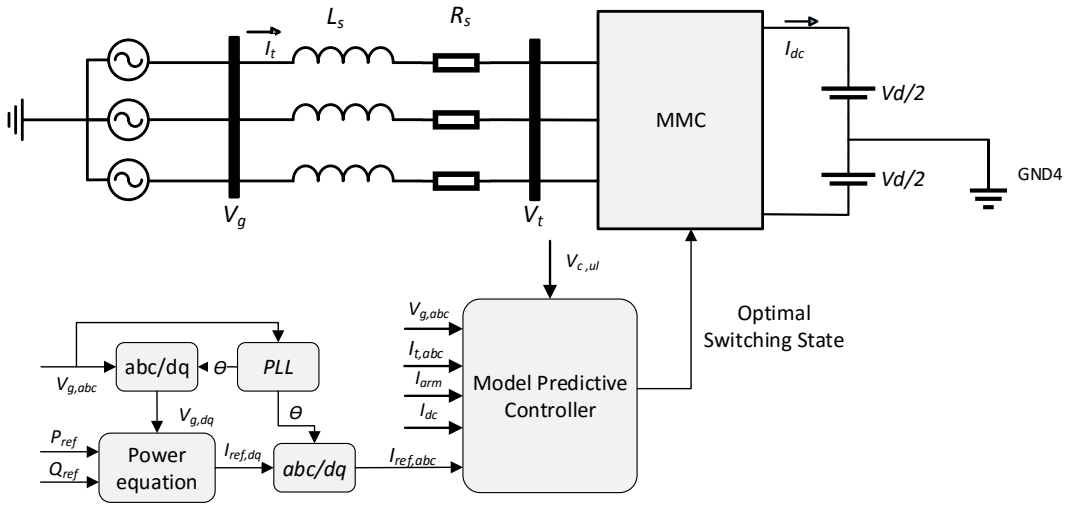

Figure 6.20 The control diagram of MPC

The principles of MPC have been introduced in Chapter 4, which will be briefly repeated here again and the simulation method and results are presented afterwards.

The dynamic equations for AC side current, SM capacitor voltages and circulating current are shown by equations below respectively based on the mathematical model in section 2.1.2 and assuming arm resistance is zero.

$$V_{u,j} - V_{u,j} = -(L_{arm} + 2L_s)\frac{di_j}{dt} + 2R_s\frac{di_j}{dt} + 2V_{g,j} \tag{6.23}$$

$$I_{dc} = C\frac{dV_{dc}}{dt} \tag{6.24}$$

$$\frac{Vdc}{2} - \frac{V_{l,j} + V_{u,j}}{2} = L_{arm}\frac{di_{diff,j}}{dt} \tag{6.25}$$

Based on these three equations and assuming a sampling period of T_s, the predicted quantities can be deduced by Euler approximation as shown by equation (6.26),(6.27) and (6.28) respectively.

$$i_j(t+T_s) = -\frac{1}{K}\left(\frac{V_{l,j}(t+T_s) - V_{u,j}(t+T_s)}{2} - V_{g,j}(t+T_s) - \frac{L'}{T_s}i_j(t)\right) \tag{6.26}$$

$$i_{diff,j}(t+T_s) = i_{diff,j}(t) + \frac{T_s}{2L_{arm}}[V_{dc} - V_{u,j}(t+T_s) - V_{l,j}(t+T_s)] \quad (6.27)$$

$$V_{cj}(t+T_s) = V_{cj}(t) + S * \frac{i_{k,j}}{C} T_s \quad (6.28)$$

where S represent the switch state for each SM, S=1 for switched-on SM and S=0 for switched-off SM.

And the cost function is defined as below. Three terms represent three different control purposes above respectively.

$$\mathrm{J} = \left|i_{jref}(t+T_s) - i_j(t+T_s)\right| + \lambda_c \left(\sum_j \left| V_{c,j}(t+T_s) - \frac{V_{dc}}{N} \right| \right) + \lambda_{cir} \left| i_{diff}(t+T_s) \right| \quad (6.29)$$

As all the terms in cost function are errors between predicted value and reference value, the MPC strategy aims to choose the switch state which results in the minimum value of cost function. Since there are always *N* SMs on and *N* SMs off in each phase, the total number of switching states are C_{2n}^n. The flow chart of the MPC algorithm is shown in Figure 6.21.

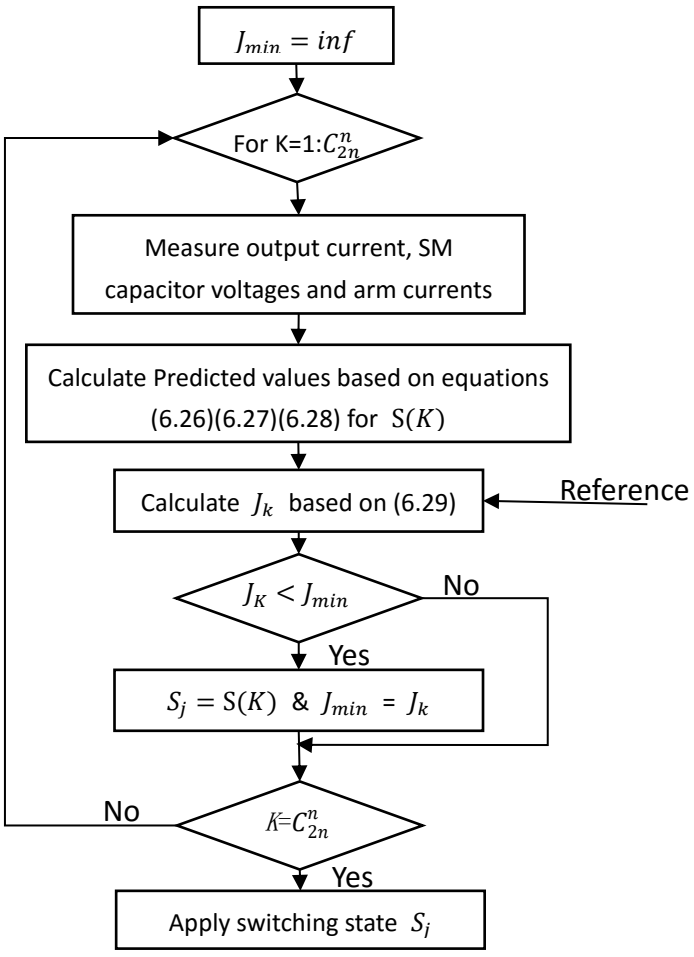

Figure 6.21 The Flowchart of MPC strategy

The model in Simulink for calculating optimal switching date of phase A, "*g*_a" is shown in Figure 6.22. The block, "MATLAB function" describes the flow chart above and the Matlab code is shown in Appendix.

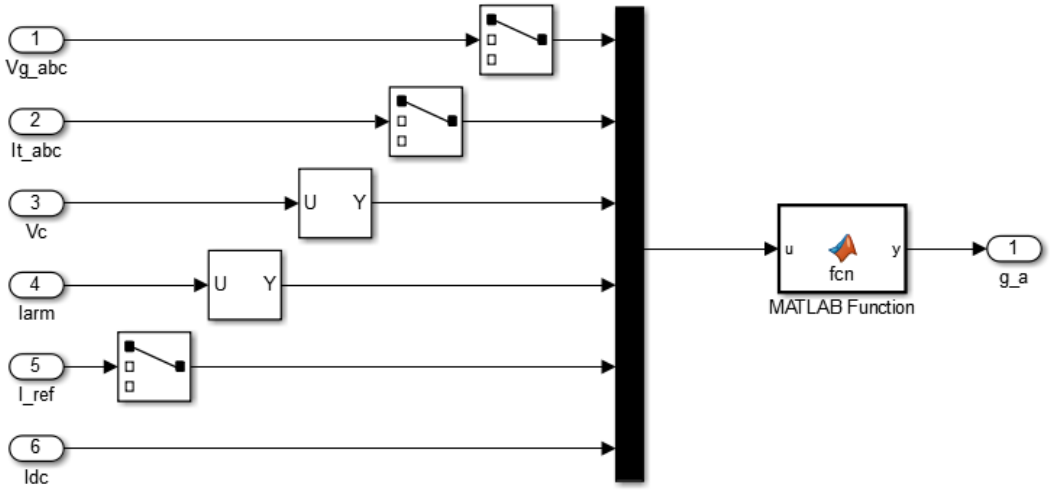

Figure 6.22 The model of MPC in Simulink

6.6.1 Tuning the weighting Factor

There are two weighting factors λ_c and λ_{cir} in cost function (6.29) needing to be decided. They determine the priority of each control constrains. Relatively higher value means higher priority and better performance on corresponding control purposes. There is still no numerical method to calculate the weighting factors, so that only the empirical method is used, which is presented in [91]. The procedure can be summarized as:

Firstly, set both λ_{cir} and λ_c zero. Then increase λ_c gradually and observe the SM capacitor voltages and AC side current. It was found by simulation that with the increase of λ_c, the voltages were balanced better and better, but the errors between AC side current and reference value become bigger. At some value of λ_c, the error on AC current became unacceptable. Choose the value of λ_c a little bit less than the critical value to leave some space for circulating current control. After that, use the same method to determine λ_{cir}. Choose a criteria for voltage balancing, based on which choose the λ_{cir} to achieve the best performance for circulating current suppression.

By simulation, it was found that it was hard to achieve the best performance for all of the three control purposes, there was always some trade-off between them and the value of them chosen in the following simulation is λ_c= 6 and λ_{cir}=1.

6.6.2 Switching Frequency Problem

Although sampling frequency can be chosen constant, the switching frequency assigned to SMs is not fixed. Because the switching state may changes every time the MPC function finishes executing. Therefore, the switching frequency will be very high, which may not be a problem for simulation, but a serious problem in reality. In order to solve them, a trigger block was used in the model to force the MPC function executing only once every 100 μs, so that the switching state would be held during 100μs period until next trigger signal arrived. In this way, the switching frequency was fixed and could be varied according to requirement. In addition the executing speed of the model became much faster and the performance of the controller did not change a lot before and after using trigger block according to the results of simulation.

6.6.3 The Simulation Results

Based on the theory above, the model was built in Simulink, three control purposes were tested and realized one by one, the sampling time used is 100e-6s:

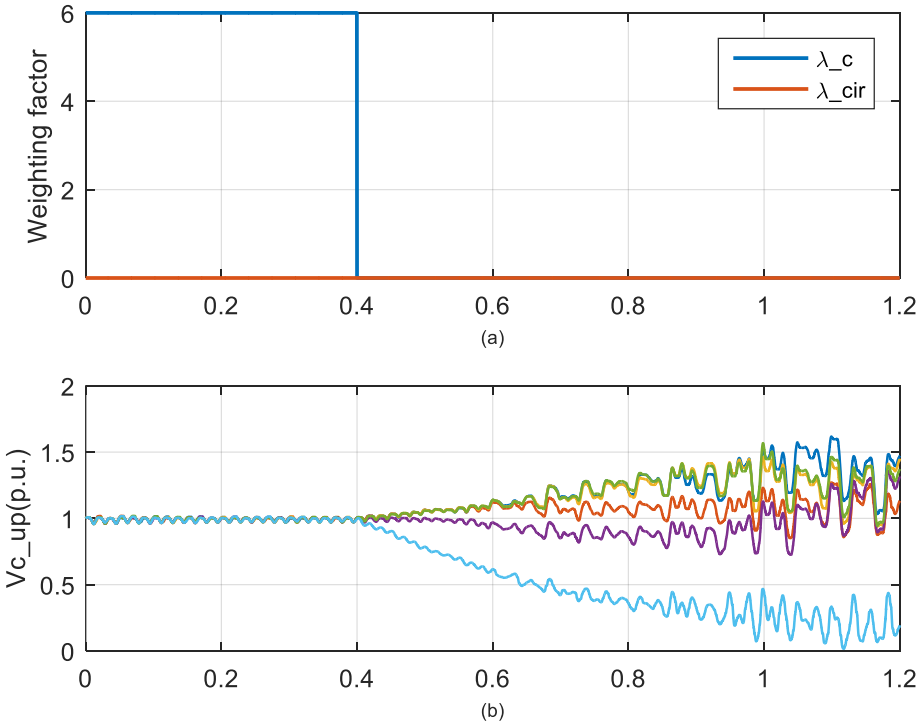

Figure 6.23 Testing voltage balancing control (a) weighting factor (b) SM voltages of upper arm in phase A

(1) **SM Capacitor Voltage balancing**. Initially, the system operated at steady state condition, active power reference was set at rated value 20MW, reactive power reference was 0 and capacitor voltage balancing was enabled (λ_c= 6). At t= 0.4s, voltage balancing was disabled by setting λ_c to be 0. During the whole process, the

circulating current control was always disabled. The response is shown in Figure 6.23.

As we can see, before t=0.4s, the capacitor voltages of upper arm in phase A was balanced well at the nominal value. After the voltage control disabled, they became badly unbalanced, which verified the effect of voltage balancing control.

(2) **Circulating current suppressing control**. The same as above, the system operated at unity power factor and the capacitor voltage balancing control was enabled, but circulating current control was disabled (λ_c= 6, λ_{cir}=0) initially. At t =0.8s, circulating current control was enabled (λ_c= 6, λ_{cir}=1). Figure 6.24 shows the response.

Figure 6.24(a) shows the change of weighting factor. Figure 6.24(b) shows the circulating current. As depicted, circulating current was well suppressed from 0.6 p.u. to less then 0.2 p.u. for peak value after the activation of circulating current control. Figure6.24(c) illustrates the SM capacitor voltages of phase A (total 12 SMs). As can be seen, the voltage ripples were reduced, the voltage value between upper arm and lower arm was balanced better after t= 0.8s, which was the reason of the elimination of circulating current. Figure 6.24(d) and (e) illustrate the output voltage and current of MMC respectively. The amplitude and the shape of waveforms are reasonable. However, if look in detail, the amplitude of voltage were unbalanced between three phases before t=0.8s , which is because of the unbalance between upper and lower arm SM voltages. After, t=0.8s, this unbalance was eliminated. All the diagrams verify the function of the predictive circulating current control.

(3) **AC side Current Control (Energy Control).** Initially, the system of Figure6.20 operated with P_ref =0, Q_ref =0 and both capacitor voltage balancing and circulating current control were enabled (λ_c= 6, λ_{cir}=1). At t= 2.8s, a step change was assigned to active power reference to transfer 1p.u. active power from AC side grid to DC side. At t= 3.2s, reactive power command was step changed to transfer 0.33 p.u. power from DC side to AC side. The results of these two step change are shown in Figure6.25.

Figure 6.25(a) and (b) are the power reference value and measured value respectively. Compared these two diagrams, it could be concluded that both active and reactive followed the reference well and the dynamics response was fast, almost without using time. However, the ripples of active and reactive are a little bit high, which may cost some errors. Figure 6.25(c) illustrated the power transferred to the DC side. As can be seen, the power transferred was around 1p.u., which is reasonable and no obvious losses can be observed. But there were some oscillations when power changed, which may be caused by the interaction between SM capacitors and arm inductors. Figure6.25(d) and (e) show the circulating current and SM capacitor voltages in phase A respectively. Both of them were controlled well and almost the same as that shown in Figure 6.24. In addition, no obvious changes occurred when power changed so that the inner dynamics were not affected by the outer dynamics of MMC, which is expected.

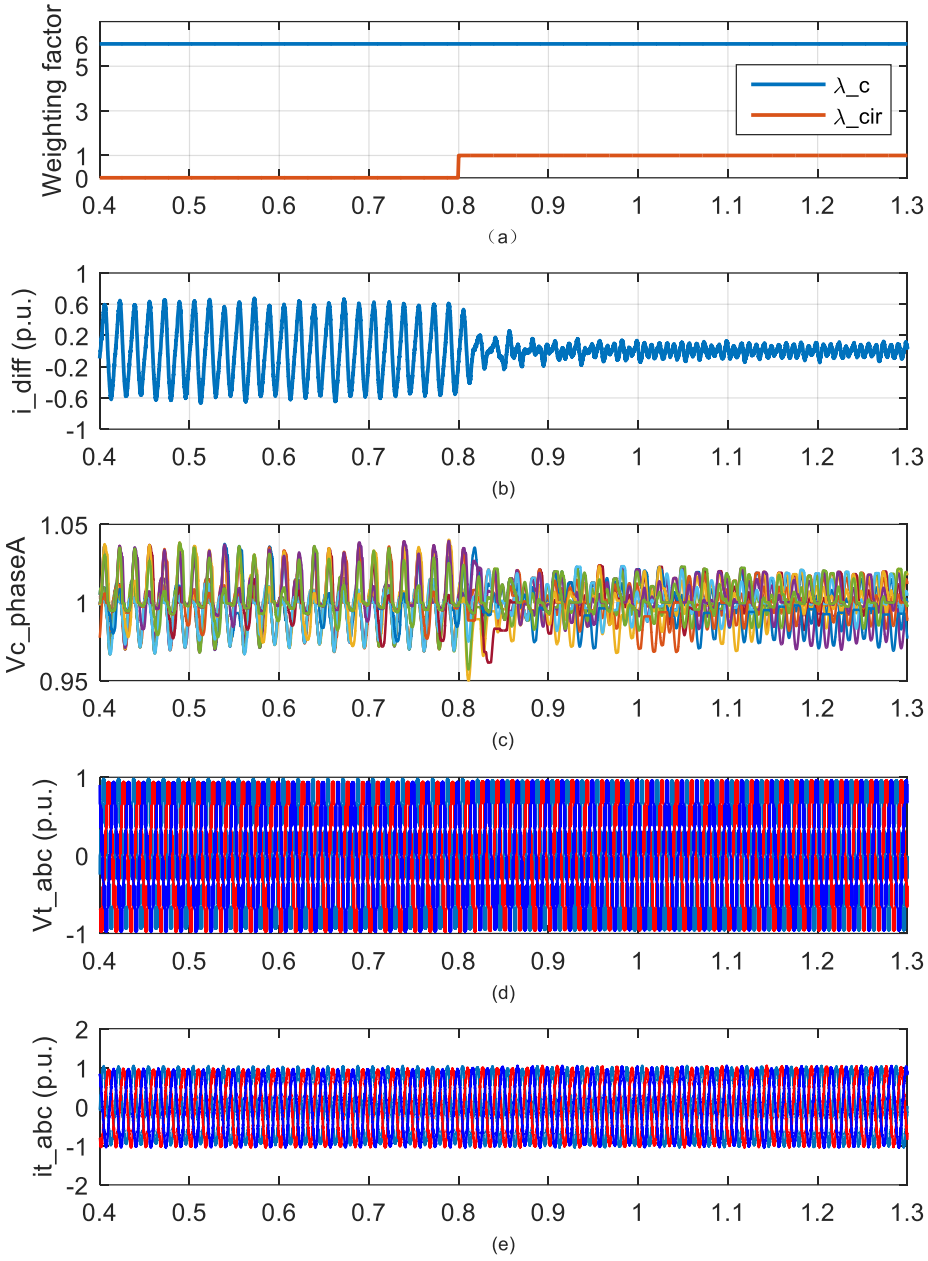

Figure 6.24 Testing Circulating Current Control (a) weighting factors (b) circulating current of phase A (c) SM voltages of phase A (d) output voltages (e) output currents of MMC (All the values are in p.u.)

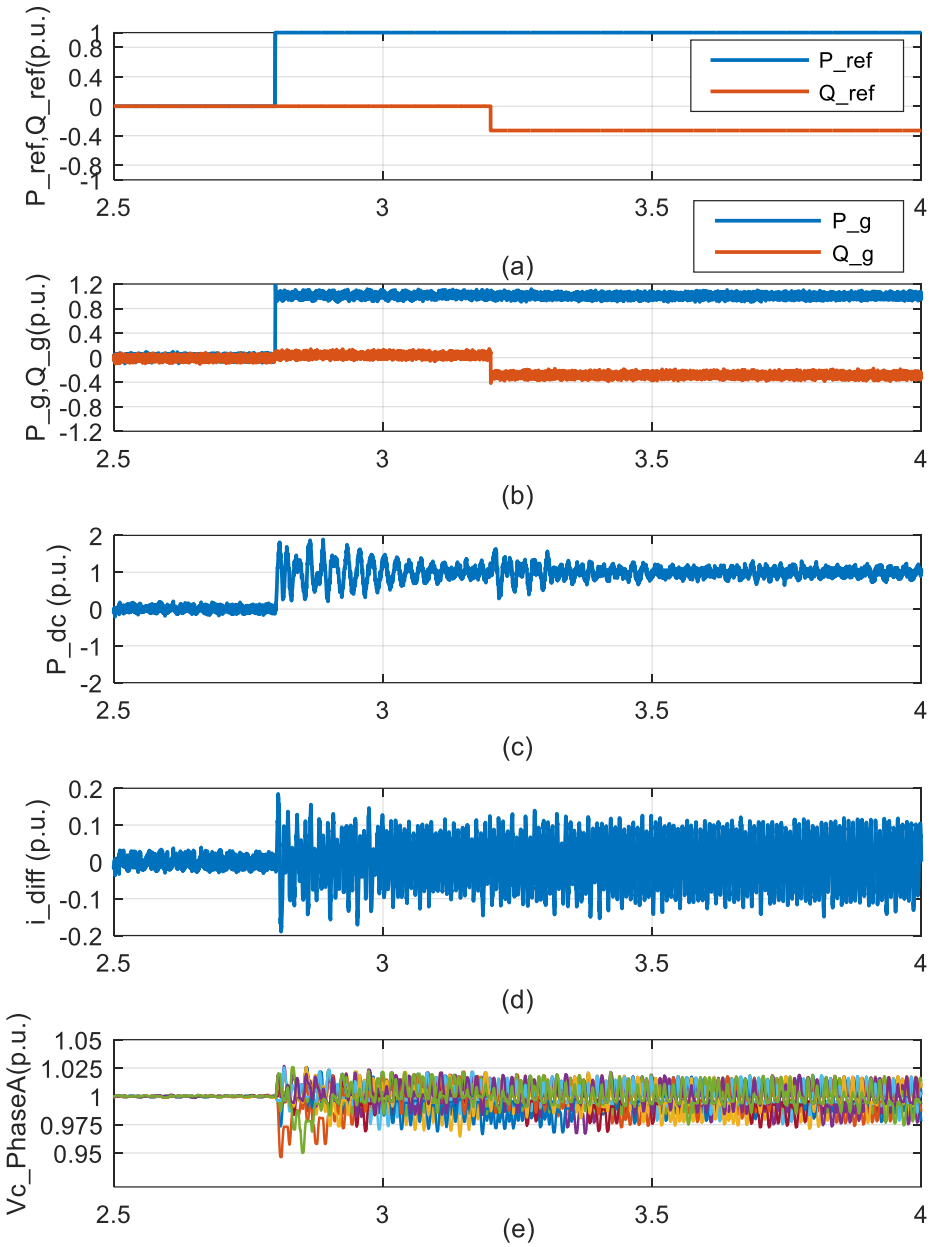

Figure 6.25 Testing of AC side current control (a) active and reactive reference (b) measured active and reactive power at grid bus (c) active power transferred to DC side (d) circulating current (e) SM capacitor voltages of phase A (all values are in p.u.)

6.6.4 Discuss

The simulation above verified the proposed MPC strategy, and the controller can balance the voltages of SMs, suppress circulating current and control the power at the

same time, which make the system simple and fast. However, there are still some problems occurred during simulation:

Firstly, the trade-off between three control performances. As we can see from Figure6.25 (b), (d) and (e), neither of the three controlled quantities got the best performance: active and reactive power had some ripples; circulating current still had some space to be suppressed further and SM voltages were not perfectly balanced. If the best performance of one of the control purposes is achieved by increasing corresponding weighting factor, the other two or one my go badly. Thus, there must be some trade-off between different control constrains by using MPC on MMC.

Secondly, the computational burden problem. In the proposed MPC strategy, the cost function is calculated for all possible switching states, the number of which is C_{2n}^{n}. That is a large number especially for MMC with large number of SMs, which makes the computational burden heavy and become a problem for hardware implementation or even for simulation. One possible solution called indirect finite control set model Predictive control (IFCS-MPC) is proposed in [85], which only concerns about the numbers of inserted SMs and uses sorting algorithm for voltage balancing, it is simulated in next section.

6.6.5 Indirect Finite Control Set Model Predictive Control

The method separate the voltage balancing control from predictive control. The difference is that the cost function is evaluated only for all possible inserted numbers of SMs in upper and lower arm, instead of for all possible switching states. So that the number of all combinations reduced from C_{2N}^{N} to N+1 (if N SMs per phase are ensured to be on at all time), which dramatically reduced the computation burden of Model predictive controller, the output of which is connected to the voltage balancing controller using sorting algorithm.

In IFCS-MPC, only the sums of the total SM voltages V_u^{Σ}, V_l^{Σ} in upper and lower arm respectively are input rather than the voltage of each SM. The arm voltages are calculated by:

$$V_{u,l} = \frac{n_{u,l} * V_{u,l}^{\Sigma}}{N} \tag{6.30}$$

where $n_{u,l}$ are the inserted number of SMs in upper or lower arm

The cost function is also changed that only the errors on the sums of SM voltages in upper and lower arms are concerned, which is shown below:

$$\mathrm{J} = \left|i_{jref}(t+T_s) - i_j(t+T_s)\right| + \lambda_c\left(\left|V_{dc} - V_u^{\Sigma}\right| + \left|V_{dc} - V_l^{\Sigma}\right|\right) + \lambda_{cir}\left|i_{diff}(t+T_s)\right| \tag{6.31}$$

The flowchart for IFCS-MPC algorithm is shown in Figure6.26. Follow the same procedure as Figure 6.25 to simulate the IFC-MPC, the results are shown in Figure 6.27.

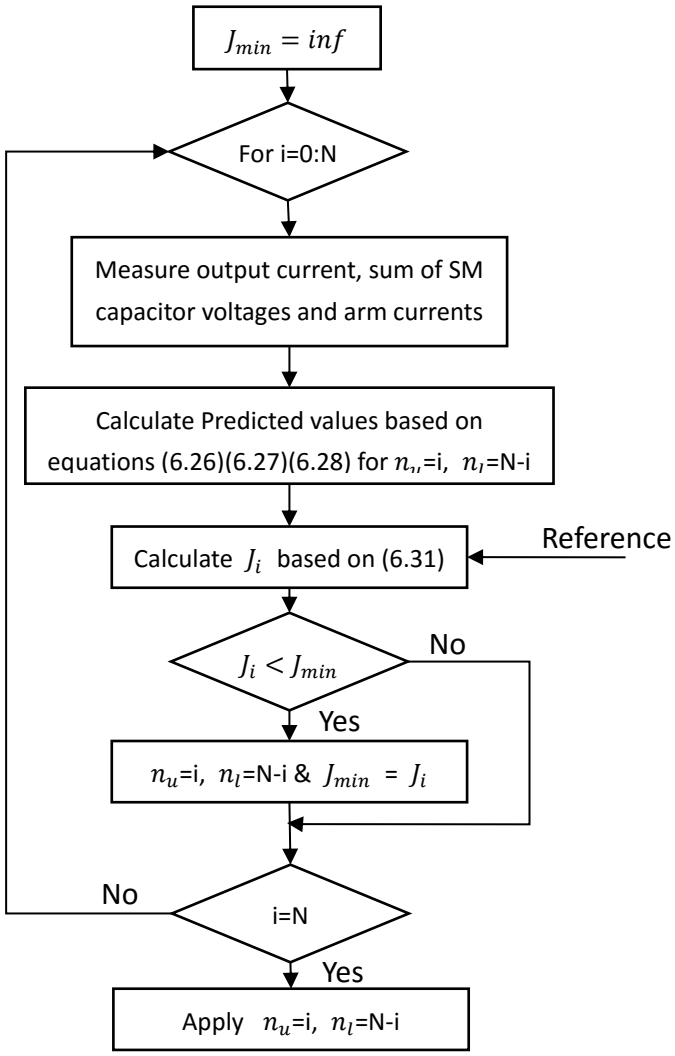

Figure 6.26 The flowchart of IFCS-MPC

Compared Figure6.27 and Figure 6.25, IFCS-MPC almost got the same performance on power control and circulating current suppression. The only difference is on the voltage balancing control. The voltages shown in Figure 6.27 were much better balanced around rated value; the ripples are also much smaller, which is about 2.5% peak-to-peak value compared to 5% in Figure 6.27. It could be concluded that the traditional sorting algorithm got better performance than predictive control.

Actually, this algorithm does not reduce the total computation burden for the whole system as all the SM voltages still need to be measured for voltage balancing controller and sorting algorithm needs huge computational efforts as well. The advantage is that IFCS-MPC separate the computation burden to two controllers, which may make it more realizable in reality.

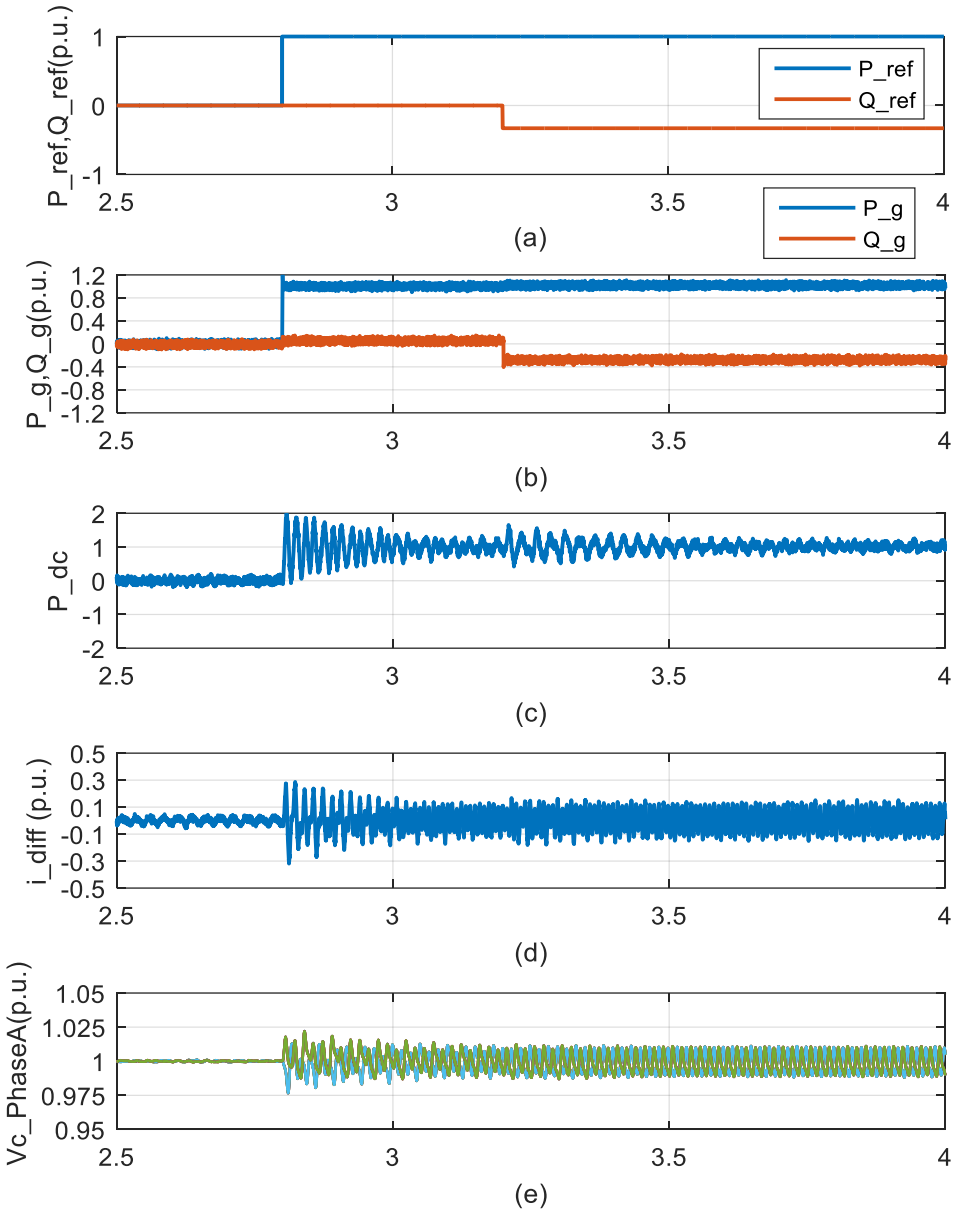

Figure 6.27 Testing of IFCS_MPC strategy (a) active and reactive reference (b) measured active and reactive power at grid bus (c) active power transferred to DC side (d) circulating current (e) SM capacitor voltages of phase A (all values are in p.u.)

6.7 Comparison between MPC and Traditional Method

In this section, the direct finite control set MPC method (distinguish with IFCS-MPC) is compared with PI controller based cascade control method with CCSC introduced in Section 6.2 for circulating current control and sorting algorithm for voltage balancing control. The results are summarized below:

1. **Performance of circulating current elimination and voltage balancing.** Comparing Figure6.19 (d), (e) and Figure6.25 (d), (e) respectively, it is found that Both method controlled the circulating current and capacitor voltage in an acceptable range, but traditional method had an obvious better performance on both of them. Using traditional method, the circulating current was suppressed to almost 0 compared to 0.1p.u.(peak value) by MPC; the voltages were balanced better in each arm and the ripple was about 2% compared to 5% by MPC.

2. **Performance on reference following and dynamic response.** Comparing Figure6.19(b) and Figure 6.25(b), it is concluded that both methods controlled the system follow the power reference well, but traditional method resulted in less error, which was almost zero, while MPC resulted some ripples around reference value. However, MPC had considerably better dynamic responds to step changes. It took no visible time to reach the new reference value for MPC, while it took more than 0.05s to reach a 0.33 p.u. change in reactive power reference for PI controller. In addition, expected amount of power was transferred to the DC side by both control method, as shown by Figure 6.25(c) and Figure 6.19(d)

3. **The simplicity of the system.** MPC can control the AC side current, SM voltages and circulating current at the same time, which make the system simpler and easy to debug. As for traditional method, three separate controllers are needed for three control purposes, which make system complex. Based on the experience of simulation, synchronizing these three controllers is not easy. Also, for hardware realization, MPC may be much easier.

4. **Comments on switching frequency.** Normally, higher switching frequency results in better performance but higher losses. As the losses is not analyzed in this thesis, the controller with higher switching frequency may have an advantage on performance. For MPC, the switching frequency is 10 kHz and PI based method uses 3.6 kHz (600 Hz for carrier waveform frequency and 6 SMs per arm, so overall switching frequency is 600*6=3.6 kHz). Even through traditional method used smaller switching frequency, it still had better performance except dynamic response speed, which makes the conclusions above even more convincing. By reducing the switching frequency of MPC in simulation, the advantage of fast dynamic response still existed

In summary, the traditional method can get more precise performance, while MPC has simpler configurations and is able to add more control purposes easily and flexibly. In addition, the fast dynamic responses is another advantage of MPC

6.8 Simulation of the Whole System with Wind Farm Model

In this section, one option of overall control scheme for the whole system with wind farm model is proposed, which is mostly based on model used in section 6.5, but wind turbine model was added to replace the gird model. Thus, PI controller based cascade control was adopted for AC side current control, CCSC method for circulating current

control and sorting algorithm for SM capacitor balancing. The whole system shown in Figure 5.1 is simulated and the model in Simulink is shown below:

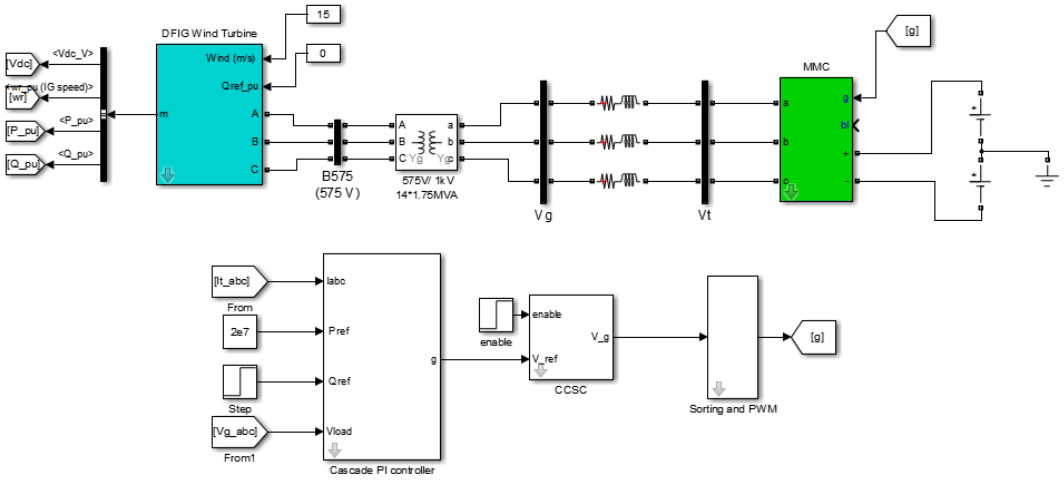

Figure 6.28 The model of the whole system in Simulink

The wind farm model consists of 14 wind turbines. Each turbine produces rated power 1.6 MW using doubly-fed induction generator at rated wind speed 15 m/s. The wind farm model is a pre-built model in Simulink Demo, in which the average model of back to back converters for generators was adopted in order to increase the speed of simulation.

In this simulation, the purpose of AC side energy control is to control the system to transfer the active power produced by wind turbine to DC side, in addition, provide reactive compensation for wind farm if necessary. Not like ideal grid, the wind farm can only produce fixed amount of active power (providing the wind speed is constant at 15m/s), so that the active power reference was always set at rated power 20 MW. The reactive power was set at zero at the beginning and had a 1MVar step at t=0.4s to test the reactive compensation ability. The CCSC was enable at t=0.3s and sorting algorithm was applied from beginning to the end to balance the voltages. The results are shown in Figure 6.29.

Figure 6.29 (a) and (b) illustrate the reference and measured value for active and reactive power respectively, which shows that both active and reactive power follow the reference. It took 0.1s for reactive power to follow the new reference after step change. After that, the HVDC system compensated 1MVar reactive power for wind turbine. Figure 6.29 (c) proved that 1 p.u. active power was transferred to the DC side. However, the ripple was high (almost 0.2p.u for peak value), which may be caused by the ripple on SM voltages because there were always energy exchange between DC source and SM capacitors. In addition, the ripples on the capacitors were squared and shown on DC side power waveform. At t= 0.3s, the CCSC was enabled and Figure 6.29(d) verified the performance of the controller. The SM voltages were kept balanced during the whole procedure, but low frequency harmonics can be observed. The waveforms

were almost the same as those in Figure 6.19.

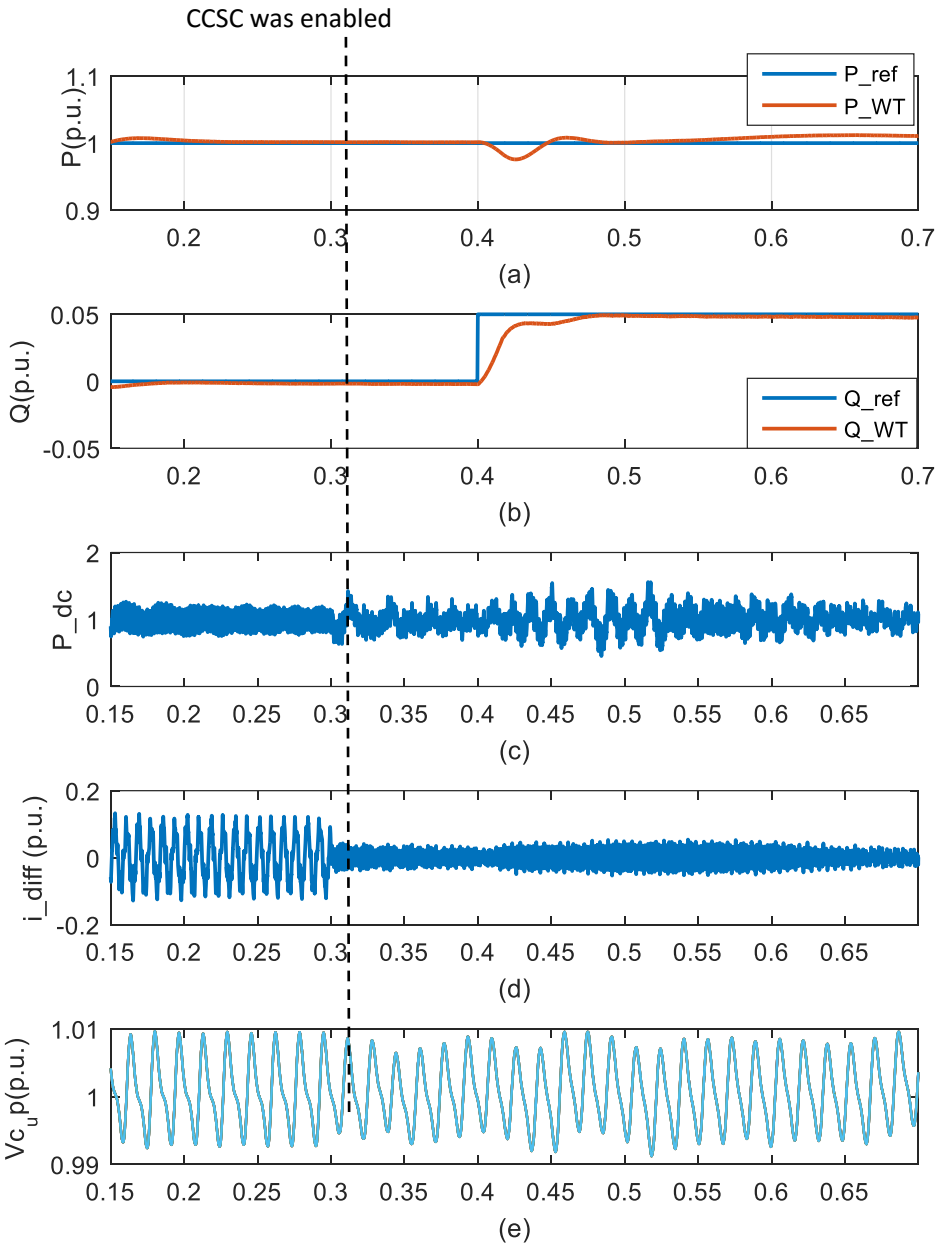

Figure 6.29 testing complete system (a),(b) reference and measured values for active and reactive power at the output of wind farm (c) DC side power (e) Circulating current (e) SM capacitor voltages of upper arm in Phase A

It should be noted that the step change of reactive power cause the oscillation on active power, which further cause the oscillation on DC side power and circulating current. This may because that wind turbine did not need any reactive power. Pushing extra reactive power cause the wind turbine oscillation inside and it took time to be stable again. The detailed study of wind turbine model was not done in this thesis, as

well as the situation of power control at varied wind speed.

6.9 Summary and Discussions

In this chapter, the chosen control strategies summarized in chapter 5 was simulated. The simulation methods were introduced and all the simulation results were presented and analyzed. In addition, different control methods for same control purposes were compared. Based on these, some conclusions were obtained in this chapter:

- CPS-PWM modulation resulted correct amplitude of output voltage and almost sinusoidal output current. In addition, the SM voltages were well balanced even without balancing controller. Compared to CPS-PWM, NLM had a much worse performance. When the number of SMs per arm is only 6, NLM lost much information and introduced harmonics to the output current. Also because the switching frequency was very low, the capacitor were much unbalanced. This method may only suitable for the system with large number of arm SMs
- Both sorting method and MPC balanced the SM voltages to an acceptable range, but sorting method performed better with much less difference between arm capacitors. However, sorting method slow down the simulation a lot, which increase the computation burden.
- CCSC method shown in section 6.2 had a more superior performance over energy control method in circulating current suppression. In addition, CCSC were easier to tune and synchronize with other controllers. The advantage of energy control is that it can control the arm energy flexibly. In addition, Compared to MPC in circulating current control part, these two methods mentioned above performed better.
- The simulations show that with the suppression of circulating current, the ripple of SM voltages were reduced, but the DC side power ripple was increased. In addition, some lower frequency harmonics were introduced to SM voltages
- For AC side current control of MMC in HVDC system, traditional PI based method had better performance on reference tracking, while MPC resulted higher ripple around references. However, much faster dynamic responses were achieved by MPC. Also, MPC can achieve all three control purposes at the same time, which simplified the systems. While PI based method needed other controllers to achieve extra functions and the synchronization between different controllers were not easy.
- One reason that MPC had less precision on each control aspects is that there must be trade-off between control purposes when all of them are controlled at the same time.
- One complete system with wind farm model, wind farm side MMC and DC side

voltage sources using PI controller based AC side current control, CCSC for circulating current suppression, sorting method for voltage balancing was simulated and the performance was verified in section 6.8. It can be an example for comprehensive control of HVDC system for offshore wind farm.

7. Conclusions

7.1 Summary

The current control of MMC can be mainly divided into three aspects: SM voltage balancing control, circulating current control and AC side current control. The main purpose of this thesis is to review the control strategies for MMC in the literature and verify some of them by simulations. Because of the rapid development of offshore wind farm and the requirement for high voltage and high power transmission system, the study of MMC was based on the application of HVDC system for offshore wind farm.

For this purpose, some background knowledge about MMC and HVDC system was introduced in chapter 2 including the structure and mathematical model of MMC, the topologies and converter technologies of HVDC system, as well as the control scheme for HVDC system.

Because MMC is multilevel VSC, most of current control strategies for two-level VSC may be extended to control MMC. Thus, the control strategies for two-level VSC were reviewed first consisting of linear control methods and non-linear control methods. After that, most of control strategies in literature for MMC in modulation and three control aspects were reviewed. The principles were explained in detail and control diagrams were presented. The name of these control strategies are summarized below

- Modulation method
  - PWM modulation- carrier phase shifted and carrier disposition PWM
  - Space vector modulation
  - Nearest level modulation
- Voltage balancing Algorithms
  - Sorting method
  - Method based on carrier shifting
  - Method based on averaging and balancing control
  - Method based on model predictive control
- Circulating current suppressing control
  - Method based on total energy and energy balancing control
  - Method based on double line-frequency dq coordinate
  - Method based on Predictive current control
  - Method based on PR controller and repetitive controller
- AC side current control
  - PI controller based cascade control
  - Model predictive control

- Hysteresis current control
- Methods based on bilinear model

At last, the model of MMC was built in Simulink and some of the control strategies were tested and compared, which is summarized in Chapter 5. Some conclusions were gained from simulations:

- CPS-PWM modulation resulted correct amplitude of output voltage and almost sinusoidal output current. In addition, the SM voltages were well balanced even without balancing controller. These are all better than NLM. NLM lost much information and introduced harmonics to the output current as the number of SMs per arm is only 6. Also because the switching frequency was very low, the capacitor were much unbalanced. This method may only suitable for the system with large number of arm SMs
- Both sorting method and MPC balanced the SM voltages to an acceptable range, but sorting method performed better with much less difference between arm capacitors. However, sorting method slow down the simulation a lot, which increase the computation burden.
- CCSC method shown in section 6.2 had more superior performance over energy control method in circulating current suppression when more amount of circulating current were eliminated by CCSC. In addition, CCSC were easier to tune and synchronize with other controllers. The advantage of energy control is that it can control the arm energy flexibly. In addition, Compared to MPC in circulating current control part, both of these two methods performed better.
- The simulations show that with the suppression of circulating current, the ripple of SM voltages were reduced, but the DC side power ripple was increased, which was reasonable and show how the circulating current was reduced to a certain extent. Also, some lower frequency harmonic (lower than fundamental frequency) was introduced to capacitor voltages by circulating current control methods.
- In AC side current control of MMC in HVDC system, traditional PI based method had better performance on reference tracking, while MPC resulted higher ripple around references. However, much faster dynamic responses were achieved by MPC. Also, MPC can achieve all three control purposes at the same time, which simplified the systems. In addition, even more control constraints can be added. While PI based method needed other controllers to achieve extra functions and the synchronization between different controllers were not easy.
- One reason that MPC had less precision on each control aspects is that there must be trading off between control purposes when all of them are controlled at the same time.
- One complete system with wind farm model, wind farm side MMC and DC side voltage sources using PI controller based AC side current control, CCSC for circulating current suppression, sorting method for voltage balancing was

simulated and the performance was verified in section 6.8. It can be an example for comprehensive control of HVDC system for offshore wind farm.

7.2 Thesis contribution

Since MMC was first proposed in 2002, intense research has been done on its control strategies. However, most of papers only focus on one control aspects or one control algorithms. This Thesis provides a general overview of most of control strategies in all three control aspects, voltage balancing, circulating current suppressing and AC side current control with detailed explanations and clear classification. In addition, some of methods were verified by simulations and different control methods for same control purposes were compared. This provides readers good reference in control aspects of MMC in both theory and simulation, which could be a basis for further advanced study on MMC or similar topologies.

Also, a complete targeted system with wind turbine models and controllers for all three control aspects was simulated and verified in Simulink, which proposed one possible comprehensive control for HVDC system for offshore wind farm.

7.3 Limitations and Future work

The main limitations of the thesis are

- Only wind farm side MMC are studied and the transmission line were not the modelled so that the power system problems were neglected.
- Most of simulations neglected the oscillations or other effects from wind farm and an ideal grid model was used
- Only half bridge configuration is considered for SMs
- Not verified by hardware implementation
- Only the control strategies for balanced system were studies.

Thus, the future work may include:

- Simulating the control strategies in whole HVDC system
- Deeper study on theories and modelling of wind farm, testing all control algorithms with wind farm model by considering the oscillation from wind farm and controlling the energy transformation according to wind speed.
- Applying half bridge configuration for SMs and comparing the results. In addition, extending the control algorithms to new multilevel topologies, like alternate arm converter [92].
- Simulating more control strategies and using new control methods for MMC
- Laboratory hardware realization of the control strategies with delays considered
- Studying control algorithms for unbalanced system.

Reference

[1] Global Wind Energy Council, Global Wind Energy Report Annual Market update 2015, http://www.gwec.net/wp-content/uploads/vip/GWEC-Global-Wind-2015-Report_April-2016_22_04.pdf

[2] European Wind Energy Association, Wind in Power 2014 European statistics, http://www.ewea.org/fileadmin/files/library/publications/statistics/EWEA-Annual-Statistics-2014.pdf

[3] Technical University of Denmark, DTU International Energy Report 2014, http://www.natlab.dtu.dk/english/-/media/Andre_Universitetsenheder/Nationallab_for_Baeredygtig_Energi/NatLabDocs/DIER2014/DTU-INTL-ENERGY-REP-2014-WIND.ashx?la=da

[4] European Wind Energy Association, The European offshore wind industry - key trends and statistics 1st half 2015, http://www.ewea.org/fileadmin/files/library/publications/statistics/EWEA-European-Offshore-Statistics-H1-2015.pdf

[5] Bresesti, P., Kling, W. L., Hendriks, R. L., & Vailati, R. (2007). HVDC connection of offshore wind farms to the transmission system. *Energy Conversion, IEEE Transactions on*, *22*(1), 37-43.

[6] Heyman, O., Weimers, L., & Bohl, M. L. (2010, September). HVDC-A key solution in future transmission systems. In *World Energy Congress-WEC* (pp. 12-16).

[7] Ackermann, T. (2005). Transmission systems for offshore wind farms. *Wind power in power systems*, 479-503.

[8] Breuer, W., Povh, D., Retzmann, D., Teltsch, E., & Lei, X. (2004, October). Role of HVDC and FACTS in future Power Systems. In *CIGER Symposium, Shang Hai*.

[9] Korompili, A., Wu, Q., & Zhao, H. (2016). Review of VSC HVDC connection for offshore wind power integration. *Renewable and Sustainable Energy Reviews*, *59*, 1405-1414.

[10] Bahrman, M., & Johnson, B. (2007). The ABCs of HVDC transmission technologies. *IEEE power and energy magazine*, *2*(5), 32-44.

[11] European Wind Energy Association, Oceans of Opportunity, http://www.ewea.org/fileadmin/files/library/publications/reports/Offshore_Report_2009.pdf

[12] Marquardt, R. (2010, June). Modular Multilevel Converter: An universal concept for HVDC-Networks and extended DC-Bus-applications. In *Power Electronics Conference (IPEC), 2010 International* (pp. 502-507). IEEE.

[13] Allebrod, S., Hamerski, R., & Marquardt, R. (2008, June). New transformerless, scalable modular multilevel converters for HVDC-transmission. In *Power Electronics Specialists Conference, 2008. PESC 2008. IEEE* (pp. 174-179). IEEE.

[14] Nami, A., Liang, J., Dijkhuizen, F., & Demetriades, G. D. (2015). Modular multilevel converters for HVDC applications: Review on converter cells and functionalities. *Power Electronics, IEEE Transactions on*, *30*(1), 18-36.

[15] Dorn, J., Huang, H., & Retzmann, D. (2008). A new multilevel voltage-sourced converter topology for HVDC applications. *CIGRE Session. Paris, France: International Council on Large Electric Systems*, 1-8.

[16] Friedrich, K. (2010, July). Modern HVDC PLUS application of VSC in Modular Multilevel Converter topology. In *Industrial Electronics (ISIE), 2010 IEEE International Symposium on* (pp. 3807-3810). IEEE.

[17] Dorn, J., Huang, H., & Retzmann, D. (2007, November). Novel voltage-sourced converters for HVDC and FACTS applications. In *Cigre Symposium, November* (pp. 1-4).

[18] Ahmed, N., Norrga, S., Nee, H. P., Haider, A., Van Hertem, D., Zhang, L., & Harnefors, L. (2012, March). HVDC SuperGrids with modular multilevel converters—The power transmission backbone of the future. In *Systems, Signals and Devices (SSD), 2012 9th International Multi-Conference on* (pp. 1-7). IEEE.

[19] Debnath, S., Qin, J., Bahrani, B., Saeedifard, M., & Barbosa, P. (2015). Operation, control, and applications of the modular multilevel converter: A review. *Power Electronics, IEEE Transactions on*, *30*(1), 37-53.

[20] Tu, Q., Xu, Z., & Xu, L. (2011). Reduced switching-frequency modulation and circulating current suppression for modular multilevel converters. Power Delivery, IEEE Transactions on, 26(3), 2009-2017.

[21] Rodriguez, J., Lai, J. S., & Peng, F. Z. (2002). Multilevel inverters: a survey of topologies, controls, and applications. *Industrial Electronics, IEEE Transactions on*, *49*(4), 724-738.

[22] Lai, J. S., & Peng, F. Z. (1996). Multilevel converters-a new breed of power converters. *Industry Applications, IEEE Transactions on*, *32*(3), 509-517.

[23] Kouro, S., Malinowski, M., Gopakumar, K., Pou, J., Franquelo, L. G., Wu, B., ... & Leon, J. (2010). Recent advances and industrial applications of multilevel converters. *Industrial Electronics, IEEE Transactions on*, *57*(8), 2553-2580.

[24] Flourentzou, N., Agelidis, V. G., & Demetriades, G. D. (2009). VSC-based HVDC power transmission systems: An overview. *Power Electronics, IEEE Transactions on*, *24*(3), 592-602..

[25] Lesnicar, A., & Marquardt, R. (2003, June). An innovative modular multilevel converter topology suitable for a wide power range. In *Power Tech Conference Proceedings* (Vol. 3, p. 6).

[26] Glinka, M., & Marquardt, R. (2005). A new AC/AC multilevel converter family.*Industrial Electronics, IEEE Transactions on*, *52*(3), 662-669.

[27] Solas, E., Abad, G., Barrena, J. A., Aurtenetxea, S., Carcar, A., & Zajac, L. (2013). Modular

multilevel converter with different submodule concepts—Part II: experimental validation and comparison for HVDC application. *Industrial Electronics, IEEE Transactions on*, *60*(10), 4536-4545.

[28] Negra, N. B., Todorovic, J., & Ackermann, T. (2006). Loss evaluation of HVAC and HVDC transmission solutions for large offshore wind farms.*Electric Power Systems Research*, *76*(11), 916-927.

[29] Bahrman, M. P. (2008, April). HVDC transmission overview. In Transmission and Distribution Conference and Exposition, 2008. T&# x00026; D. IEEE/PES (pp. 1-7). IEEE.

[30] Junyent-Ferré, A., Clemow, P., Merlin, M. M., & Green, T. C. (2014, August). Operation of HVDC Modular Multilevel Converters under DC pole imbalances. In *Power Electronics and Applications (EPE'14-ECCE Europe), 2014 16th European Conference on* (pp. 1-10).

[31] Kazmierkowski, M. P., & Malesani, L. (1998). Current control techniques for three-phase voltage-source PWM converters: a survey. Industrial Electronics, IEEE Transactions on, 45(5), 691-703.

[32] Irwin, J. D. (2002). Control in power electronics: selected problems. M. P. Kazmierkowski, R. Krishnan, & F. Blaabjerg (Eds.). Academic press.

[33] Mohan, N., & Undeland, T. M. (2007). *Power electronics: converters, applications, and design*. John Wiley & Sons.

[34] Zhang, G., & Xu, Z. (2001). Steady-state model for VSC based HVDC and its controller design. In *Power Engineering Society Winter Meeting, 2001. IEEE*(Vol. 3, pp. 1085-1090). IEEE.

[35] Bajracharya, C., Molinas, M., Suul, J. A., & Undeland, T. M. (2008). Understanding of tuning techniques of converter controllers for VSC-HVDC. In Nordic Workshop on Power and Industrial Electronics (NORPIE/2008), June 9-11, 2008, Espoo, Finland. Helsinki University of Technology.

[36] Du, C., Sannino, A., & Bollen, M. H. (2005, June). Analysis of the control algorithms of voltage-source converter HVDC. In *Power Tech, 2005 IEEE Russia* (pp. 1-7). IEEE.

[37] Ruihua, S., Chao, Z., Ruomei, L., & Xiaoxin, Z. (2005). VSCs based HVDC and its control strategy. In *Transmission and Distribution Conference and Exhibition: Asia and Pacific, 2005 IEEE/PES* (pp. 1-6). IEEE.

[38] Papavasiliou, A., Papathanassiou, S. A., Manias, S. N., & Demetriadis, G. (2007, June). Current control of a voltage source inverter connected to the grid via LCL filter. In *Power Electronics Specialists Conference, 2007. PESC 2007. IEEE* (pp. 2379-2384). IEEE.

[39] Viswanathan, V., & Jeevananthan, S. (2011). A Novel Current Controlled Space Vector Modulation based Control Scheme for Reducing Torque Ripple in Brushless DC Drives. *International Journal of Computer Applications*,*28*(2).

[40] Timbus, A. V., Ciobotaru, M., Teodorescu, R., & Blaabjerg, F. (2006, March). Adaptive

resonant controller for grid-connected converters in distributed power generation systems. In *Applied Power Electronics Conference and Exposition, 2006. APEC'06. Twenty-First Annual IEEE* (pp. 6-pp). IEEE.

[41] Dirscherl, C., Fessler, J., Hackl, C. M., & Ipach, H. (2015, September). State-feedback controller and observer design for grid-connected voltage source power converters with LCL-filter. In *Control Applications (CCA), 2015 IEEE Conference on* (pp. 215-222). IEEE.

[42] Pradeepa, S., Rao, K. U., Deekshit, R., & Shantha, M. S. (2013, February). State-feedback control of a voltage source inverter-based STATCOM. In*Power, Energy and Control (ICPEC), 2013 International Conference on* (pp. 120-123). IEEE.

[43] Gabe, I. J., Massing, J. R., Montagner, V. F., & Pinheiro, H. (2007, September). Stability analysis of grid-connected voltage source inverters with LCL-filters using partial state feedback. In *Power Electronics and Applications, 2007 European Conference on* (pp. 1-10). IEEE.

[44] Kukkola, J., & Hinkkanen, M. (2014). Observer-based state-space current control for a three-phase grid-connected converter equipped with an LCL filter. *Industry Applications, IEEE Transactions on*, *50*(4), 2700-2709.

[45] Cortés, P., Kazmierkowski, M. P., Kennel, R. M., Quevedo, D. E., & Rodríguez, J. (2008). Predictive control in power electronics and drives.*Industrial Electronics, IEEE Transactions on*, *55*(12), 4312-4324.

[46] Yang, S. M., & Lee, C. H. (2002). A deadbeat current controller for field oriented induction motor drives. *Power Electronics, IEEE Transactions on*,*17*(5), 772-778.

[47] Abu-Rub, H., Guzinski, J., Krzeminski, Z., & Toliyat, H. A. (2001). Predictive current control of voltage source inverters. In *Industrial Electronics Society, 2001. IECON'01. The 27th Annual Conference of the IEEE* (Vol. 2, pp. 1195-1200). IEEE.

[48] Zeng, Q., & Chang, L. (2008). An advanced SVPWM-based predictive current controller for three-phase inverters in distributed generation systems.*Industrial Electronics, IEEE Transactions on*, *55*(3), 1235-1246.

[49] Han, J., Ma, Z., & Peng, D. (2013). Analysis of Model Predictive Current Control for Voltage Source Inverter. Research Journal of Applied Sciences, Engineering and Technology 6(21): 3986-3992.

[50] Preindl, M., Schaltz, E., & Thogersen, P. (2011). Switching frequency reduction using model predictive direct current control for high-power voltage source inverters. *Industrial Electronics, IEEE Transactions on*, *58*(7), 2826-2835.

[51] Mariéthoz, S., & Morari, M. (2009). Explicit model-predictive control of a PWM inverter with an LCL filter. *Industrial Electronics, IEEE Transactions on*,*56*(2), 389-399.

[52] Vargas, R., Cortés, P., Ammann, U., Rodríguez, J., & Pontt, J. (2007). Predictive control of a three-phase neutral-point-clamped inverter. *Industrial Electronics, IEEE Transactions on*, *54*(5), 2697-2705.

[53] Malesani, L., & Tenti, P. (1990). A novel hysteresis control method for current-controlled voltage-source PWM inverters with constant modulation frequency. *IEEE Transactions on Industry Applications*, *26*(1), 88-92.

[54] Zeng, J., Yu, C., Qi, Q., Yan, Z., Ni, Y., Zhang, B. L., ... & Wu, F. F. (2004). A novel hysteresis current control for active power filter with constant frequency. *Electric power systems research*, *68*(1), 75-82.

[55] Brod, D. M., & Novotny, D. W. (1985). Current control of VSI-PWM inverters.*Industry Applications, IEEE Transactions on*, (3), 562-570.

[56] Kaźmierkowski, M. P., Dzieniakowski, M., & Sulkowski, W. (1991). Novel space vector based current controllers for PWM-inverters. *Power Electronics, IEEE Transactions on*, *6*(1), 158-166.

[57] Wuest, D., & Jenni, F. (1993, June). Space vector based current control schemes for voltage source inverters. In *Power Electronics Specialists Conference, 1993. PESC'93 Record., 24th Annual IEEE* (pp. 986-992). IEEE.

[58] Rosyadi, M., Muyeen, S. M., Takahashi, R., & Tamura, J. (2012, October). Fuzzy logic controlled voltage source converter in grid connected application via LCL filter. In *Electrical Machines and Systems (ICEMS), 2012 15th International Conference on* (pp. 1-6). IEEE.

[59] Rukonuzzaman, M., & Nakaoka, M. (2000). Fuzzy logic current controller for three-phase voltage source PWM-inverters. In *Industry Applications Conference, 2000. Conference Record of the 2000 IEEE* (Vol. 2, pp. 1163-1169). IEEE.

[60] Jasinski, M., Liserre, M., Blaabjerg, F., & Cichowlas, M. (2002, November). Fuzzy logic current controller for PWM rectifiers. In *IECON 02 [Industrial Electronics Society, IEEE 2002 28th Annual Conference of the]* (Vol. 2, pp. 1300-1305). IEEE.

[61] Bo, Q., Xiao-yuan, H., Wen-xi, Y., Zheng-yu, L., & Guerrero, J. M. (2009, February). An optimized deadbeat control scheme using fuzzy control in three-phase voltage source PWM rectifier. In *Applied Power Electronics Conference and Exposition, 2009. APEC 2009. Twenty-Fourth Annual IEEE*(pp. 1215-1219). IEEE.

[62] Ruan, S. Y., Li, G. J., Jiao, X. H., Sun, Y. Z., & Lie, T. T. (2007). Adaptive control design for VSC-HVDC systems based on backstepping method.*Electric power systems research*, *77*(5), 559-565.

[63] Dash, P. K., & Nayak, N. (2014). Nonlinear control of voltage source converters in AC–DC power system. *ISA transactions*, *53*(4), 1268-1285.

[64] Moharana, A., & Dash, P. K. (2010). Input-output linearization and robust sliding-mode controller for the VSC-HVDC transmission link. *Power Delivery, IEEE Transactions on*, *25*(3), 1952-1961.

[65] Ayari, M., Moez Belhaouane, M., & Benhadj Braiek, N. (2015, April). Optimal control design of voltage source converter using bilinear state-space representation. In *Systems and Control (ICSC), 2015 4th International Conference on* (pp. 169-174). IEEE.

[66] Konstantinou, G. S., & Agelidis, V. G. (2009, May). Performance evaluation of half-bridge cascaded multilevel converters operated with multicarrier sinusoidal PWM techniques. In *Industrial Electronics and Applications, 2009. ICIEA 2009. 4th IEEE Conference on* (pp. 3399-3404). IEEE.

[67] Saeedifard, M., & Iravani, R. (2010). Dynamic performance of a modular multilevel back-to-back HVDC system. *Power Delivery, IEEE Transactions on*, *25*(4), 2903-2912.

[68] Siemaszko, D., Antonopoulos, A., Ilves, K., Vasiladiotis, M., Ängquist, L., & Nee, H. P. (2010, June). Evaluation of control and modulation methods for modular multilevel converters. In *Power Electronics Conference (IPEC), 2010 International* (pp. 746-753). IEEE.

[69] Hagiwara, M., & Akagi, H. (2009). Control and experiment of pulsewidth-modulated modular multilevel converters. *Power electronics, IEEE Transactions on*, *24*(7), 1737-1746.

[70] Saeedifard, M., & Iravani, R. (2010). Dynamic performance of a modular multilevel back-to-back HVDC system. *Power Delivery, IEEE Transactions on*, *25*(4), 2903-2912.

[71] Qin, J., & Saeedifard, M. (2013). Reduced switching-frequency voltage-balancing strategies for modular multilevel HVDC converters. *Power Delivery, IEEE Transactions on*, *28*(4), 2403-2410.

[72] Guan, M., Xu, Z., & Chen, H. (2011, November). Control and modulation strategies for modular multilevel converter based HVDC system. In *IECON 2011-37th Annual Conference on IEEE Industrial Electronics Society* (pp. 849-854). IEEE.

[73] Ilves, K., Harnefors, L., Norrga, S., & Nee, H. P. (2015). Predictive sorting algorithm for modular multilevel converters minimizing the spread in the submodule capacitor voltages. *Power Electronics, IEEE Transactions on*,*30*(1), 440-449.

[74] Deng, F., & Chen, Z. (2014). A control method for voltage balancing in modular multilevel converters. *Power Electronics, IEEE Transactions on*,*29*(1), 66-76.

[75] Qin, J., & Saeedifard, M. (2012). Predictive control of a modular multilevel converter for a back-to-back HVDC system. *Power Delivery, IEEE Transactions on*, *27*(3), 1538-1547.

[76] Antonopoulos, A., Ängquist, L., & Nee, H. P. (2009, September). On dynamics and voltage control of the modular multilevel converter. In *Power Electronics and Applications, 2009. EPE'09. 13th European Conference on*(pp. 1-10). IEEE.

[77] Ängquist, L., Antonopoulos, A., Siemaszko, D., Ilves, K., Vasiladiotis, M., & Nee, H. P. (2010, June). Inner control of modular multilevel converters-an approach using open-loop estimation of stored energy. In *Power Electronics Conference (IPEC), 2010 International* (pp. 1579-1585). IEEE.

[78] Bergna, G., Garces, A., Berne, E., Egrot, P., Arzandé, A., Vannier, J. C., & Molinas, M. (2014). A generalized power control approach in abc frame for modular multilevel converter hvdc links based on mathematical optimization.*Power Delivery, IEEE Transactions on*, *29*(1), 386-394.

[79] Pou, J., Ceballos, S., Konstantinou, G., Agelidis, V. G., Picas, R., & Zaragoza, J. (2015). Circulating current injection methods based on instantaneous information for the modular multilevel converter. *Industrial Electronics, IEEE Transactions on*, *62*(2), 777-788.

[80] Darus, R., Pou, J., Konstantinou, G., Ceballos, S., & Agelidis, V. G. (2013, June). Circulating current control and evaluation of carrier dispositions in modular multilevel converters. In *ECCE Asia Downunder (ECCE Asia), 2013 IEEE* (pp. 332-338). IEEE.

[81] She, X., Huang, A., Ni, X., & Burgos, R. (2012, October). AC circulating currents suppression in modular multilevel converter. In *IECON 2012-38th Annual Conference on IEEE Industrial Electronics Society* (pp. 191-196). IEEE.

[82] Li, Z., Wang, P., Chu, Z., Zhu, H., Luo, Y., & Li, Y. (2013). An inner current suppressing method for modular multilevel converters. *Power Electronics, IEEE Transactions on*, *28*(11), 4873-4879.

[83] He, L., Zhang, K., Xiong, J., & Fan, S. (2015). A repetitive control scheme for harmonic suppression of circulating current in modular multilevel converters.*Power Electronics, IEEE Transactions on*, *30*(1), 471-481.

[84] Abildgaard, E. N., & Molinas, M. (2012). Modelling and control of the modular multilevel converter (MMC). *Energy Procedia*, *20*, 227-236.

[85] Vatani, M., Bahrani, B., Saeedifard, M., & Hovd, M. (2015). Indirect Finite Control Set Model Predictive Control of Modular Multilevel Converters. *Smart Grid, IEEE Transactions on*, *6*(3), 1520-1529.

[86] Mei, J., Ji, Y., Du, X., Ma, T., Huang, C., & Hu, Q. (2014). Quasi-Fixed-Frequency Hysteresis Current Tracking Control Strategy for Modular Multilevel Converters. *Journal of Power Electronics*, *14*(6), 1147-1156.

[87] Martinez-Rodrigo, F., de Pablo, S., & Herrero-de Lucas, L. C. (2015). Current control of a modular multilevel converter for HVDC applications. *Renewable Energy*, *83*, 318-331.

[88] Vatani, M., Hovd, M., & Saeedifard, M. (2015). Control of the Modular Multilevel Converter Based on a Discrete-Time Bilinear Model using the Sum of Squares Decomposition Method.

[89] Münch, P., Görges, D., Izák, M., & Liu, S. (2010, November). Integrated current control, energy control and energy balancing of modular multilevel converters. In *IECON 2010-36th Annual Conference on IEEE Industrial Electronics Society* (pp. 150-155). IEEE.

[90] Zygmanowski, M., Grzesik, B., & Nalepa, R. (2013, September). Capacitance and inductance selection of the modular multilevel converter. In Power Electronics and Applications (EPE), 2013 15th European Conference on (pp. 1-10). IEEE.

[91] Cortés, P., Kouro, S., La Rocca, B., Vargas, R., Rodríguez, J., León, J. I., ... & Franquelo, L. G. (2009, February). Guidelines for weighting factors design in model predictive control of power converters and drives. In Industrial Technology, 2009. ICIT 2009. IEEE International Conference on (pp. 1-7). IEEE.

[92] Merlin, M., Green, T. C., Mitcheson, P. D., Trainer, D. R., Critchley, R., Crookes, W., & Hassan, F. (2014). The alternate arm converter: A new hybrid multilevel converter with dc-fault blocking capability. *Power Delivery, IEEE Transactions on*, *29*(1), 310-317.

Appendix

A. Park and Inverse-Park Transformation in Simulink

A.1 abc to dq0:

$$\begin{bmatrix} d \\ q \\ 0 \end{bmatrix} = \begin{bmatrix} sin\theta & -\cos\theta & 0 \\ \cos\theta & sin\theta & 0 \\ 0 & 0 & 1 \end{bmatrix} \cdot \begin{bmatrix} a \\ b \\ c \end{bmatrix}$$

A.2 dq0 to abc

$$\begin{bmatrix} a \\ b \\ c \end{bmatrix} = \begin{bmatrix} sin\theta & \cos\theta & 1 \\ \sin(\theta - \frac{2\pi}{3}) & \cos(\theta - \frac{2\pi}{3}) & 1 \\ \sin(\theta + \frac{2\pi}{3}) & \cos(\theta + \frac{2\pi}{3}) & 1 \end{bmatrix} \cdot \begin{bmatrix} d \\ q \\ 0 \end{bmatrix}$$

B. Per unit system

In this thesis, all the diagram are shown in per unit value, this is the process to calculate the base values. The parameter values are shown in Table 5.1:

At AC side:

S_b: Nominal three phase power = $\sqrt{20^2 + 3.3^2}$ = 20.27 MVA

V_b: Nominal peak phase voltage at AC side = 14.14 kV;

As the rated power can be calculated by the formula below:

$$S_{3-phase} = 3V_{phase,rms}I_{phase,rms}$$

I_b: Nominal peak phase current= $\frac{2S_b}{3V_b}$ = 955 A ;

Z_b: Nominal AC impedance = $\frac{V_b}{I_b}$ = 14.8 Ω ;

At DC side:

In order to keep the modulation in linear region, the half DC voltage $V_{dc}/2$, should be equal or higher than peak value of AC phase voltage. In this thesis, $V_{dc}/2$ is chosen to be $V_b/0.8$, so that when modulation index is 0.8, the output voltage of MMC is equal to AC grid voltage. In this way, so space has been left for control. Thus:

$V_{dc,b}$: Nominal DC side voltage = 2*V_b/0.8 = 35.35 kV;

There are always N SMs on per phase, so the base value for SM voltage is :

$V_{SM,b}$ = $V_{dc,b}/N$ = 5892 V;

$I_{dc,b}$: Nominal DC side current = $\frac{S_b}{V_{dc,b}}$ = 573.4 A;

In this way, all the quantities are guaranteed to be 1 p.u. when the system works in rated power. As the maximum value of MMC output voltages can be equal to $V_{dc}/2$, they are shown in p.u. using $V_{dc}/2$ as the base value (like Figure 6.2 and 6.4), even though they are in AC side. So that better illustration can be achieved.

C. Matlab codes for Model Predictive Control

1. Initial file (define the parameters for the system)

```
clear all;
clc;
%% parameter values for MMC model
Ts = 100e-6;                                % sampling time
n = 6;                                      % number of SMs per arm
Vdc = 20000*sqrt(2)/0.8;                    % DC voltage
C = 0.01;                                   % SM capactitance
L_grid = 3.17e-3;
R_grid = 0.062;                             % grid side impedance
L_arm = 1.59e-3;

L_eq = L_grid + L_arm/2;
K = R_grid + L_eq/Ts;

% nominal value
S_n = 20e6;
V_n = 1e4*sqrt(2);              % peak pahse voltage
I_n = 2/3*S_n/V_n;
Vc_n = Vdc/n ;

%% create all switch state for one phase
j = 1;
S_M= zeros(nchoosek(2*n,n),2*n);
for i = 0:1:2^(2*n)
    S = bitget(i,12:-1:1);
    if sum(S)==6;
        S_M(j,:) = S;
        j= j+1;
    end
end
```

```
%% Save variables for future calculations
save('Initial');
```

2. Predictive algorithm for direct FCS-MPC

```
function y = fcn(u)
in = load('Initial');
% declare variables
Vg = u(1);                          % grid votlages
it = u(2);                          % grid currents
Vc_up = u(3:8)';                    % SM capacitors in upper arm
Vc_low = u(9:14)';                  % SM capacitors in lower arm
iarm_up = u(15);                    % upper arm current
iarm_low = u(16);                   % lower arm current
it_ref = u (17);                    % reference current
Idc = u (18);                       % DC current
Lamda_c = u(19);
Lamda_cir = u(20);                  % weighting factor

% circulating current
i_cir = (iarm_up + iarm_low)/2 - Idc/3;

% define and minimize cost function
[r,c]= size(in.S_M);
J = zeros (1, r);
for i = 1:1:r;
    % AC current control
    V_up = sum(Vc_up.* in.S_M(i,1:6));
    V_low = sum(Vc_low.* in.S_M(i,7:12));
    it_new = -1/in.K*(V_low/2 - V_up/2 - Vg - in.L_eq/in.Ts * it);

    % voltage balancing control
    Vc_add_up = iarm_up/ in.C * in.Ts;
    Vc_add_low = iarm_low/ in.C * in.Ts;
    Vc_up_new = Vc_up + Vc_add_up * in.S_M(i,1:6);
    Vc_low_new = Vc_low + Vc_add_low * in.S_M(i,7:12);

    % circulating current control
    i_cir_new = in.Ts/(2*in.L_arm)*(in.Vdc - V_low - V_up) + i_cir;

    %cost function
    J(i) = abs(it_ref - it_new) + ...
            Lamda_c * sum(abs([Vc_up_new,Vc_low_new]-in.Vc_n))+ ...
            Lamda_cir * abs(i_cir_new);
```

```
end
J_op = min(J);
S_op = in.S_M(J==J_op,:);
y = S_op(1,:);
```

3. **Predictive algorithm for indirect FCS-MPC**

```
function y = fcn(u)
in = load('Initial');
% declare variables
Vg = u(1);                          % grid votlages
it = u(2);                          % grid currents
Vc_up = u(3:8)';                    % SM capacitors in upper arm
Vc_low = u(9:14)';                  % SM capacitors in lower arm
iarm_up = u(15);                    % upper arm current
iarm_low = u(16);                   % lower arm current
it_ref = u (17);                    % reference current
Idc = u (18);                       % DC current
Lamda_c = u(19);
Lamda_cir = u(20);                  % weighting factor

% arm votlage
V_ups = sum(Vc_up);
V_lows = sum(Vc_low);

% circulating current
i_cir = (iarm_up + iarm_low)/2 - Idc/3;

% define and minimize cost function
J_op= inf;
n_up = 0;
n_low = 0;
for i = 0:1:in.n
        j=in.n-i;
        % AC current control
        V_up = i * V_ups/in.n;
        V_low = j * V_lows/in.n;
        it_new = -1/in.K*(V_low/2 - V_up/2 - Vg - in.L_eq/in.Ts * it);

        % voltage balancing control
        V_up_add = iarm_up/ in.C * in.Ts;
        V_low_add = iarm_low/ in.C * in.Ts;
        V_ups_new = V_ups + V_up_add * i;
        V_lows_new = V_lows + V_low_add * j;
```

```
            % circulating current control
            i_cir_new = in.Ts/(2*in.L_arm)*(in.Vdc - V_low - V_up) + i_cir;

            %cost function
            J = abs(it_ref - it_new) + ...
                Lamda_c * (abs(V_ups_new - in.Vdc)+ abs(V_lows_new - in.Vdc))+ ...
                Lamda_cir * abs(i_cir_new);
            if J_op >= J;
               J_op=J;
               n_up = i;
               n_low = j;
            end
end
y = [n_up , n_low];
```

D. Detailed Diagram of Overall Control Scheme (Figure 6.18)

Show in next page.

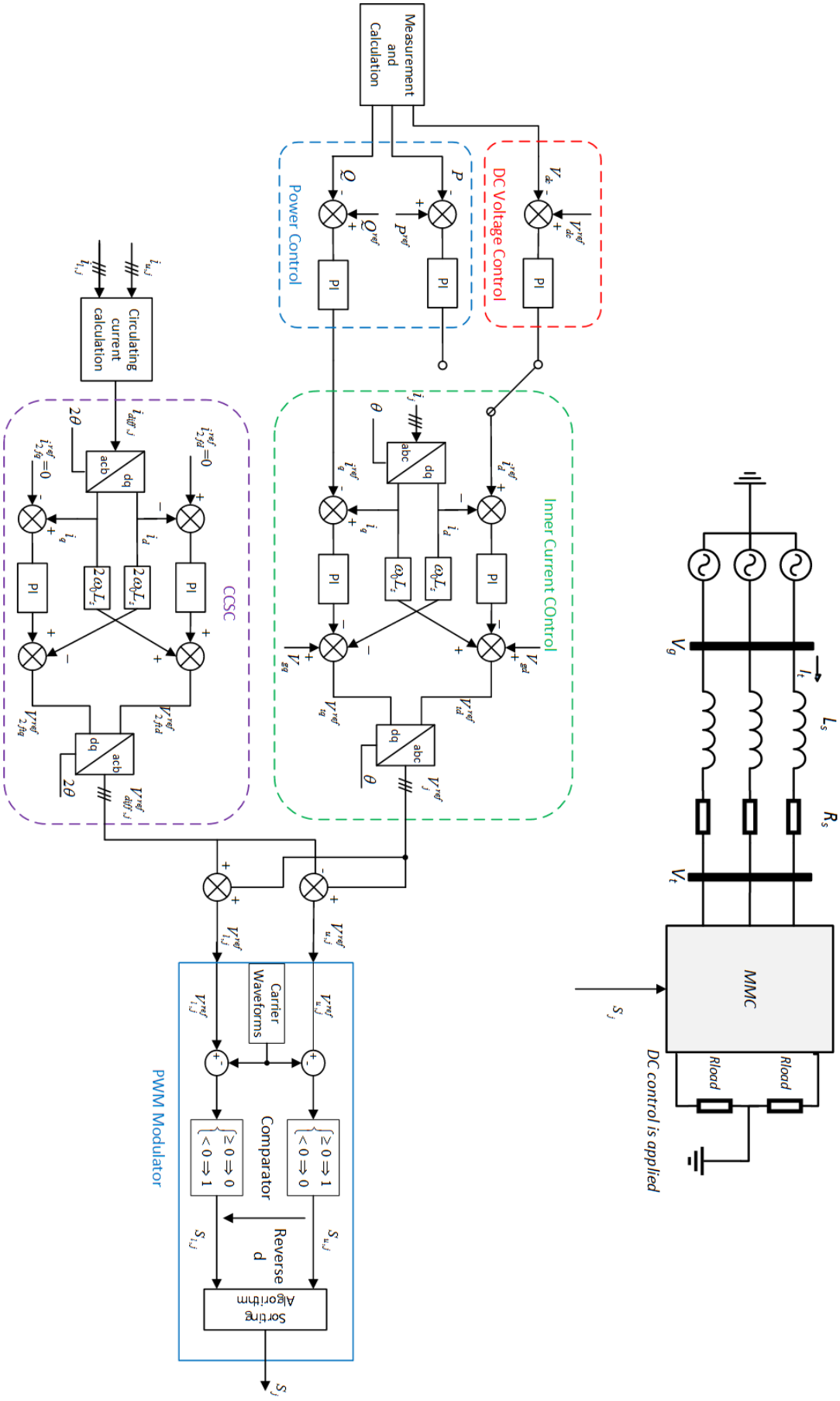
Measurement and Calculation
Power Control
DC Voltage Control
Inner Current COntrol
CCSC
Circulating current calculation
PWM Modulator
Carrier Waveforms
Comparator
Reverse d
Sorting Algorithm
PI
abc
dq
acb
MMC
Rload
Rload
DC control is applied